Long-term variability of storm track characteristics

Dissertation zur Erlangung des Doktorgrades der Naturwissenschaften im Fachbereich Geowissenschaften der Universität Hamburg

vorgelegt von Lan Xia

aus Yunnan, China

Hamburg 2012

Als Dissertation angenommen vom Fachbereich Geowissenschaften der Universität Hamburg

auf Grund der Gutachten von Prof. Dr. Hans von Storch
und Dr. Frauke Feser

Hamburg, den 03.12.2012

Prof. Dr. Dirk Gajewski
(Sprecher des Fachbereichs Geowissenschaften)

Long-term variability of storm track characteristics

Lan Xia

Abstract

The variability of storm track characteristics is studied in terms of polar lows in the North Atlantic and extratropical cyclones in the Northern Hemisphere by detection and tracking algorithms. Two different cyclone-tracking algorithms to detect North Atlantic polar lows, which are very intense mesoscale cyclones, are compared. Both approaches include spatial filtering, detection, tracking and constraints specific to polar lows. Comparisons between these two methods show that different filters lead to different numbers and locations of tracks. The discrete cosine transform is more precise in scale separation than the digital filter and the results of this study suggest that it is more suited for the bandpass filtering of mean sea level pressure fields. The detection and tracking parts also influence the numbers of tracks although less critically. The winter storm activity over the North Hemisphere during the last one thousand years within a global climate simulation was also investigated by tracking and clustering analysis. The numbers of extratropical winter storms exhibit notable inter-annual variability, but only little variability on centennial time scales. The respective storm track clusters also show only small changes between the different centuries. Storm track clusters with longest lifetime and largest deepening rates are found over the North Atlantic and Pacific oceans, with negative correlations between the numbers of members of neighboring oceanic clusters. A linear relationship was found between the numbers of members per storm track clusters over the North Pacific or North Atlantic Ocean and specific atmospheric circulation patterns using a canonical correlation analysis.

Contents

Acknowledgements

My PhD studying was funded by the China Scholar Council (CSC) and the Institute of Coastal Research, Helmholtz-Zentrum Geesthacht (HZG) within the framework of the Junior Scientist Exchange Program organized by the CSC and the Helmholtz Association of German research centers (HGF). I would like to thank the CSC, HZG and HGF for giving me the opportunity to work in the Department of Coastal Climate (KSA) at the HZG in Geesthacht, Germany. During the last over three yeas, it is my honor to meet and work with many people, who taught me how to think and research the scientific questions.

First of all I would acknowledge sincerely my supervisor, Prof. Hans von Storch for leading me to this interesting topic, his continuous support and patient guidance. I heartly appreciate the sharing of his scientific knowledge, experience, and constructive comments. I learn the scientific spirit and the cooperative way from him. I also would like to thank him for providing very open and free discussion atmosphere, which makes me feel comfortable in my studying.

I would like to thank my two co-adviser − Dr. Matthias Zahn and Dr. Frauke Feser. I am very grateful to Dr. Matthias Zahn for providing me the CLM simulation data, the programs and scripts of tracking algorithm. In the beginning of my study, he helped me a lot on dealing with technical problems of programs and GMT. I also benefited from his valuable experience and suggestions on PhD studying. I am thankful to Dr. Frauke Feser for her helpful comments and assistances to my work. I extend my great thankfulness to her for solving my administrative problems and other living difficulties in Germany. Without her kindly aid, I could not concentrate on my research.

I would like to thank Dr. Eduardo Zorita for providing ECHO-G simulation data and supporting with statistic routines. I am also grateful for the constructive discussions about my clustering analysis with him. A special thanks to Dr. Kevin I. Hodges of Reading University for sharing his tracking algorithm which was used for my study. I am very thankful for his hosting me when I visited him and giving me the chance to use his algorithm and work with him. I would like to thank Dr. Beate Geyer from the Department of Regional Atmospheric Modelling (KSR) for providing the NCEP/NCAR reanalysis data and technical supports. I also thank Dr. Jens Meywerk and Dr. Hermann Kuhn for the computational sever supporting and Beate Gardeike for her help to prepare the figures. I acknowledge Dr. Thomas Frisius

from Hamburg University who is the chair of my panel meeting. He organized my panel meetings, supervised my progress and gave helpful suggestions on my work. I also thank Dr. Sebastian Wagner for reading this thesis and giving constructive comments.

Many thanks to Monika Barcikowska, Fei Chen, Xi Lu, Oliver Krueger, Anja Hermans, Armineh Barkhordarian, Frederik Schenk, Katharina Klehmet, other PhD students and colleagues of the HZG, for their companies and supports, which made my study and life colorful in Germany. I would like to express my thankfulness to Sabine Billerbeck and Sabine Hartmann for providing the assistance of administrative work, and Peter Kummerow for supporting on resident permit. At last, I would like to thank my parents and family, who support my decisions permanently. I could not finish my PhD study without their enthusiastic encouragement.

Chapter 1 Introduction

1.1 Polar lows

Polar lows are severe small and meso-scale cyclones over the sea at polar areas or high latitudes associated with strong winds, precipitations and occasionally heavy snow (Rasmussen and Turner 2003). They are also called Arctic hurricanes, Arctic instability lows, polar air depressions, polar airstream cyclones, and Arctic mesocyclones. During historical times, polar lows were already known by coastal residents and seamen. There are many stories and tales between seafarers in Scandinavian countries about polar lows which caused shipwrecks. These storms usually happen during winter time along the northern coast of Norway. They deepen very rapidly with strong winds near or above gale force and show heavy precipitation. The Norwegian meteorological office has noticed these lows, but it still is very hard to predict them.

In the Northern Hemisphere, the area west of Spitsbergen in the Arctic is an active region for polar lows genesis. The warm North Atlantic current provides favorable baroclinic development conditions, so usually polar lows travel southward to Scandinavia. It's also possible that polar lows move southeast to the Kara Sea. Polar lows are also found in the Labrador Sea, in the area of eastern Greenland, the Norwegian Sea and the Barents Sea. Except for the North Atlantic, many polar lows occur in the North Pacific and in the Japan Sea (Fu et al. 2004). In the Southern Hemisphere, polar lows show up around the Antarctic. Thus polar lows are marine cyclones. There is always severe weather accompanied with polar lows, such as storm waves, strong winds, heavy precipitation and snow showers (Rasmussen and Turner 2003). The horizontal diameter of polar lows ranges from approximately 200 to 1000 kilometers. The life span of most polar lows is less than 24 hours. And the travelling speed of polar lows can be up to 50 km/h. Polar lows will disappear rapidly after landfall (Rasmussen and Turner 2003, Zahn et al. 2008).

Many studies analyzed the formation and development of polar lows. Baroclinic instability is considered as one mechanism for polar low formation (Mansfield 1974, Duncan 1977), while conditional instability of the second kind (CISK) is also suggested to be responsible for the development of polar lows (Rasmussen 1979). It is sure that both baroclinic instability and convection play important roles in the development of polar lows. For example, when cold air warms up over warm ocean surface, baroclinic instability increases and favors the formation

of polar lows. Zahn and von Storch (2008 b) studied the linkage between MSLP fields and polar low time series over the North Atlantic by Canonical Correlation Analysis (CCA) and found that cold air outbreaks and upper air troughs do favor the formation of polar lows. Fluxes of sensible and latent heat can also provide warming, so baroclinic instability could cooperate with air-sea interaction (Emanuel and Rotunno 1989). But more stable atmospheric conditions are found in the Antarctic region and surface fluxes there are also relatively smaller than in the Arctic region (Rasmussen and Turner 2003, Mokhov et al. 2007). Topography may also provide an initial disturbance needed for the formation of polar lows, but this mainly for large topography differences like the ones around Greenland.

The satellite measurements since the 1970s enabled great advances in the analysis of polar lows. The satellite images of clouds provide more records of polar lows than observation data like ship measurements or station data in former times. Polar lows can be divided into different types according to their cloud shapes. Figure 1.1 from Mokhov et al. (2007) shows polar lows of spiral type (Figure 1.1 a) and of comma shape (Figure 1.1 b). The comma polar lows happen more often than the spiral type. And polar lows with comma shape clouds may show a clear eye like tropical cyclones (see Figure 1.1 b).

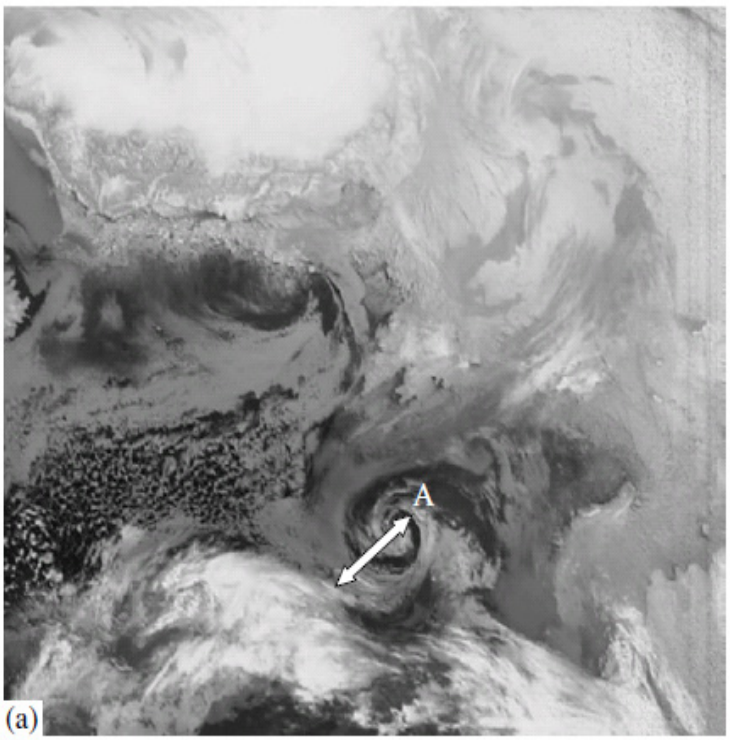

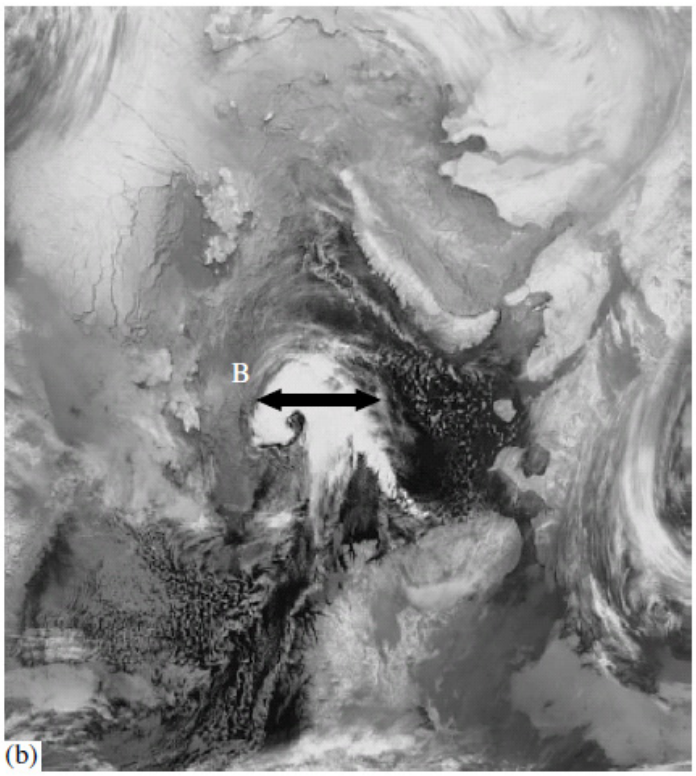

Fig. 1.1 Polar lows in the form of (a) spiral (size A about 520-540 km) on March 20, 2002, and (b) comma (size B about 430-450 km) on January 20, 2002, over the Barents Sea in NOAA-14 and NOAA-15 satellite images, respectively (Mokhov et al. 2007).

Mokhov et al. (2007) studied the polar low size distribution of different cloud shapes. They found that the average diameter of polar lows with comma shape is 177 km and that of spiral shape is 283 km. So the spiral-shape polar lows are usually larger than the comma-shape ones.

In addition to satellite observations, some aircraft and ship observations are available for polar lows (Shapiro et al. 1987). But all these observations suffer from the problem that they are available only for certain periods or lack of homogeneity due to changing observation tools and skills. Reanalysis data like NCEP-NCAR re-analyses with relatively coarse temporal and spatial resolutions are insufficient to diagnose polar lows (Zahn et al. 2008). So a major barrier to polar low research has been shortage of data, especially for long, homogeneous time periods and data sets with high resolutions. Without solving this problem it is not possible to construct climatological statistics, assess decadal trends and variability, or evaluate possible changes of future polar low occurrences. To overcome the limitation of too short and inhomogeneous data, Zahn et al. (2008) introduced a dynamical downscaling strategy to

simulate polar lows. A higher resolution atmospheric regional model was used to reproduce polar low features over the North Atlantic. It used global re-analyses at the lateral and lower boundaries as input data. The regional climate model taken was CLM (now renamed to COSMO-CLM or CCLM, www.com-community.eu) (Steppeler et al. 2003). A spectral nudging technique (von Storch et al. 2000) was also applied to constrain the large-scale atmosphere of the regional model to not deviate too much from the global forcing reanalyzes. Sensitivity studies with different initial conditions and with or without spectral nudging for polar low cases were compared by Zahn et al. (2008). Their results showed that the dynamical downscaling set-up of CLM with spectral nudging can generate polar low features. The simulations of polar low cases were compared to satellite data and weather analyses of the German Weather Forecast Service (DWD): polar lows principally developed at the right time and location while the core pressures were shallow in the CLM simulation. Spectral nudging practices lead to a more realistic upper-level development for polar lows. A subsequently computed long-term simulation extends for the last about 60 years from January 1948 to February 2006 and covers the whole North Atlantic, including the Labrador Sea, western Greenland and the Barents Sea (Zahn and von Storch 2008 b). A similar simulation for polar lows in the North Pacific over the Bering Sea, the Gulf of Alaska and the Japan Sea was later computed by Chen et al. (2012).

Based on these sufficiently long and presumably homogeneous simulations, Zahn and von Storch (2008 a) investigated trends and variability for polar lows. Zahn and von Storch (2008 b) studied the climatological statistics of polar low frequency over the North Atlantic from 1948-2006 and found that there is strong year-to-year variability but no obvious trend. Mokhov et al. (2007) found similar results from satellite data: no significant trend for polar lows over the North European Basin in the late 20th century. Zahn and von Storch (2010) analysed changes of polar lows over the North Atlantic for possible future climate scenarios. They looked at different global climate change scenarios from the Intergovernmental Panel of Climate Change (IPCC) and showed that the occurrences of polar lows over the North Atlantic will decrease. Related to increasing greenhouse gas concentrations a northward shift of polar low genesis areas emerges.

All of the analyses presented above are based on an automatic detection and tracking method by Zahn and von Storch (2008 a) especially designed for tracking polar lows. It is based on a digital bandpass filter (Feser and von Storch 2005) which filters MSLP fields in the spatial

range of about 200−600 km. The tracking technique provides a convenient way to study temporal and spatial distributions of polar lows. There are also many other detection and tracking algorithms for tracking extratropical cyclones. The following questions emerge: can other tracking methods for extratropical cyclones also be applied to track polar lows? Do the climatological statistics of polar lows change when using different tracking methods? What is the sensitivity for polar lows to various tracking procedures?

To answer these questions, another detection and tracking algorithm was also applied to track North Atlantic polar lows. The results were compared with the method of Zahn and von Storch (2008 a). Both algorithms were applied to the same regional climate model output fields. Differences between polar lows identified and tracked by the two methods were analysed by comparing the technical features of the two algorithms. In addition polar low case studies and polar low numbers were investigated using both methods.

1.2 Cyclone tracking

There are basically two ways to diagnose cyclone activity: The Eulerian and the Lagrangian approach. The Eulerian approach calculates the variance or covariance of filtered mean sea level pressure (MSLP) or geopotential height fields which stand for synoptic time scales (about 2.5-8 days) (Blackmon 1976, Ulbrich and Christoph 1999, and Wollings et al. 2012). It gives combined information of intensity and frequency of cyclone activity. For example it uses the standard deviation of the 2-6 or 8 days bandpass filtered variability of sea level pressure fields (Wollings et al. 2012) or 500 hPa geopotential heights (Ulbrich and Christoph 1999). In many studies, the results are also called “storm tracks” (Ulbrich et al. 2009).

The Lagrangian approach known as tracking method also provides an effective way to study spatial and temporal variability of extratropical weather systems (Murray and Simmonds 1991; Hodges 1994, 1995; Serreze 1995; Blender et al. 1997; Gulev et al. 2001; Muskulus and Jacob 2005; Wernli and Schwierz 2006; Zahn and von Storch 2008a). Using numerical tracking algorithms is essential to detect long-term changes of storms or cyclones objectively. Automatic tracking algorithms make it possible to analyse long-term cyclone trends, cyclone formation and decay, travelling speed, lifetime as well as cyclone intensities. Tracking methods can also enable us to study the formation and the decay of storms or cyclones, as well as a possible merging or separation of cyclones during their lifetime (Inatsu 2009).

Generally automatic Lagrangian tracking methods can be divided into three parts: preprocessing (filtering), detection, tracking. Additionally, the tracks are classified according to intensity, structure and activity. Spatial filters are often used before storm or cyclone identification to remove the large-scale background (Hoskins and Hodges 2002, Anderson et al. 2003) and to select the spatial scales of interest especially for tracking mesoscale and small-scale lows (Zahn and von Storch 2008a).

The points used for the tracking are typically chosen as local extremes of some field, for example, minima of the mean sea level pressure field (MSLP) (Serreze 1995, Gulev et al. 2001, Muskulus and Jacob 2005, Wernli and Schwierz 2006, and Zahn and von Storch 2008a), the 1000hPa geopotential height surface (Z1000) (Blender et al. 1997), maxima of the relative vorticity field (Hodges 1995 and Scharenbroich et al. 2010) in the NH and minima in the SH, and geostrophic vorticity computed as the Laplacian of pressure or geopotential (Murray and Simmonds 1991).

Typically the local extremes are detected based on a comparison with the surrounding grid points. The extremes can be found by searching the whole gridded data using a raster scan, but more sophisticated methods can improve the efficiency of the search by first identifying sub-regions. Muskulus and Jacob (2005) segmented pressure fields into areas by a watershed segmentation algorithm and detected minima or maxima in these segmented areas. Wernli and Schwierz (2006) detected minima encircled by at least one closed contour line on Z1000. Scharenbroich et al. (2010) used connected component analysis to define locally connected regions with extremes found in every connected region. Similarly Hodges (1994) used CCA based on hierarchical quad trees.

The next stage links the local extremes to form tracks. Murray and Simmonds (1991) used past motion and pressure tendency to decide the most likely track point at the next time step. Gulev et al. (2001) performed tracking using an interactive approach. Muskulus and Jacob (2005) used a Kalman filtering approach to perform the tracking which takes into account the whole cyclone history and not just two consecutive timesteps to form tracks. Scharenbroich et al. (2010) applied a probabilistic model to decide the most probable tracks of storms. Other simpler methods have also been employed such as those based on nearest neighbour search (Blender et al. 1997). Methods based on the steering-level flow (Marchok, 2002) have also been used. Finally, further criteria are often applied to pick out particular types of cyclones,

such as some requirements of lifetime or intensity. In this paper, selection criteria previously used by Zahn and von Storch (2008a) are applied to both the Hodges and Zahn algorithms to pick out tracks of potential polar lows.

The steps described above will all influence the cyclone track results. The filter range chosen also decides which features will be identified. For a low-pass filter, the long waves will be retained and the track method will select large-scale systems; similarly, a high-pass filter will remove the contributions of long waves and short wave systems will be tracked. The detection part records the location and values of local extremes which are used for the tracking. Different techniques and additional requirements in this part can lead to differences in the systems that are identified. The tracking is applied in the next step together with further criteria which can also affect the final results. For example Raible et al. (2008) compared three cyclone detection and tracking schemes and found deviations of track length due to different technical aspects in the detection and tracking procedures.

Of course the use of different datasets also influences cyclone characteristics and climatologies. The ECMWF reanalysis (ERA-40) has been shown to produce systematically more cyclones than the NCEP-NCAR reanalysis dataset (Raible et al. 2008) when using MSLP for identification. The study of Feser and von Storch (2008a, b) which used dynamically downscaled global reanalyses data produced by a limited area model showed that lower pressure and higher wind speeds were obtained for typhoon events which are closer to observations although the tracks of the typhoon events were not improved. The use of different fields and levels has also been shown to result in different numbers of cyclones, even if using the same source data set (Hoskins and Hodges, 2002). The use of projections for the data can also have an impact on the final results via both the identification and tracking. For example, using the standard latitude-longitude projection (plate carrée) preferentially samples the high latitudes (Sinclair, 1997), whilst distance and direction become distorted relative to their true values on the surface of a sphere. This can be circumvented to some extent by the choice of a different projection and measuring distance and direction on a sphere (Hodges, 1995). Blender and Schubert (2000) and Jung et al. (2006) studied the influences of different horizontal resolutions on extratropical cyclone characteristics. Numbers of extratropical cyclones could be underestimated within low horizontal resolution data. Cyclones are more sensitive and influenced by resolutions over the regions like the northern Pacific, the Arctic,

Baffin Bay and the Labrador Sea (Jung et al. 2006). Uncertainties of cyclone frequency may also be linked to different temporal resolution (Zolina and Gulev 2002).

1.3 Extratropical cyclones

Extratropical cyclones are defined as synoptic low pressure systems developing in the mid- and high latitudes (>30°N). These systems are connected with baroclinic instability and accompanied with outbreaks of cold air, heavy rains, gales and thunderstorms (Weisse and von Storch 2009). Therefore, extratropical cyclones are very important weather phenomena in the mid- and high latitude areas. Due to the Coriolis force, extratropical cyclones rotate counterclockwise in the northern hemisphere and clockwise in the southern hemisphere. Extratropical cyclones usually form along frontal areas near the upper level jetstream with pronounced temperature and dewpoint gradients (Hewson 2009). The divergence in the upper level is favored by the jetstream forces upward air motion and convergence in the lower level. This upward air motion leads to reduce the surface pressure and strengthens the cyclone. Thus extratropical cyclones are usually regarded as baroclinic systems. Tropical cyclones can transit into extratropical cyclones when they reach mid-latitude areas between 30° and 40° north and south, respectively (Jones et al. 2003). In contrast to tropical cyclones, extratropical cyclones move relatively fast and occur more frequently.

In the Northern Hemisphere, cyclone activity mainly occurs over the North Atlantic and North Pacific. The secondary maxima are over the Asian continent and the Mediterranean Sea. Cyclone genesis of North Pacific cyclones occur in Mongolia, southeast China, eastern Japan and in the central Pacific (Hoskins and Hodges 2002, Inatsu 2009). Genesis of North Atlantic cyclones is located in the lee of the Northern Rocky Mountains, along the northeast of Cape Hatteras, in Iceland and the Norwegian Sea regions (Hoskins and Hodges 2002). Other genesis areas are found over the Mediterranean Sea and Caspian Sea.

Cyclones generated in the Mongolian Plateau move east to the Japan Sea (Adachi and Kimura 2007). The Majority of these systems is generally weak (Hoskins and Hodges 2002). Cyclones generated in the East China Sea or southeast China around the mouth of the Yangtze River move to the southern coast of Japan (Adachi and Kimura 2007). Cyclones generated over the Japan Sea go to the central or northern Pacific (Hoskins and Hodges 2002). In the northern Atlantic, cyclones from the northern Rockies terminate in the northeast of

America. Cyclones starting from Cape Hatteras move north or north-eastwards finishing in the Norwegian Sea. Cyclones in the North Atlantic can also travel to Western Europe.

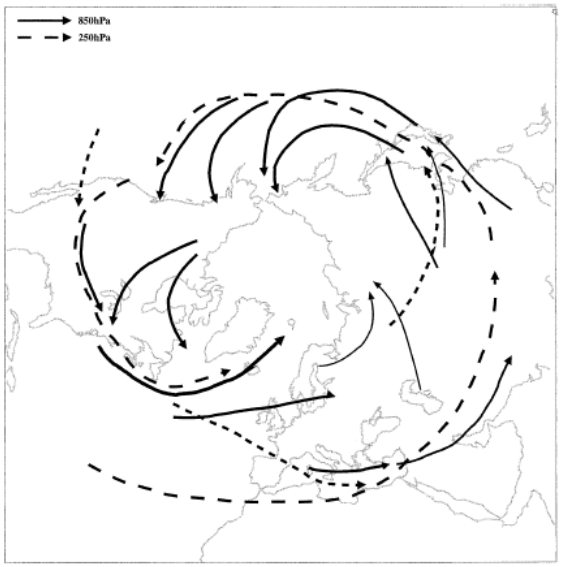

Fig. 1.2 Schematic of principal tracks for lower- (solid line) and upper- (dashed line) tropospheric storm track activity based on 850 hPa vorticity (ξ_{850}) fields and potential temperature on the potential vorticity= 2 PVU surface (θ_{pv2}) (Hoskins and Hodges 2002).

Figure 1.2 from Hoskins and Hodges (2002) gives the principal tracks of upper and lower level for storm track activity using 850 hPa vorticity (ξ_{850}) and potential temperature on a potential vorticity=2 PVU surface (θ_{pv2}). We can see that track bands spiral around the northern hemisphere occurring sequentially in the Mediterranean, southeast China, to the east of Japan, in the central Pacific, in the lee of the Rockies mountains, around the eastern American coasts, in the Norwegian Sea and Western Europe (Hoskins and Hodges 2002) .

There are many studies that deal with perspectives of changing storm statistics in the course of emerging anthropogenic climate change. Schubert et al. (1998) found that for North Atlantic cyclones their frequency increases northeastward using ECHAM3 in the double CO_2 scenario and northward in the triple CO_2 scenario but the cyclone intensities do not change in both scenarios. Ulbrich and Christoph (1999) found that an increasing number of storm tracks over the east Atlantic and Western Europe are related to a northeastward shift of the North Atlantic Oscillation (NAO) due to rising greenhouse gas forcing. Bengtsson and Hodges (2006) concluded that the intense storms do not increase in the future climate either in the tropics or extratropics. Pinto et al. (2007) studied cyclone activity in three climate scenarios.

Cyclone track density decreased over the mid-latitudes in the future scenarios, especially over the Mediterranean Basin. Woolings et al. (2012) suggested that in contrast to cyclones in other regions, the North Atlantic cyclones tracks do not shift polewards due to effects related to the oceanic Meridional Overtuning Circulation (MOC) that could potentially reduce greenhouse-induced sea-surface warming.

However, apart from assessing the significance of expected future changes, it is needed and interesting to study the natural changes of cyclone frequencies and characteristics in the past. Sickmöller et al. (2000) showed that in the Atlantic the intense cyclones decrease and in the Pacific the intense cyclones increase during the period 1979 – 1997 based on re-analyses of the European Center for Medium-Range Weather Forecasts (ECMWF). Gulev et al. (2001) used NCEP/NCAR reanalysis data from 1958 to 1999 and found that cyclone numbers increase in the Arctic and in the western Pacific but decrease over the Gulf Stream in the North Atlantic and the subpolar Pacific. Geng and Sugi (2001) found cyclones over the northern North Atlantic to increase from 1958 to 1998. Simmonds and Keay (2002) tracked extratropical cyclones over the Pacific and Atlantic from 1958 to 1997 using the NCEP/NCAR reanalysis data. They showed there are positive trends for the numbers of intense cyclones over the pacific and Atlantic. But the increase over the Atlantic really depends on the definition of extreme cyclones. Wang et al. (2006) compared the ECMWF reanalysis and the NCEP/NCAR reanalysis for 1958-2001. Both datasets showed a significant increasing trend for winter intense cyclones in the high-latitude North Atlantic and the mid-latitude North Pacific, but a decreasing trend in the mid-latitude North Atlantic. Raible et al. (2008) also compared the 40-years ECMWF reanalysis with the NCEP/NCAR reanalysis data. The cyclone trends and characteristics are sensitive to the reanalysis dataset.

The storm activity changes for the last century were also investigated by using proxies based on air pressure or winds statistics. Bärring and von Storch (2004) studied Scandinavian storms since about 1800 derived from pressure observations in Lund and Stockholm. They found that storminess is remarkably stable during the entire historical period and there is no obvious sign of any long-term trend for storminess indices. Alexander et al. (2005) used observation data of stations in the United Kingdom and Iceland to analyse the changes of severe storms. A significant increase of severe storm numbers over the United Kingdom during the late twentieth century was found. Matulla et al. (2008) showed that geostrophic wind's high percentiles over Europe increased in the early twentieth century, then descended, and rose up

again in the late twentieth century. This is in line with Alexander et al. (2005). However, these studies looked at the past changes of storms in the limited scope of the last century. Only Fischer-Bruns et al. (2005) examined multi-centennial data – from coupled atmosphere-ocean global climate model (GCM) simulations subject to estimated external (volcanic, solar and anthropogenic) forcing. They showed that the storm frequency had no noteworthy long-term trends until recently. In particular no obvious link between temperature variations and extratropical storm activity emerged.

How storm track activity relates to changes of circulation has been studied often: the effect of the North Atlantic Oscillation (NAO) (Hurrell 1995, Ulbrich and Christoph 1999, Gulev et al. 2001, Pinto et al. 2007 and Raible et al. 2007) on storm statistics has been studied; also the effects of the Southern Oscillation (SO) (Sickmöller et al. 2000), the North Pacific Oscillation (PNA) (Christoph and Ulbrich 2000, Sickmöller et al. 2000, and Gulev et al. 2001) as well as anomalies of midlatitude sea surface temperature (SST) anomalies (Brayshaw et al. 2008). In this study, the variability of Northern Hemisphere extratropical storms and their relation to changes in winter (December – February, DJF) circulation is studied. This is achieved with the help of a Canonical Correlation Analysis of seasonal anomalies of mean sea level pressure fields (MSLP) and the seasonal number of members in the storm track clusters.

In addition to tracking algorithms, extratropical cyclones can also be studied by clustering analysis. The cluster analysis was developed for sorting objects into different categories. Gulev et al. (2001) studied cyclone characteristics from different genesis areas. Wang et al. (2006) separated extratropical cyclones into mid-latitude cyclones and high-latitude cyclones. Blender et al. (1997) classified cyclone tracks in the North Atlantic/European region into three distinct groups of stationary, zonally and north-eastward travelling storms. Elsner (2003) clustered North Atlantic tropical cyclones into three clusters − one cluster presents straight-moving hurricanes and two clusters present recurving hurricanes. Nakamura et al. (2009) considered the locations and shapes of tropical cyclone tracks of the North Atlantic and classified them into six clusters. Chu et al. (2010) classified tropical storms over the western North Pacific according to their shapes into three straight types, four recurved types and one mixed straight-recurved type.

1.4 Research aims

In this study, long-term variability of storm track characteristics were investigated in terms of polar lows over the North Atlantic and extratropical cyclones in the Northern Hemisphere. This thesis aims to answer two major scientific questions:

1. Could other detection and tracking algorithms designed for tracking extratropical cyclones be applied for tracking polar lows and what are the influences on polar low climatology when using various tracking procedures?

2. What is the variability of the winter extratropical cyclone activity in the Northern Hemisphere for the last one thousand years? Do the numbers of extratropical winter storms show any trend in a simulation of the past millennium?

To answer the first question, two tracking methods were applied to track polar lows of the North Atlantic using the same Regional Climate Model (RCM) output fields produced from dynamically downscaling the NCEP/NCAR reanalysis data. The technical features of both tracking methods were compared for polar low identification and tracking by analyzing their filtering, detection and tracking parts.

To make the two algorithms comparable, the settings were adapted to be as similar as possible. The reasons for differences between the two algorithms are studied by comparing distinctive details in filter construction, detection methods and tracking. In order to identify common tracks between the two different methods a simple track-to-track comparison algorithm was applied. Polar low criteria which find and pick out potential polar lows are applied additively to see the influences on the tracks of the two tracking methods.

To answer the second question, a global climate simulation for the last one thousand years was used to study winter cyclone activity in the Northern Hemisphere. These long simulations mostly operate with spatial resolutions suitable for extratropical storms, but not for tropical cyclones. Therefore we limit ourselves to such mid-latitude baroclinic storms as in Fischer-Bruns et al. (2005).

The intention of this study is to determine and discuss the variability of extratropical cyclone tracks from century to century. The statistics and frequency of storm tracks are studied

through the lens of regional clustering. Cyclone characteristics such as life span, frequency, or intensity are also analyzed for each cluster. Variations of the numbers of members of the clusters in the marine sectors of the North Pacific and North Atlantic are related to mean winter circulation anomalies by Canonical Correlation Analysis. It is favorable to know the link between cyclone activity and large-scale systems.

1.5 Dissertation structure

The scientific aims mentioned in Section 1.4 are studied in this dissertation which is organized as follows: In Chapter 2 a comparison of two identification and tracking methods for polar lows is analyzed. This chapter is based on the article "a comparison of two identification and tracking methods for polar lows" by Xia et al. (2012a) published in Tellus A. In Section 2.2 the Regional Climate Model (RCM) used to dynamical downscale the NCEP/NCAR reanalysis data is introduced. In Section 2.3 two spatial filters used in the two tracking algorithms are compared. The technical details of these two tracking methods are described in Section 2.4 and 2.5. How each part in the tracking process influences the tracks is shown in Section 2.6. A simple track-to-track comparison algorithm to identify common tracks is described in Section 2.7. In Section 2.8 comparisons of tracks of potential polar lows derived from two tracking methods are also given.

A tracking and clustering analysis for centennial extratropical cyclone activity in a simulation of the past millennium is studied in Chapter 3. This chapter is based on the publication "quasi-stationary of centennial Northern Hemisphere midlatitude winter storm tracks" in Climate Dynamics by Xia et al. (2012b). The millennial simulation, obtained with the coupled atmosphere-ocean global climate model ECHO-G exposed to time variable solar, volcanic and greenhouse gas forcing is introduced in Section 3.2. The availability of millennial simulations on studying extratropical storms was examined by various researchers (e. g. Fischer-Bruns et al. 2005). The Lagrangian-type tracking algorithm of Hodges (1994, 1995, and 1999) to gain the tracking results is described in Section 3.3.1. For validation reasons, tracks are compared with results derived from coarsened NCEP/NCAR reanalysis data to evaluate the model simulation in Section 3.3.2. The variability of numbers of extratropical winter storms for the quasi-millennium period is shown. Tracks are consecutively clustered into ten groups for hundred years' segments in Section 3.4. The changes and activities of the clusters of these storm tracks between the centuries are also analyzed in Section 3.4.3. A linear relationship was found between the numbers of members per storm track clusters over

the Pacific or Atlantic Ocean and seasonal mean atmospheric circulation patterns by a canonical correlation analysis (CCA) in Section 3.4.5. The caveats of this study due to coarse resolution of ECHO-G data and the potential uncertainties of results are discussed in Section 3.5. Summary and discussions as well as ideas for future work are presented in Chapter 4, followed by the Acknowledgements and References.

Chapter 2 Comparisons of two tracking methods for polar lows

2.1 Overview

In this chapter, we compare two different cyclone-tracking algorithms to detect and track North Atlantic polar lows, which are very intense mesoscale cyclones. The differences between two different methods are examined by comparing the technical features of the filtering, detection and tracking parts of the two methods. The methods explored are those of Hodges (1994, 1995, and 1999) and Zahn and von Storch (2008a). These were applied to detect polar lows in the North Atlantic. Polar lows are associated with intense low-level winds and heavy precipitation and are an important risk factor for maritime operations at high latitudes (Rasmussen and Turner, 2003).

The first tracking method is that of Zahn and von Storch (2008a) which is based on a digital bandpass filter of the MSLP in the spatial range 200-600km. The filter was originally designed by Feser and von Storch (2005). This method was especially designed for tracking polar lows. The other method is that of Hodges (1994, 1995 and 1999) which uses a bandpass filter based on the discrete cosine transforms (DCT) and can be applied to MSLP and vorticity fields. The Hodges' program was designed for tracking weather systems in general but for this study was adapted for tracking polar lows.

For abbreviation, we use the acronyms "MZ" for Zahn and von Storch's method (2008a) and "KH" for the Hodges' algorithm (1994, 1995 and 1999). Both methods include three parts: filter, detection and tracking. MZ's algorithm has a fourth part to assign tracks of polar lows according to given constraints and these are also applied to KH's method to identify polar lows.

As discussed in Section 1.2, the use of different datasets also influences tracking characteristics and climatologies. So both algorithms are applied on the same regional climate model output fields produced from dynamical downscaling of the NCEP/NCAR reanalysis data. To make the two algorithms comparable, the settings were adapted to be as similar as possible.

The regional climate model and the data we used are described in Section 2.2. Different filters approaches using in two algorithms are compared in Section 2.3. We show the differences in terms of the filters and detection techniques resulting from applying two methods in section 2.4. The different settings in tracking parts of both methods are introduced in section 2.5. Processes involved in tracking polar lows and their influences on the tracks are investigated in section 2.6, including the application of different combinations of the two methods in order to analyse the origin of differences. Track-to-track comparisons between the two methods are analyzed in section 2.7. Section 2.8 contains the application of further criteria on the tracking algorithms to indentify potential polar lows and an evaluation on the influences of each criterion. Section 2.9 gives a summary and conclusions of the results obtained in this chapter.

2.2 Data sets

The data used in this study are based on a previous study focusing on long-term polar low frequency (Zahn and von Storch, 2008b) by numerically downscaling the NCEP/NCAR re-analyses (Kalnay et al. 1996). The downscaling was performed by means of a regional climate model called CLM (Steppeler et al. 2003) (now renamed to COSMO-CLM or CCLM, www.clm-community.eu) version 2.4.6 using spectral nudging (von Storch et al. 2000).

CCLM was developed on the basis of the Lokalmodell (LM) of the German Weather Service (DWD) (Steppeler et al. 2003, Rockel et al. 2008). Due to the requirement of convection weather simulations, DWD developed a new non-hydrostatic model − the LM, which served as weather forecast model. The LM model was also used for regional climate simulations. In 2002, CCLM was finished as the first climate version of the LM (CLM). The CCLM-Community was organized for international network of scientists to develop the CCLM systematically and cooperatively. CCLM was also used for future climate scenarios from 1960-2100 driven with the boundaries by ECHAM5 (Rockel et al. 2008). In 2007 the CLM and the LM were merged into the limited area model for weather forecast and regional climate modeling in the framework of the Consortium of Small Scale Modeling (COSMO-model). This new model for climate simulations is named COSMO-CLM or CCLM. It uses a hybrid coordinate system with 32 σ-levels with prognostic variables of temperatures, pressure, specific humidity, cloud liquid water content, and horizontal and vertical wind. Initial and boundary conditions are provided by the NCEP/NCAR re-analysis data with a horizontal

resolution of 2° (about 220 km) every 6 hour. The regional model is nudged at its boundary zone (sponge zone) every 6 hours (Davies 1976).

A number of studies investigated the ability and reliability of CCLM simulating extremes and climate changes. Böhm et al. (2004) developed a methodology to assess the performance of CLM for different meteorological fields. The authors concluded that the performance of CCLM is similar to another regional climate model REMO, a global climate model ECHAM4 and analyses from the European Centre for Medium-Range Weather Forecasts (ECMWF) in terms of near-surface temperature and precipitation. These results are also confirmed in a further study by Böhm et al. (2006) indicating that CCLM is able to reproduce the spatial patterns of the gridded reference data sets. CCLM was also used to study climate change over Europe (Déqué et al. 2005) and North Sea storm surge extremes (Woth et al. 2006). Zahn et al. (2008) applied CCLM for investigations of polar lows. In their study, three cases of polar low formation in the North Atlantic have been simulated by dynamically downscaling NCEP/NCAR reanalysis data using CCLM. The lateral boundary conditions used for spectral nudging (von Storch et al. 2000) was provided by the NCEP/NCAR re-analysis. Spectral nudging was applied to ensure a similar evolution of the large-scale circulation in the interior domain of CCLM and the driving NCEP reanalysis data. This is important as without constraint of spectral nudging, the observed polar lows can not be reproduced by CCLM. Spectral nudging procedure is particularly suitable for polar lows, which favors in providing more realistic upper level disturbances.

A dynamically downscaled long-term simulation with CCLM driven by the NCEP/NCAR reanalysis over the North Atlantic was carried out by Zahn and von Storch (2008b). Spectral nudging (von Storch et al. 2000) was also applied to constraint the RCM results to follow the large-scale situation given by the NCEP/NCAR reanalysis. The regional simulation was used to investigate long-term climatological characteristics of polar lows over the North Atlantic. The simulation covers the period between January1948 and February 2006. The data used in this study is taken from this simulation which investigated the long-term frequency of polar lows (Zahn and von Storch 2008b).

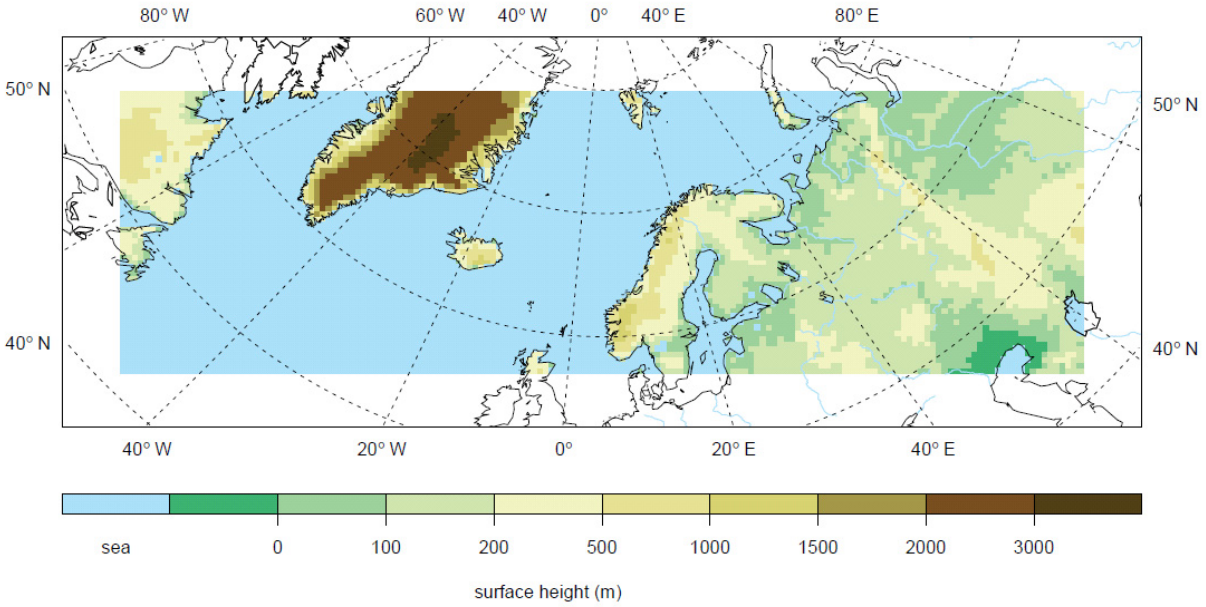

Fig. 2.1 Model domain used for the regional model simulation. White zone at the border represent the sponge zone.

2.3 Filter

Spatial filters provide ways to separate atmospheric fields based on the definition of certain wave number ranges. There are several methods to employ spatial filtering, for instance Fourier filtering, the discrete cosine transform, and digital filters. The different methods show different performances and usability depending on the application. The discrete cosine-filter method has advantages in describing spatial trends but suffers from artificial wavy contributions (Denis et al. 2002). Digital filters operate within a finite base and can be constructed flexibly but have the disadvantage of being less effective in scale separation than Fourier filters (Shuman 1957, Shapiro 1975, Feser and von Storch 2005). Concerning the frequency characteristics the applied filter range determines the temporal and spatial features that will be identified. For a low-pass filter, the long waves will be retained, whereas a high-pass filter will remove contributions of long waves and short-wave systems will be conserved.

Spatial filters are often applied in the context of storm or cyclone identification to remove the influence of atmospheric large-scale circulation, i.e. the planetary waves (Hoskins and Hodges 2002, Anderson et al. 2003) or to select the spatial scales of interests, especially for tracking mesoscale and small-scale lows (Zahn and von Storch 2008a). To track polar lows, spatial filters are applied in a first step to extract mesoscale features from the full fields.

The tracking methods used in this study both contain spatial filters as pre-processing tools prior to the application of detection and tracking. Spatial bandpass filters are applied by both methods to separate mesoscale systems from mean sea level pressure (MSLP) fields. An important difference between the two methods is the implementation of different spatial filters. KH uses the discrete cosine transform (DCT) based on the discrete Fourier transform with a symmetrisation process (Denis et al. 2002). MZ uses a near-isotropic two-dimensional spatial digital filter (Feser and von Storch 2005). These two spatial filter methods for polar lows are compared in this section.

2.3.1 Digital filter

Polar lows are mesoscale systems with horizontal scales of up to 1000 km. Accordingly, a bandpass filter as preprocessing tool is applied before the actual tracking. A near-isotropic two-dimensional spatial digital filter, developed by Feser and von Storch (2005), was used in the MZ tracking scheme. The same configuration as presented by Zahn et al. (2008a) is employed to detect polar lows with higher accuracy. Wave numbers from 6 to 15 are chosen, i.e. scales smaller than ~ 200 km and larger than ~ 600 km are removed by the spatial filtering algorithm.

Before applying the digital bandpass filter, the non-linear trends which spatial trends could disturb the filtering process were subtracted from the full fields (Feser and von Storch 2005). The filter array should be symmetrical in the zonal and meridional directions requiring the introduction of a sponge zone. The filter weights for the spatial bandpass filter are shown in Figure 2.2 indicating that the smaller structures are conserved while a large mean value will be filtered out.

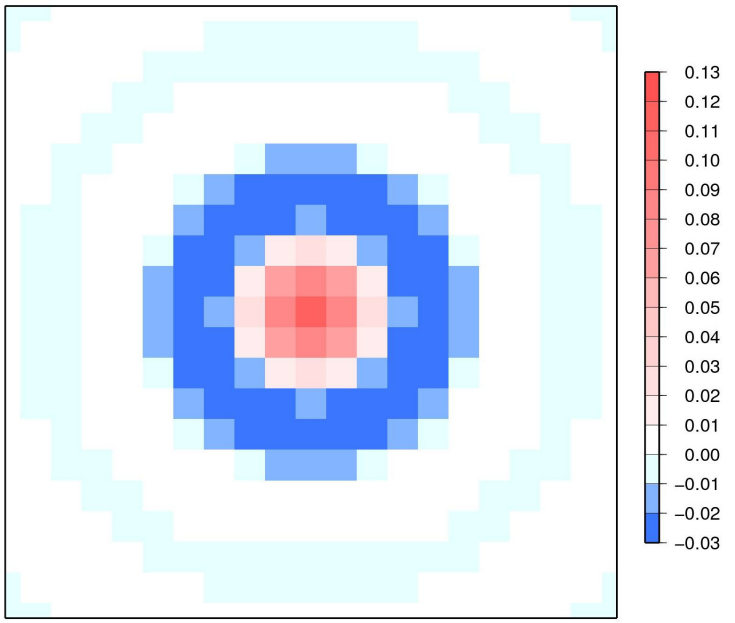

Fig. 2.2 Filter weights for the spatial bandpass filter. Filters were chosen with N=10 points, so the spatial extension is (2N+1) × (2N+1) = 21×21 points.

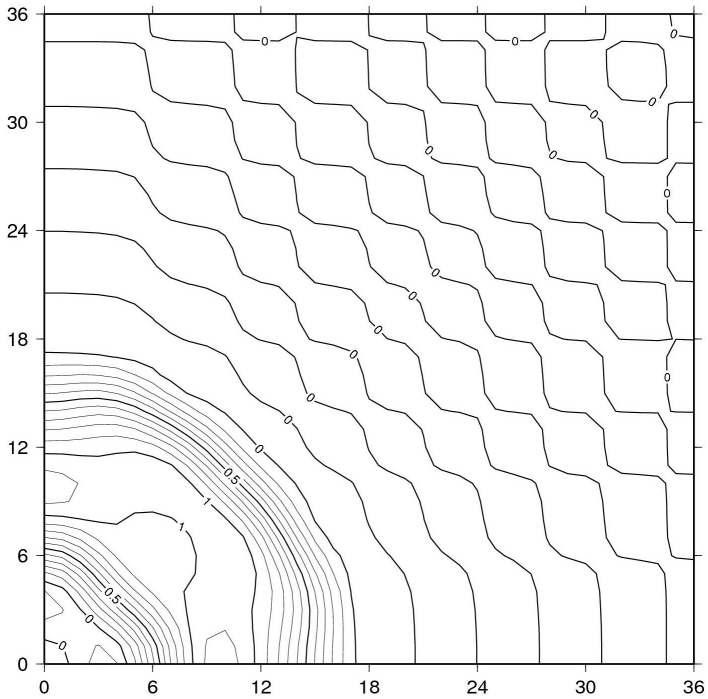

Fig. 2.3 Response function for the bandpass filters with the filter weights of Fig. 2.2. The axes are the zonal wavenumbers k (x axis) and the meridional wavenumbers l (y axis).

The periodical function is expanded into Fourier components and a response function is given by the ratio of Fourier coefficients between the filtered function and the original function (Feser and von Storch 2005). Figure 2.3 shows the response function accounting for the application of the filter weights. The response function shows a smooth transition area to response values from 0 to 1 according to the wavenumber ranges. The wavenumber ranges are defined as follows for the bandpass filter:

$$\kappa(k^*) = 0 \quad \text{for all } k^* \leq 6,$$

$$\kappa(k^*) = 0 \quad \text{for all } k^* \geq 15.$$

A polar low which is called Le Cygne (the swan) developed early on 14 October 1993 mainly because of baroclinic instability over the Barents Sea, then moved equator ward along the Norwegian coast and disappeared after landfall in southern Norway on 16 October 1993 (Grønås and Kvamstø 1995, Zahn et al. 2008). From the satellite image at 1529 UTC 14 October (Figure 2.4), this polar low initially displayed a distinct comma cloud signature and the developing disturbance resembles a swan figure in the cloud fields over the Norwegian Sea (Claud et al. 2004). Due to its silhouette it was therefore named after a swan.

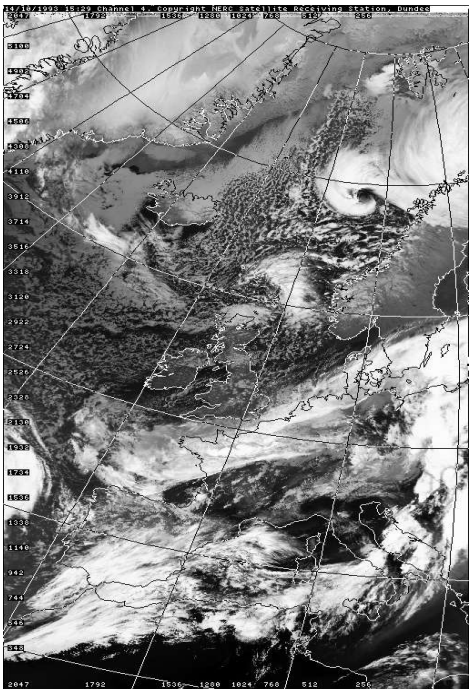

Fig. 2.4 NOAA11/AVHRR channel 4 thermal infrared for 1529 UTC 14 October 1993 (from http://www.sat.dundee.ac.uk/)

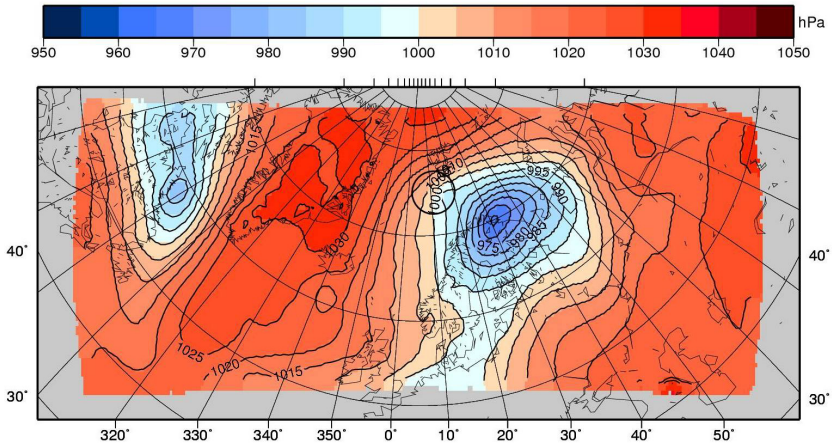

Fig. 2.5 Unfiltered MSLP field on 06:00 14 October 1993 (hPa)

Figure 2.5 shows the "Le Cygne" genesis stage as a trough around 72 N, 5-10 E at 06 UTC 14 October within the CCLM simulation (marked with a circle in Figure 2.5). It is located in the proximity of a synoptic low in the north of Scandinavia. The low caused the outbreak of cold air leading to baroclinic instability caused by temperature differences between the sea surface and the lower air troposphere. In the following hours it intensified due to an intensified air-sea interaction process (Zahn et al. 2008). However, the genesis stage of Le Cygne is still not so obvious and distinguished from the synoptic low (Figure 2.5), even with the higher resolved 50 km CCLM simulation. Therefore, a digital bandpass filter is applied to extract the disturbance in the genesis process of the polar low.

Figure 2.6 a and b show the filtered MSLP field at 06 UTC with the digital filter of Feser and von Storch (2005), which is used by MZ, for 14 October 1993. Accordingly, the mesoscale disturbances become more distinct after bandpass filtering. The initial stage of Le Cygne, which is not easy to identify in the unfiltered data, becomes more obvious in the filtered fields (cf. circle in Figure 2.6). For the digital filter, there is a margin around the model domain with values of 0, as the digital filter needs data in a symmetric neighbourhood around a point to be filtered (Feser and von Storch 2005).

The digitally filtered MSLP field displayed in Figure 2.6a shows distinct mesoscale systems but still has a similar pattern to the unfiltered MSLP field (Figure 2.5). The reason for this

phenomenon relates to the response function of the digital filter being smooth opposed to a step function employed in a Fourier filter (Feser and von Storch 2005). This means for the digital filter there is no exact cut-off at a certain wave number and it will thus retain some long-wave parts in the vicinity of the selected band boundaries. To decrease the influences of the large scales, the monthly mean fields of MSLP were subtracted prior to subtracting the quadratic polynomials. This process weakens the influences of the large scales in specific areas as shown in Figure 2.6b. Moreover, it helps to solve this drawback of the digital filter although it does not completely remove the large-scale background. Therefore, in the following, both, the monthly mean fields of MSLP and the quadratic polynomials related to spatial trends are subtracted before filtering.

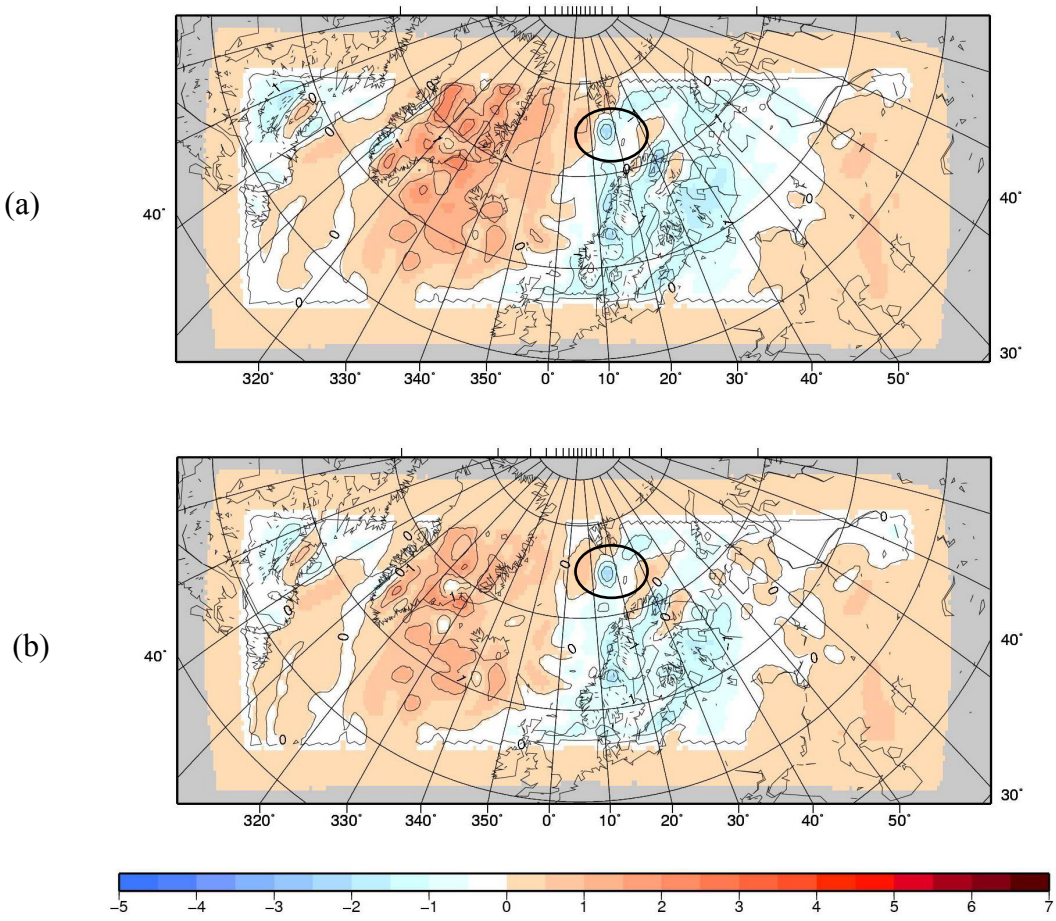

Fig. 2.6 Bandpass filtered MSLP fields by digital filter on 06:00 14 October 1993 (hPa): (a) only subtracting the quadratic polynomials before filtering; (b) monthly mean fields of MSLP were subtracted before subtracting the quadratic polynomials.

2.3.2 Discrete cosine transform (DCT)

The Fourier filter has the advantage in scale separation. However, when the filter is applied over a limited area, it shows some problems within trend-contaminated time series, by artificially adding wave contributions (Denis et al. 2002, Feser and von Storch 2005). This results in the destruction of the normal spectrum and leads to distortion. DCT based on the discrete Fourier transform with a symmetrisation process (Denis et al. 2002) reduces this feature, but does not allow for full elimination. This process will be implemented by using the original function as a mirror image before applying the Fourier transform. Then this special Fourier transform is called the discrete cosine transform (DCT), employed as filter procedure in KH to differentiate scale systems.

KH's filter was originally not designed to track polar lows but to track synoptic scale cyclones (Hodges 1994, 1995, and 1999). For comparison studies, it is reconfigured in accordance to the dynamics of polar lows. Therefore the same filter range of 200–600 km is used with the DCT to filter MSLP.

Figure 2.7 shows the filtered MSLP field by DCT on 06 UTC 14 October 1993. The initial turbulence of Le Cygne can also be extracted by DCT. The pattern based on DCT clearly differs from the pattern using the digital filter (Figure 2.6). The different structure compared to the unfiltered field is also clearly visible (Figure 2.5). Compared to the digital filter, DCT therefore removes the large-scale systems more effectively. As outlined above, the digital filter is less exact in wave number selection than DCT due to the response function.

The digital filter and DCT are also applied to the 850 hPa vorticity field. The filtered patterns are much more similar for both filters than MSLP as shown in Figure 2.8. This is because the large-scale background for vorticity is much weaker compared to MSLP. The MSLP is more influenced by large-scale systems, and even a small portion of large scales retained will affect the filter results greatly. Accordingly, the DCT is more effective in an exact scale selection than the digital filter and it is thus more suitable for MSLP. However, when applying the digital filter and DCT onto the vorticity fields, there is no obvious difference between the two different filter methods.

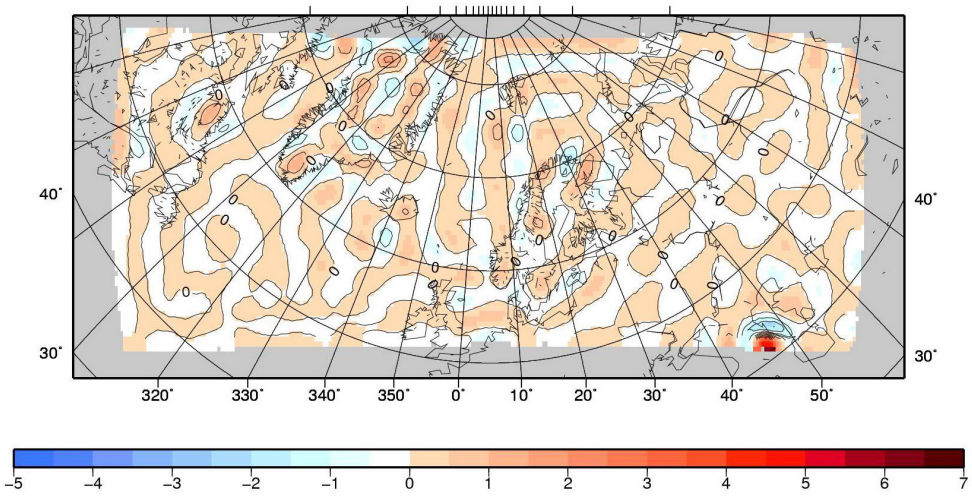

Fig. 2.7 Bandpass filtered MSLP field by DCT on 06:00 14 October 1993 (hPa)

(a)

(b)

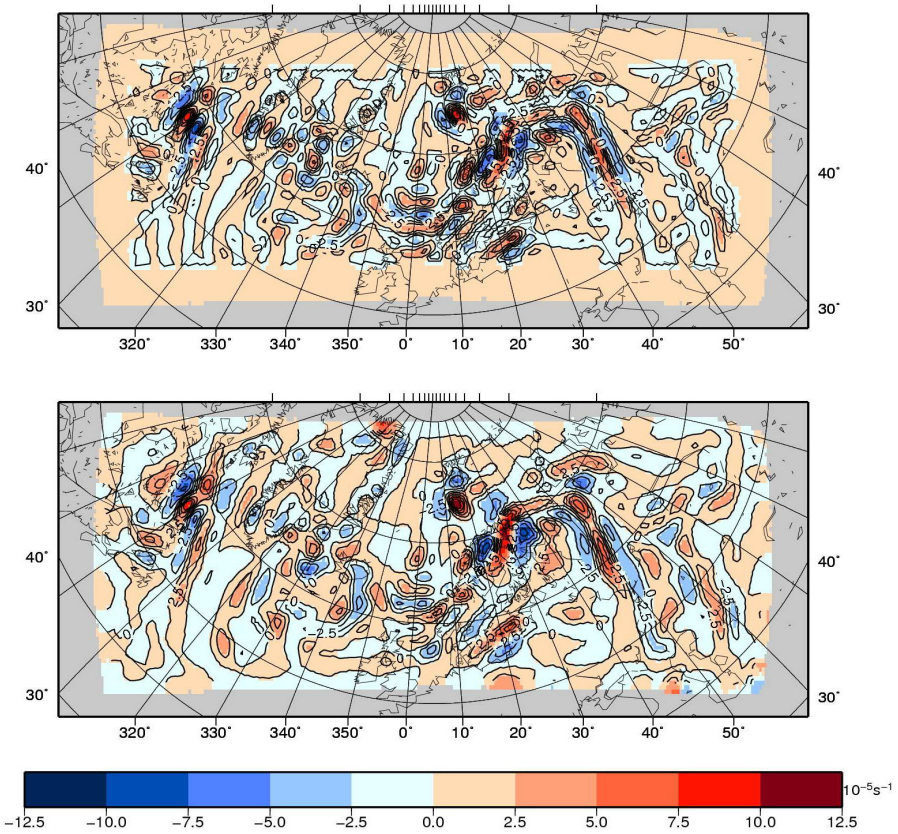

Fig. 2.8 Bandpass filtered 850hPa relative vorticity fields on 06:00 14th October 1993 ($10^{-5}s^{-1}$): (a) digital filter, (b) DCT.

2.4 Detection

The detection part of the tracking scheme records all positions of minima or maxima in the filtered output fields below or above pre-defined thresholds. Here MSLP was used for both methods. A threshold value of the bandpass-filtered MSLP smaller than -1hPa was chosen.

The MZ method was designed to detect minima located exactly on the model grid points. The gradient from the cyclone center has to be larger than 0.3 hPa/100km. Minima over land are excluded. The KH method in a first step separates fields into distinct regions by connected component labelling (CCL). In a second step, the method detects extremes in each region (Hodges 1994, 1995). KH finds minima that are located between grid points by using B-spline interpolation (Dierckx 1981) and steepest ascent maximization. This procedure results in smoother tracks.

Figure 2.9 shows the detection results by the MZ and KH methods based on bandpass filtered MSLP fields for digital filter and DCT, respectively. The green points in Figure 2.9a and b are the detected minima using the MZ method, red squares are the detected minima using the KH method. As a case study the polar low called Le Cygne (the swan) is analysed. The genesis disturbance on 06 UTC 14 October 1993 is not so visible within the unfiltered MSLP fields (Figure 2.5), but it becomes more obvious and detectable by applying the MZ and KH methods (marked with a circle in Fig. 2.9a and b). For the digital-filtered field, a margin around the model domain with values of 0 results, as the digital filter needs data in a symmetric neighborhood around a point to be filtered (Feser and von Storch 2005). For comparison purposes this margin zone was removed for the DCT-filtered fields when the KH method detects the minima (Figure 2.9b).

As discussed in Section 2.3, there are large differences between both filtered fields. Most important, the differences between the two fields produced by the two different filtering methods lead to differences in the numbers and detected locations of the minima. Most of the green points almost coincide with red squares for both filtered fields but some minima over land are only detected by the KH method. As previously mentioned this is because the MZ method was specifically designed for tracking polar lows. Usually polar lows are generated over the ocean. Accordingly, the MZ method just detects minima over oceanic areas and excludes the minima over land. Still the minima detected by the MZ method (green points in Figure 2.9a and b) are much fewer than those detected by the KH method (red squares in

Figure 2.9a and b). It was already noted that the MZ detection part uses a gradient criterion to exclude systems with a weak pressure gradient. This compares the surrounding grid points and keeps those minima, which fulfill the gradient criterion of 0.3 hPa/100 km. Applying this criterion to the filtered fields also leads to fewer minima for the MZ method.

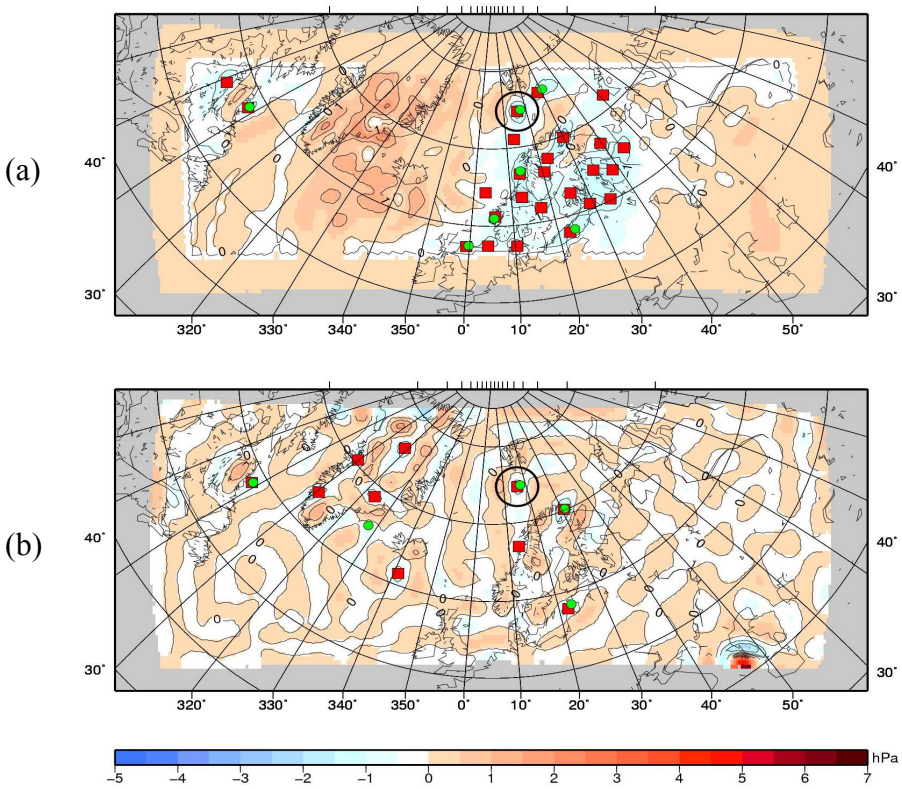

Fig. 2.9 Bandpass filtered MSLP fields on 06:00 14th October 1993 (hPa): (a) digital filter, (b) DCT, and detected minima: red by KH and green by MZ with a gradient criterion of 0.3 hPa/100 km.

To establish a common basis for comparisons between the two methods in this study, the gradient criterion is set to 0.0 hPa/100 km in the MZ detection part. The detection results are shown in Figure 2.10a and b. Using the new criterion results in larger numbers of minima detected by the MZ method. And there is a better correspondence between the points detected by both methods results from the data being at such a high resolution. However, comparing Figure 2.10a and b the detected minima differ greatly based on different filter procedures applied. Therefore it can be concluded that the detection differences stem mainly from the different filter patterns related to the digital filter and DCT, respectively. Although the detection parts of MZ and KH also lead to changes in detected extremes, the detection related differences are less important compared to the filters related differences, especially when the gradient criterion of MZ is set to 0.0 hPa/100 km.

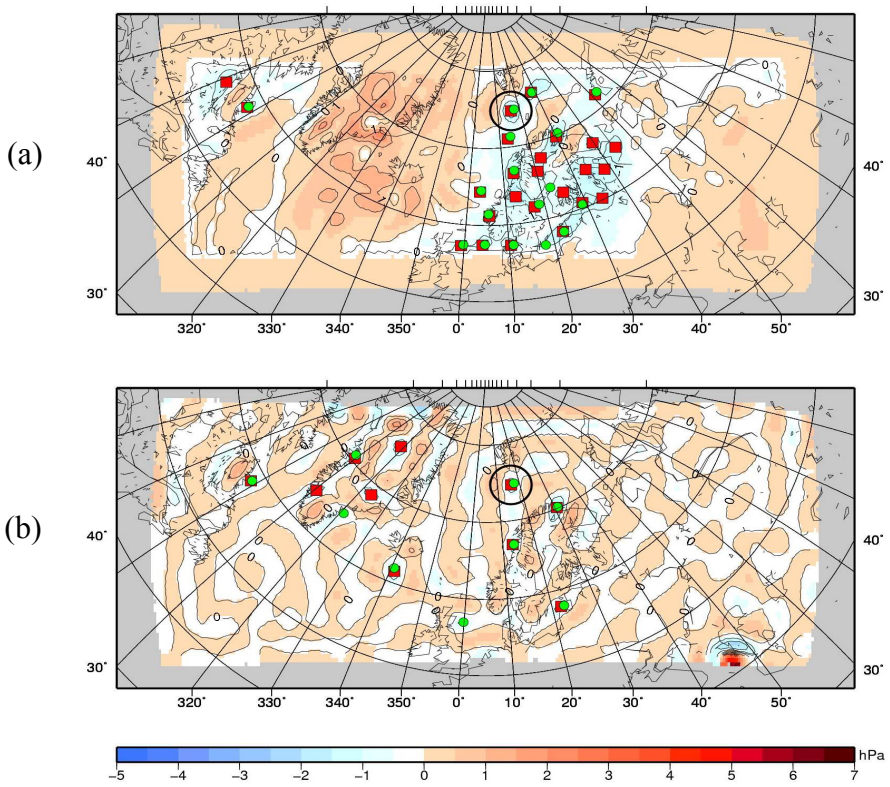

Fig. 2.10: Bandpass filtered MSLP fields on 06:00 14th October 1993 (hPa): (a) digital filter, (b) DCT, and detected minima: red by KH and green by MZ with a gradient criterion of 0.0 hPa/100 km.

2.5 Tracking

The next step is to link the detected positions to form tracks. In KH method the tracks are initialized based on a nearest neighbour method by linking the points in consecutive time steps which in this study are 3 hours apart (3h) if their horizontal distance is less than 2° (about 222 km). A cost function is constructed to measure the track smoothness which is determined over three consecutive time steps and summed along the tracks (Hodges 1994, 1999). In order to gain the smoothest tracks, the cost function is minimized subject to constraints on displacement and track smoothness. The smoothness constraints are applied adaptively so that the constraint is less stringent if the system moves slowly and stricter if the system moves fast (Hodges, 1999). This minimization process iterates with direction forward and backward in time to ensure that all points of a track fulfil the minimum of the smoothness function.

For MZ, the maximum travel distance for a vortex in a time step is considered to be smaller than 200 km. If more than one position is detected for the next time step, and they all fulfil the maximum distance requirement, the closest one to the current track is selected. In this study,

the tracks have to last at least one day (8 time steps) to be retained. This is a post-tracking filter on the lifetimes. Further differences of tracking procedures of MZ and KH are investigated below.

2.6 Comparison of two methods

As discussed above, different settings in the detection can lead to large differences in track numbers between the KH and MZ tracking schemes. In MZ within the original detection part the gradient from the cyclone centre being larger than 0.3hPa/100km is required, whereas the KH method does not employ the gradient requirement. The existence of the gradient constraint in MZ definitely leads to fewer extremes as shown Figure 2.9 and Figure 2.10 of Section 2.4 and hence fewer tracks. According to Table 2.1, without gradient criterion (0.0 hPa/100km) the application of MZ results in 1421 tracks, opposed to 483 tracks with a gradient criterion of 0.3 hPa/100km.

Table 2.1: Comparison between different cyclone gradient criterions applied to tracking scheme of MZ.

	filter	*detection*	*tracking*	*0.3 hPa/100km*	*0.0 hPa/100km*
7	**MZ**	**MZ**	**MZ**	**483**	**1421**

Another implication is that the KH method in contrast to the MZ method also includes tracks over land areas. Therefore the KH method results in larger numbers of tracks (cf. Table 2.2). In order to make the two methods suitable for comparison, we excluded the tracks of KH over land areas.

Table 2.2: Comparison between the classical KH method including all grid points and the method with land area excluded from analysis.

	filter	*detection*	*tracking*		*no land*
1	**KH**	**KH**	**KH**	**2575**	**856**

In this part we show how different parts of the whole tracking set-up influence the tracking results by comparing different combinations of the KH and MZ methods. Table 2.3 shows the number of tracks obtained for different combinations of filter, detection and tracking parts of

the MZ and KH methods. All the numbers shown in Table 2.3 are based on MSLP fields from October 1993 to September 1995. Several combinations of filter, detection, and tracking parts were tested with changing settings for these individual parts according to both MZ's and KH's methods. For example, combination 1 is the original KH method with DCT filter. Combination 3 is the KH method but based on the digital filter which is used in the MZ method. The MZ method is also applied on DCT realized as combination 5. Other combinations are also tested, for example the KH method using MZ's tracking part (combination 2), the KH method using MZ's detection part (combination 6), and the MZ method using KH detection part (combination 4) and KH tracking part (combination 8). Employing this strategy allow us to disentangle how each part leads to the differences between the two methods.

Analyzing the track numbers in Table 2.3 for different combinations of filtering, detection and tracking indicates a large spread of the results. However, it should be noted that using the same filter and tracking parts, track numbers are more similar when either using KH's detection or MZ's detection. The largest difference is between combinations 1 and 6 (number difference=155) and the smallest difference between combinations 4 and 7 (number difference=21). Figure 2.11 shows the tracks in October 1993 based on the original MZ's tracking scheme (combination 7) and the same scheme for filter and tracking but using KH's detection part (combination 4). According to Figure 2.11 both combinations show a high degree of similarity. Based on the discussion of the detection part of both methods in Section 3.3, we already know that the detection part of both methods leads to small differences using a gradient of 0.0 hPa/100km in the MZ method. Due to the exclusion of tracks over land in the KH's method track numbers and tracks are quite similar to MZ.

Table 2.3: Numbers of tracks resulting from different combinations between MZ and KH tracking schemes (for 2 year test period: October 1993– September 1995).

	filter	detection	tracking	numbers of tracks
1	KH	KH	KH	856
2	KH	KH	MZ	833
3	MZ	KH	KH	1509
4	MZ	KH	MZ	1400
5	KH	MZ	MZ	819
6	KH	MZ	KH	971
7	MZ	MZ	MZ	1421
8	MZ	MZ	KH	1570

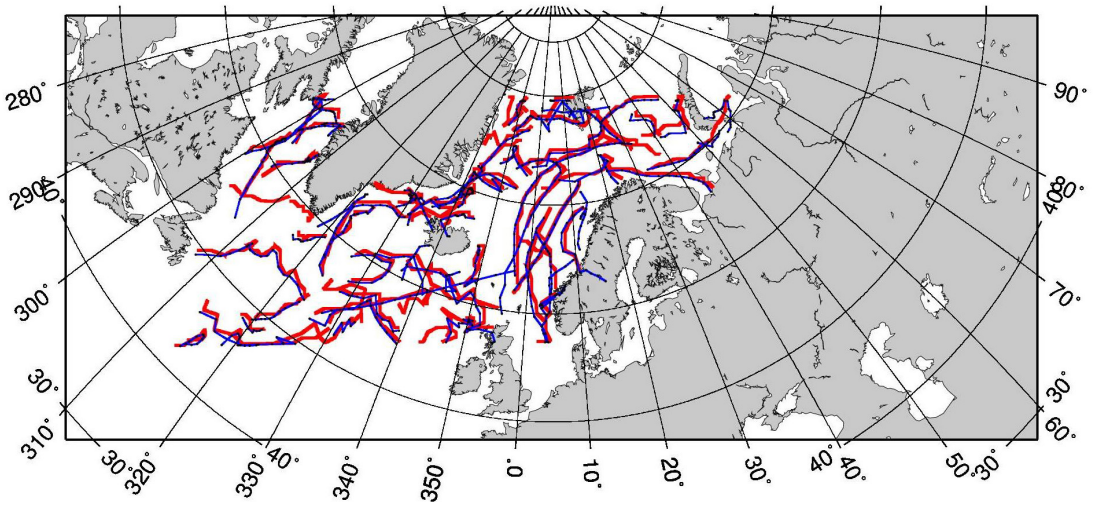

Fig. 2.11 Tracks in October 1993 for combination 4 (blue with points) and combination 7 (red) of Table 2.3.

Given the filter and detection parts are the same, the track numbers are also similar between KH's tracking and MZ's tracking scheme: here the largest difference can be seen between combinations 5 and 6 (number difference=152) and the smallest difference between combinations 1 and 2 (number difference=23, cf. Table 2.3). Figure 2.12 shows the tracks in October 1993 for combination 1 and combination 2 outlined in Table 2.3, which are only different in the tracking part. The comparison shows a high degree of similarity between the two combinations.

In the KH tracking part, adaptive tracking constraints are applied to allow for a more flexible tracking. The tracking constraints are adaptive and vary according to the travel velocity of different synoptic systems. For instance, for slow moving system a less restrictive track smoothness constraint is required, whereas a more restrictive constraint is required for fast moving systems. Based on meteorological reasoning these tracking constraints could demand more restrictive track smooth constraints for extratropical cyclones than for tropical cyclones. The cost function based on each of the three steps of tracks is minimized according to adaptive smooth constraints. Tracks are split if the constraints are not fulfilled. This process iterates both forward and backward in time of a track to ensure that all points fulfil the minimum of cost function. From table 2.3 you can see that numbers of combination 1 (856) and 2 (833) are very similar. Moreover, also the tracks in October 1993 for combination 1 and 2 do not differ from tracks to a large extent (Figure 2.12). Therefore some different technical

settings in the KH's and MZ's tracking part actually do not lead to large differences on track numbers and track paths.

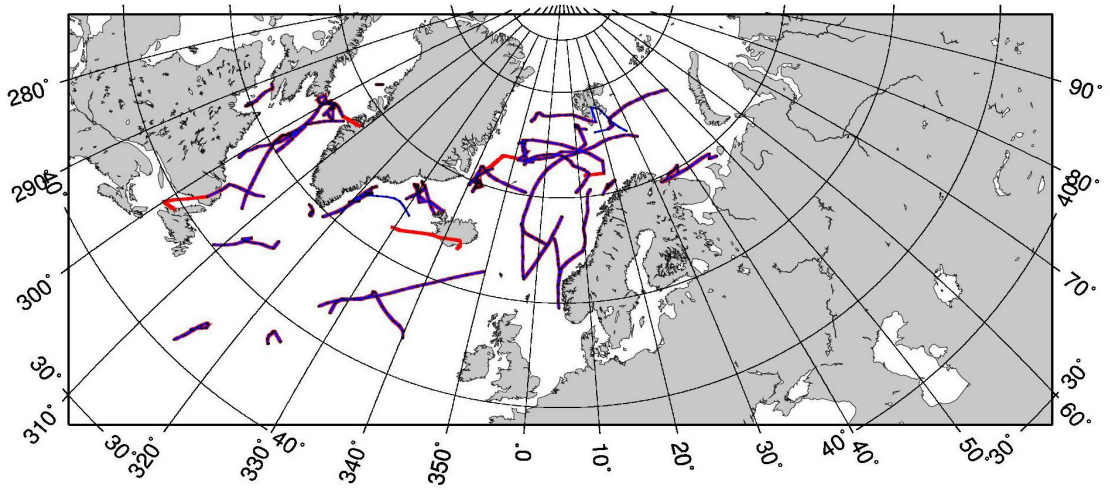

Fig. 2.12 Tracks in October 1993 for combination 1 (red) and combination 2 (blue with points) of Table 2.3.

In contrast to the detection and tracking parts, the changes in the filter parts lead to larger differences in track numbers. The digital filter used in MZ leads to a larger number of detected tracks than the DCT filter of KH: the largest difference is 653 between combinations 1 and 3, whereas the smallest difference is 567 between combinations 2 and 4 (Tale 2.3). Figure 2.13 shows the tracks in October 1993 by the MZ method based on the DCT (combination 5: blue with points) and the digital filter (combination 7: red). According to Table 2.3 and Figure 2.13 the number of tracks based on the DCT is considerably lower compared to the digital filter. Moreover, only a small number of red tracks based the digital filter overlap with the blue tracks (Figure 2.13). As discussed in the Section 2.3 and Section 2.4, the DCT and digital filter result in different filtered MSLP patterns. More minima are detected based on the digital-filtered fields (Figure 2.10a and b), leading to more detected tracks. Therefore different filters result in large variations of track numbers even using the same tracking method.

In this section, different combinations of filter, detection and tracking parts in two methods are used to investigate the differences between the two methods. A gradient of 0.0 hPa/100km was chosen for the MZ method and tracks over land were dismissed in KH to establish a common basis for comparison. The results show that the detection and tracking parts do not lead to pronounced differences between MZ and KH in contrast to the filter applied. The

differences are obviously not only related to track numbers but also to track paths. This is because the filtered-fields by the DCT and digital filter result in various minima and definitely influence the track numbers and tracks. However, not all of these tracks are necessarily polar lows.

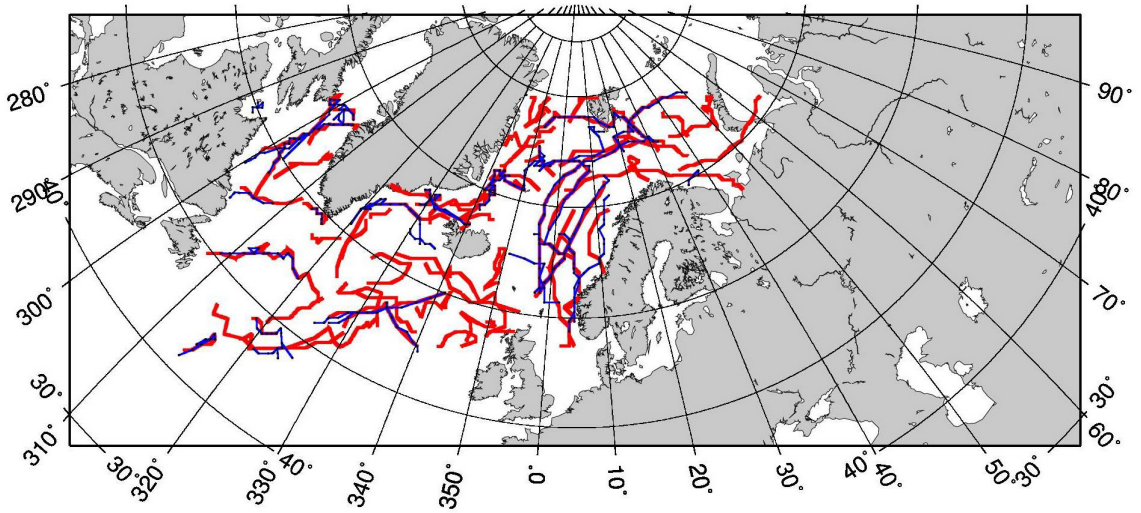

Fig. 2.13 Tracks in October 1993 for combination 5 (blue with points) and combination 7 (red) of Table 2.3.

2.7 Track-to-track comparison

In order to identify common tracks between the different combinations a simple track-to-track comparison algorithm was applied. When the points of two tracks correspond to the same time, then the distances between these points on a great circle are calculated. The algorithm defines common tracks as two tracks (with points corresponding to the same times) which overlap for more than 60% of their points with mean separation distance of less than 3 degrees and a closest distance of less than 100 km occurring at least once. Different threshold criteria can be applied. For instance, less stringent requirements for distance and percentage of overlapped points can definitely lead to more common tracks. The thresholds for common tracks used here are relatively restrictive and conservative. Figure 2.14 shows the common tracks of the MZ method applied to data derived from the different filters for October 1993: red lines are tracks of MZ using the digital filter (combination 7) and the blue ones are for MZ with the DCT filter (combination 5).

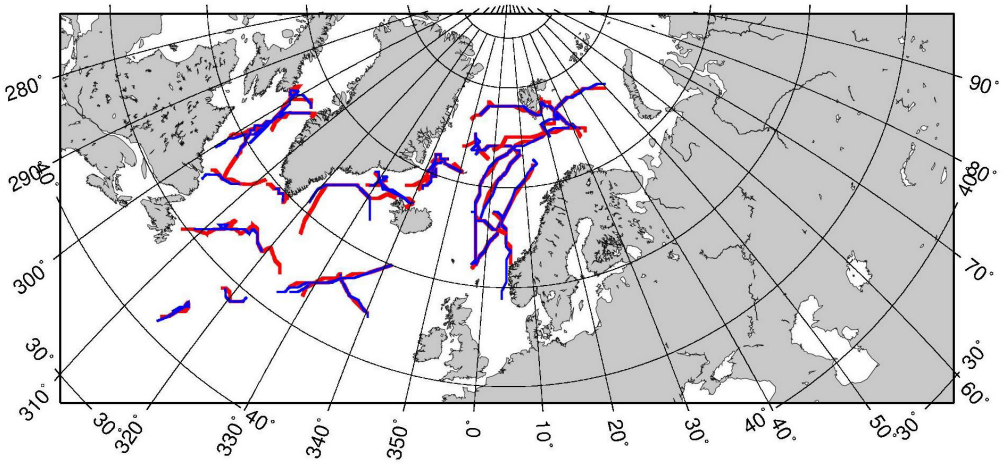

Fig. 2.14: Overlapping tracks in October 1993 for combination 5 (blue) and combination 7 (red) of Table 2.3.

A quantitative measure of the matched and non-matched tracks is provided by the probability of track overlap. The probability P_o of the overlap between two sets of tracks is defined as:

$$p_o = \frac{2N_o}{(N_1 + N_2)}.$$

Where N_1 and N_2 are the numbers of tracks in the two different combinations, N_o is the number of common tracks between the two track sets. P_o=0 indicates the two sets of tracks are completely different and P_o=1 that the same tracks are present in both sets.

The second probability that can be determined is P_m, the probability of non-overlapping tracks and is defined as:

$$p_m = \frac{(N_1 + N_2 - 2N_o)}{(N_1 + N_2)},$$

where P_m >0 indicates that there is no perfect match between the two track sets. Table 2.4 shows the probability of common tracks based on comparing different combinations with combination 1, the original KH method as reference. Table 2.5 is the same with combination 7, the original MZ method as reference.

Table 2.4: Number N_o of overlapping tracks, probability P_o for overlapping tracks and ratio P_m of non-overlapping tracks for different combinations using combination 1 as reference (for combination 1−8 refer to Table 2.3).

	1	2	3	4	5	6	7	8
N_o	856	768	385	387	608	713	372	380
P_o	1.00	0.91	0.33	0.34	0.73	0.78	0.33	0.31
P_m	0.00	0.09	0.67	0.66	0.27	0.22	0.67	0.69

Table 2.5: Number N_o of overlapping tracks, probability P_o for overlapping tracks and ratio P_m of non-overlapping tracks for different combinations using combination 7 as reference (for combination 1−8 refer to Table 2.3).

	1	2	3	4	5	6	7	8
N_o	372	377	989	1025	401	416	1421	1247
P_o	0.33	0.33	0.68	0.73	0.36	0.35	1.00	0.83
P_m	0.67	0.67	0.32	0.27	0.64	0.65	0.00	0.17

The highest P_o with combination 1 is combination 2, with more than 90% of common tracks. The only difference between combination 1 and 2 is the tracking part. The highest P_o with combination 7 is combination 8, with 83% of the common tracks. Here the only difference is also related to the tracking part. The tracking parts of both methods lead to similar numbers and a large number of common tracks. It confirms again that KH's and MZ's tracking part actually do not lead to large differences of track numbers and track paths.

The second highest P_o with combination 1 is combination 6 and with combination 7 is combination 4. Here the difference in the methods relates to the detection part. The detection part of MZ with a gradient setting of 0.0 hPa/100km is similar to that of KH and leads to a small difference and also to a large number of common tracks. This confirms the analysis given above, that the detection and tracking parts are not the main reasons for the differences.

It is notable that in Table 2.4 the combinations based on the DCT filter such as combination 1 show slightly higher probabilities P_o (over 70%), such as combinations 2, 5 and 6, whereas

combinations with the digital filter (combination 3, 4, 7 and 8) find only about 30% tracks to overlap with combination 1. Similar results are also found in Table 2.5. Combinations based on the digital filter such as combination 7 also show relatively high probabilities P_o, such as combination 3, 4 and 8. Other combinations with DCT indicate relatively low probabilities P_o, like combination 1, 2, 5 and 6. This analysis proves again that different filters lead to differences not only in track numbers but also in track paths. The underlying reason is that different filtered patterns differ in their detected minima, eventually influencing the track numbers and track paths.

2.8 Tracks of potential polar lows

After connecting the minima to form tracks, the numbers of detected tracks are still too high and not all are related to polar lows. To identify polar lows further criteria are required. Therefore in this section we apply further criteria as presented in Zahn and von Storch (2008a) to pick out potential polar lows. The criteria that have to be fulfilled are as follows:

1) Filtered MSLP should be below -2 hPa at least once along a track. Polar lows are strong mesoscale cyclones. This criterion therefore excludes weak cyclones and only retains the stronger ones. The threshold of -2 hPa has been chosen based on polar low case studies (Zahn et al., 2008). All three studied polar lows in their study are below this value. In the following the term “Filtered minimum” is used as acronym for this criterion.

2) The maximum 10m wind speed within a distance of 100 km around the storm center has to be larger than 13.9 m/s at least for 20% of the positions. Polar lows are connected with strong surface wind speeds. The acceptable definition for mesoscale cyclones to be denoted “polar low”, requires 10m wind speeds near or above gales of 13.9 m/s (Rasmussen and Turner 2003, Zahn et al. 2008). In the following the acronym “wind speed” is used for this criterion.

3) The temperature difference between the sea surface temperature (SST) and the 500 hPa temperature (T_{500}) must exceed 43°C at least once along the track. In general polar lows are thermal instability systems. In a convectively triggered atmosphere, the temperature is colder in the high levels than in the low levels. The threshold chosen follows the favourable developing conditions for polar lows suggested by the Norwegian Meteorological Institute (Noer and Ovhed 2003). The acronym “vst” is used for this constraint in the following.

4) The detected tracks taking paths along coastal grid boxes for more than 50% of their time are discarded. Zahn et al. (2008) suggested that the filtering procedure can be influenced by mountainous orography along coastlines and there might be some "artificial" polar lows induced over regions with complex terrain. To avoid detecting these "artificial" disturbances, this constraint is applied. The acronym "no land" is used for this criterion.

5) It requires a southward moving track, i.e. the first detected position has to be about 100 km farther north than the last. Polar lows typically occur with cold air outbreaks and mostly take a southward path. However, it should be noted that some possible polar lows in the Labrador Sea or in the east Greenland might be wrongly excluded by this criterion (Zahn and von Storch 2008a). For this criterion the acronyms "NS" is used.

6) If the filtered MSLP falls below -6 hPa at least once along the track and criterion 4) is fulfilled, the system will also be regarded as a polar low track. Otherwise it should fulfil all five criteria given above. The -6 hPa criterion assumes a very strong mesoscale disturbance and hence overrides other criteria. This criterion is similar to the operational cyclone detection, and the acronyms "supmin" is used to stand for this criterion in the following.

Practically these criteria can be applied individually and the respective thresholds can be changed. These are applied in an additive way to tracks which result from applying the MZ and KH methods. Table 2.6 shows the selection results based on combinations 1, 3, 5 and 7 of Table 2.3.

After applying the polar low identification criteria, the numbers of tracks identified by the KH and MZ methods mostly differ because of the use of different filters. The KH method based on the DCT results in 84 potential polar lows and based on the digital filter in 135 potential polar lows. The MZ method based on the DCT filter and the digital filter results in 79 and 127 potential polar lows, respectively. Therefore a larger number of tracks are retained for the digital filter than for the DCT filter. However, for the same filter, the numbers of tracks are much closer even for different detection and tracking methods. From a meteorological point of view different mesoscale systems are retained by the DCT filter and the digital filter. As a consequence, variables such as filtered wind speed, temperature or MSLP, used to describe the various mesoscale systems, also differ. These differences eventually lead to the varying track numbers after applying further criteria.

Table 2.6: Numbers of retained potential polar lows after applying the respective criteria in October 1993 – September 1995 ("noland" excludes tracks over land area [criterion 4]; "filtered minimum" means that filtered MSLP should be below -2 hPa at least once along a track [criterion 1]; "wind speed" means that the maximum 10m wind speed around the storm center has to be larger than 13.9 m/s at least for 20% of the positions [criterion 2]; "vst" means that vertical instability should be fulfilled [criterion 3]; "NS" requires the tracks to travel from north to south [criterion 5]; "supmin" means that the filtered MSLP falls below -6 hPa at least once along the track and "noland" is also fulfilled [criterion 6]. "Sum" is the final number of retained potential polar lows.)

	noland	filtered minimum	wind speed	vst	NS	supmin	sum
1	856	533	508	231	81	3	84
3	1509	818	744	352	127	8	135
5	819	442	419	186	78	1	79
7	1421	738	680	303	120	7	127

The incremental implementation of the polar low identification criteria has the following impact on the number of systems: The "filtered minimum" constraint dismisses 38% and 46% of all tracks from combinations 1 and 3 (Table 2.6) which use the detection and tracking of KH but employ the DCT and digital filters and returns 533 and 818 tracks, respectively. For the MZ detection and tracking applied to the DCT and digital filters this constraint dismisses 46% and 48% of all tracks, as shown in Table 2.6 for combinations 5 and 7.

The vertical stability (vst) criterion dismisses 55% and 53% of the tracks for the KH detection and tracking using the DCT and the digital filter, respectively. For the MZ method, it dismisses 56% of all tracks using the DCT and 55% when using the digital filter. This criterion is a stronger criterion than the previous two and can dismiss over half of the tracks resulting from both methods.

The strongest constraint is the directional criterion which requires the tracks to go from north to south (by the acronym "NS"). It dismisses 65%, 64%, 58% and 60% of the tracks, respectively, for combinations 1, 3, 5 and 7 in Table 2.6. As mentioned before, this criterion is very subjective and could dismiss potential polar lows wrongly. The "wind speed" criterion reduces the numbers by 5%, 9%, 5% and 8% of the tracks for each combination in Table 2.6.

The last criterion of "supmin" means that the filtered MSLP minima falls below -6hPa at least once along the track and that the "no land" criterion is fulfilled. Even if all other criteria are not fulfilled and this criterion is fulfilled then the track is considered as a polar low. Table 2.6 shows that for the DCT filter and the KH detection and tracking parts there are 3 tracks fulfilling the "supmin" criterion and there is 1 track for the MZ detection and tracking which fulfil this criterion. Using the digital filter there are 8 tracks for the KH method and 7 tracks for the MZ method that fulfil this criterion. However, this criterion highly depends on the filter method applied, with the DCT filter retaining less deep low pressure systems than the digital filter.

For other combinations shown in Table 2.3 that use the same filter comparable numbers result, e.g. combination 2 returns 79 tracks of potential polar lows which is the same as combination 5, whilst combination 4 gives 124 tracks which is close to the numbers of combination 7.

Figure 2.15 shows as an example one month (October 1993) of tracks of potential polar lows after applying the polar low identification criteria to combination 1 (red) of KH and combination 7 (blue) of MZ. Combination 1 gives 3 tracks while combination 7 leads to 6 tracks. Three tracks are almost overlapping for both methods. One track of combination 7 which parallels the Norwegian coast over the Norwegian Sea overlaps partly with a track of combination 1 in the southern Norwegian Sea. The other two tracks generally overlap very well for both combinations. The track of Le Cygne which appeared south of Spitsbergen and decayed at the southern Norwegian coast is tracked well by both methods.

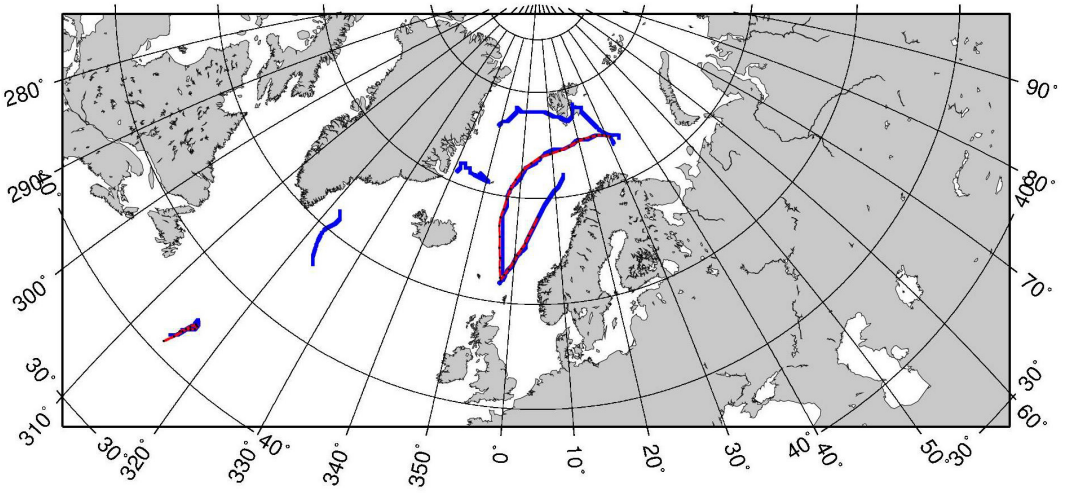

Fig. 2.15 Tracks of potential polar lows after applying criteria to combination 1 (red with points) of KH and combination 7 of MZ in October 1993 (blue)

It is notable that applying the criteria to pick out tracks of potential polar lows still retains the differences of numbers based on the DCT and digital filters. The “vst” and “NS” criteria are the most powerful constraints for both methods and can dismiss more than half of the remaining tracks.

2.9 Outcome

In this chapter two methods Zahn and von Storch’s method (2008a) (abbreviate as “MZ”) and Hodges’ algorithm (1994, 1995 and 1999) (abbreviate as “KH”) for tracking polar lows are compared. Two years of simulation data (October 1993 – September 1995) with relatively high resolution are used to compare the two method’s abilities to identify and track polar lows. Bandpass filters by the DCT and a digital filter are applied by two methods to select mesoscale systems to track polar lows. The detection parts of two methods based on the DCT and digital filter are compared. The detected minima vary mainly due to the different filter patterns. The setting of a gradient criterion for detected minima in MZ’s detection part could lead to retain much less minima than KH’s detection. MZ’s detection part only detects minima over sea because the MZ method is designed for tracking polar lows which are strong marine cyclones. To establish a better basis for comparisons for the two methods, the gradient criterion of MZ’s detection part is set to zero and tracks over land areas in the KH method are excluded.

Different combinations of filter, detection and tracking parts from the two methods are studied to investigate the influence of each part on the tracking results. If the gradient criterion of MZ's detection part is set to zero, the detection and tracking part between both methods show only small differences in track numbers for the same spatial filter. A simple algorithm for track-to-track comparison also confirms that the detection and tracking parts are not the main reasons for differences in track numbers and track paths. The largest differences on track numbers are related to the implementation of different filters. The probabilities for overlapping tracks between combinations which are based on different filters are also relatively small. This indicates that different filters lead to differences not only in track numbers but also in track paths. Moreover, the DCT and digital filter show different filtered MSLP patterns. The various filtered patterns differ in their detected minima, eventually influencing also the track numbers and paths. In this context more minima are detected for the digital-filtered fields which results in more detected tracks.

A shortcoming of the tracking algorithms relates to the fact that not all of these tracks are polar lows. To overcome this problem the polar low identification criteria of MZ were applied to both tracking schemes in order to assign tracks to potential polar lows. The vertical stability criterion represents a quite strong constraint and can dismiss more than half of the remaining tracks. The directional criterion, requiring tracks to travel from north to south, is also strong and probably excludes some polar lows in the Labrador Sea and east Greenland. After applying these criteria, the differences in track numbers and locations are still very dependent on the selection of the spatial filter applied.

Based on the comparative analysis it can be concluded that the different filters used in the two methods are the main reasons for variations in track numbers and paths. The digital filter used by MZ is less precise at scale separation according to wave numbers. The MSLP fields contain large values that influence the filter result, even if only small wave remnants are conserved after digital filtering. Thus we suggest that the DCT filter is more suited for this application, especially for MSLP fields. The filtered vorticity fields obtained by the digital and DCT filters show larger similarities, hence it might be expected that smaller differences might occur between detected polar lows obtained by KH and MZ methods for this field. Future work will explore this issue to investigate if the spatially filtered vorticity is a better alternative to the spatially filtered MSLP by applying both KH and MZ methods.

Chapter 3 Quasi-stationarity of centennial Northern Hemisphere midlatitude winter storm tracks

3.1 Overview

There is great interest in the issue of changing statistics of extratropical cyclones because of the impacts associated with the passage of such storms, in particular related to strong wind and heavy precipitation. Therefore many studies deal with perspectives of changing storm statistics in the course of emerging anthropogenic climate change (e.g., Schubert et al. 1998; Ulbrich and Christoph 1999). In order to assess the significance of expected future changes, knowledge about the natural variability of storminess is also needed (IDAG 2005). However, most analysis of recent and ongoing change of extratropical storm activity concentrated on analyzing re-analyses of recent decades such as Sickmöller et al. (2000) and Weisse et al. (2005), or on the last century such as Alexandersson et al. (1998) and Matulla et al. (2008) who used proxies based on air pressure statistics to reconstruct past storminess.

Only Fischer-Bruns et al. (2005) examined multi-centennial data – from coupled atmosphere-ocean global climate model (GCM) simulations subject to estimated external (volcanic, solar and anthropogenic) forcing. They showed that the storm frequency had no noteworthy long-term trends until recently. In particular no obvious link between temperature variations and extratropical storm activity emerged. In this study we examine a similar GCM simulation, extending for almost 1000 years, by studying the statistics through the lens of regional clustering and frequency of storm tracks.

This study is based on the availability of millennial simulations, which by now are routinely computed after their first appearance in the late 1990s (von Storch et al. 1997). These long simulations mostly operate with spatial resolutions suitable for extratropical storms, but not for tropical cyclones. Therefore we limit ourselves to such mid-latitude baroclinic storms as analysed in Fischer-Bruns et al. (2005).

Unfortunately, the spatial resolution of this simulation is relatively coarse, namely T30 (approx. 370 x 370 km), and the output is stored only every 12 hours. Jung et al. (2006) state that extratropical cyclone numbers obtained within low horizontal resolution model data are 40% lower compared to reanalysis data. Uncertainties of cyclone frequency also rise due to the coarse temporal resolution (Zolina and Gulev 2002). However, previous analyses have employed just this configuration, such as Raible and Blender (2004) and Fischer Bruns et al.

(2005). Assessing storm activity in terms of variance of 500 hPa geopotential height, Stendel and Roeckner (1998) found that T30 generates reasonable patterns and the deviations are less than 10% compared to ERA/ECMWF reanalysis data. A comparison of our results with other tracking studies is difficult, because different tracking methods use different settings. However, most important is that the spatial patterns and the relative frequencies of the different tracks are similar. The intention of this study is to determine and discuss the variability of storm tracks on multi-centennial time scales. We argue that the underestimation of the total number and length of tracks acts in the same way throughout the simulation: our track numbers may be biased negatively, but uniformly, so that the variability should hardly be affected.

Various automatic tracking algorithms for describing cyclone activity in long-term datasets are available (Murray and Simmonds, 1991; Hodges, 1994, 1995; Serreze, 1995; Blender et al., 1997; Gulev et al., 2001; Muskulus and Jacob, 2005; Wernli and Schwierz, 2006; Zahn and von Storch, 2008a). We adopt in our study Hodges (1994, 1995 and 1999) well-documented and frequently applied method. The cluster analysis was developed for sorting objects into different categories, and can of course be applied to cyclones, e.g. Blender et al. (1997) and Sickmöller et al. (2000) for North Atlantic baroclinic storms, and Elsner (2003), Nakamura et al. (2009) and Chu et al. (2010) for tropical storms.

How storm track activity relates to changes of circulation has been well studied in the past, for instance the effect of the North Atlantic Oscillation (NAO) on storm statistics has been studied by Hurrell (1995), Ulbrich and Christoph (1999), Gulev et al. (2001). Also the effects of the Southern Oscillation (SO) (Sickmöller et al. 2000), the North Pacific Oscillation (PNA) (Sickmöller et al. 2000, Gulev et al. 2001) as well as anomalies of mid-latitude sea surface temperature (SST) anomalies (Brayshaw et al. 2008) have been studied in the link of changes in storminess. Sickmöller et al. (2000) showed that there are intermediate correlations between the northeastward travelling cyclones in the Pacific and the northeastward and zonal travelling ones in the Atlantic. Storm track activity of different clusters or over different regions is always studied in connection with the dominant patterns of atmospheric variability. In this respect the North Atlantic storms are closely related to the north Atlantic Oscillation (NAO). The shift of the NAO increases storm tracks over Europe (Hurrell 1995, Ulbrich and Christoph 1999, Gulev et al. 2001). In addition to the NAO index, Sickmöller et al. (2000) also studied the relation of North Atlantic cyclones with the Southern Oscillation Index (SOI).

Authors concluded that during El Nino winters (with low SOI) the stationary cyclones are more frequent. Cyclone activity in the Pacific such as frequency or density is highly associated with the Pacific/North American Pattern (PNA) (Sickmöller et al. 2000, Gulev et al. 2001). Brayshaw et al. (2008) showed that the storm-track also responses to mid-latitude sea surface temperature (SST) anomalies. In this chapter, variability of Northern Hemisphere extratropical storms and its relation to changes in winter circulation is studied. This is done with the help of a Canonical Correlation Analysis of seasonal anomalies of mean sea level pressure fields (MSLP) and the time-variable number of members in the storm track clusters.

The long-term GCM simulation, carried out with the coupled atmosphere-ocean GCM ECHO-G forced with variable solar, volcanic and greenhouse-gas forcing of the last millennium, is described in section 3.2. In section 3.3 tracking results using a Lagrangian-type tracking algorithm (Hodges 1994, 1995, and 1999) are shown and compared with results derived from NCEP/NCAR reanalysis data in order to evaluate the model simulation. Time series of cyclone numbers for the 990 years (quasi-millennium) and for the 10 centuries are also shown. In section 3.4 tracks are clustered into ten groups by the K-means clustering method; characteristics such as life span, frequency, or intensity are analyzed for each cluster. Century-to-century variability of cyclones for each cluster is also analyzed. Interactions of storm counts between different clusters are studied in section 3.5. Variations of the numbers of members of the clusters in the marine sectors of the North Pacific and North Atlantic related to mean winter circulation anomalies are presented in section 3.6. In section 3.7 results are discussed and conclusions are drawn.

3.2 Data

The quasi-millennial (1000–1990 AD) simulation used in this study has been carried out with the global climate model ECHO-G (Min et al., 2005 a, b). The ECHO-G model consists of the atmospheric model ECHAM4 (Roeckner et al. 1996) and the ocean model HOPE-G (Wolff et al. 1997). The atmospheric general circulation model (AGCM) is ECHAM4, which is the fourth version of the Hamburg AGCM. Considering the balance between computational costs and resolution requirement, ECHAM4 performs on triangular truncation at wave number 30 (T30). It is shown that the ocean model HOPE-G performs similarly forced by ECHAM4 T30 model data or T42 data (Legutke et al. 1996 and Min et al. 2005 a). For the atmospheric part the horizontal resolution is approximately 3.75°× 3.75° for a regular longitude-latitude grid

with 19 hybrid sigma-pressure levels. A more technical description for ECHAM4 can be found in Roeckner et al. (1996).

The global ocean circulation model HOPE-G is the Hamburg Ocean Primitive Equation (HOPE) model. The HOPE-G model was implemented with a horizontal resolution of 2.8°×2.8° (corresponding to T42) with a grid-refining to 0.5° in the tropical regions. HOPE-G consists of 20 irregularly spaced levels with 10 levels located in the upper 300 m. ECHAM4 and HOPE-G are coupled by the OASIS software by exchanging mean atmospheric fluxes and surface conditions. More technical details about coupling HOPE-G are described by Legutke and Voss (1999). The model time step for ECHAM4 is 30 min and for HOPE-G is 12h. The output is stored every 12 hours. In order to prevent an artificial climatic drift the ECHO-G model is corrected for heat- and freshwater fluxes.

The estimated historical forcing for driving the model such as solar variations, CO_2 and CH_4 concentrations as well as volcanic effects have been described previously by von Storch et al. (2004) and Zorita et al. (2005). Figure 3.1 from Müller (2004) shows the changes of CO_2 and methane (CH_4) concentrations after 1500 AD. An obvious increase of greenhouse gases (CO_2 and CH_4) can be seen after 1800 AD. The ECHO-G simulations have been found skillfully in simulating the seasonal mean climatology and inter-annual variability of mean sea level pressure and surface temperature (Min et al. 2005 a, b; Gouirand et al. 2007). The atmospheric circulation of the Northern Hemisphere in winter including the NAO pattern is also simulated realistically by ECHO-G (Min et al., 2005b), although the ECHO-G model underestimates the number of blocking events compared to observations (Müller 2004). The North Atlantic sea level pressure anomalies and response to the El Nino Southern Oscillation (ENSO) are similar to observed patterns and other climate reconstructions (Gouirand et al. 2007), although the modeled frequency of El-Nino is too regular and centered around three years.

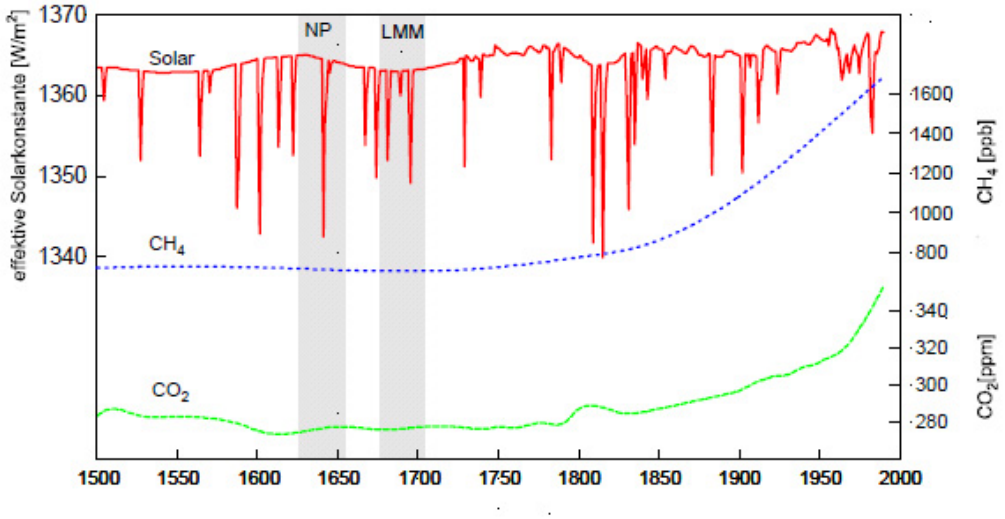

Fig. 3.1 Effective solar constant, concentration of CO_2 and methane (CH_4) since 1500; in gray: normal period (1625–1655 AD) and Late Maunder Minimum (LMM) (1675–1705 AD) (Müller 2004).

Investigations of shorter simulations done with ECHO-G have already shown that the grid resolution of T30 is sufficient to study midlatitude baroclinic cyclones (Stendel and Roeckner 1998, Raible and Blender 2004, Fischer-Bruns et al. 2005). The storm tracks were found to agree well with ERA-15/ECMWF reanalysis data and deviations from ERA-15 are below 10% (Stendel and Roeckner, 1998). Simulations carried out on higher spatially resolved grids could lead to an increase in the numbers of cyclones due to the presence of smaller and weaker cyclones.

The key added value of this simulation is the homogeneous presentation of a possible development during the last millennium. Due to the limited availability of observational data a conventional validation of the simulation is hardly possible. However, with respect to the development of Northern Hemisphere temperature, comparisons with different proxy reconstructions are possible, including tree ring data and borehole temperatures (González-Rouco et al. 2003, Tan et al. 2009). These proxies indicate that this simulation lies within the envelope of reconstructions of the past temperature evolution. Other simulations extending over 1000 and more years also exhibit qualitatively similar characteristics. Some have argued that ECHO-G temperature variations would be too large. However, this does not question our main conclusion, namely that the mid-latitude winter storm activity is remarkably stationary on centennial time scales (see below).

3.3 Strom tracks

3.3.1 Cyclone tracking

For cyclone identification and tracking 12-hourly mean sea level pressure (MSLP) fields with T30 spatial resolution simulated by ECHO-G are used. An automatic tracking algorithm developed by Hodges (1994, 1995, and 1999) is applied. This algorithm is widely used to study the climatology of extratropical cyclones (Hoskins and Hodges 2002, Hoskins and Hodges 2005), tropical storms and monsoon depressions (Hodges 1999), or specific cyclones such as polar lows (Xia et al. 2012a). In this study, only winter cyclones (DJF) at mid-latitudes (≥30° N) over the Northern Hemisphere (NH) are considered.

The use of different fields and levels has also been shown to result in different numbers of cyclones, even if using the same source data set (Hoskins and Hodges, 2002). The use of projections for the data onto a plane can also have an impact on the final results via both the identification and tracking. Here a cylindrical projection (plate carrée) which is adequate for tropics and midlatitudes has been used (Hodges 1994). Using the standard latitude-longitude projection preferentially samples the high latitudes (Sinclair, 1997), whilst distance and direction become distorted relative to their true values on the surface of a sphere. This can be circumvented to some extent by the choice of a different projection and measuring distance and direction on a sphere (Hodges, 1995).

For high resolution data, it could be perfectly adequate for tracking. However, for a coarse grid, such as T30, the data could be sparse and fail to produce smooth tracks resulting in a staircase effect. Therefore data are interpolated by the B-spline method of Dierckx (1984). The interpolated surface is periodic in longitude up to the pole. The extrema are analysed by first identifying sub-regions to improve the efficiency. The segmentation refers to the threshold to identify “objects” using connected component analysis based on hierarchical quad trees (Hodges 1994). The minima or maxima in each object are detected and recorded with locations and strength.

Before applying the tracking algorithm, a spatial filter is applied on the MSLP fields to remove the influence of large-scale systems. Wave numbers less than or equal to 5 are removed following a suggestion by Hoskins and Hodges (2002). Planetary wave are removed without significantly affecting the synoptic weather systems. Afterwards the tracking algorithm extracts all minima below -1 hPa in the filtered MSLP fields. Minima are connected

to form tracks if their distance is less than 12° (about 1333 km) within 12 hours. The minimum lifetimes of tracks is set to 2 days.

A cost function with three time steps is constructed with the terms of similarity of direction and speed to estimate track smoothness and defined as (Hodges 1994, 1995 and 1999):

$$\psi(P_i^{k-1}, P_i^k, P_i^{k+1}) = 0.5w_1[1 - \widehat{T}_i^{(k-1,k)} \cdot \widehat{T}_i^{(k,k+1)}] + w_2(1 - \frac{2[\left\|P_i^{k-1}P_i^k\right\|\left\|P_i^k P_i^{k+1}\right\|]^{1/2}}{[\left\|P_i^{k-1}P_i^k\right\| + \left\|P_i^k P_i^{k+1}\right\|]}), \quad \text{(Eq. 3.1)}$$

where P_i^k is the position for a detected point on track i of time step k. The first term is a measure of directional similarity, while the second term represents the speed similarity. The smoothness measure weights are chosen as w_1=0.2 for direction and w_2=0.8 for speed.

For applications in 2D Cartesian space (Hodges 1994), $P_i^k P_i^{k+1}$ is the displacement vector from P_i^k to P_i^{k+1}. The $\left\|P_i^k P_i^{k+1}\right\|$ is a measure of Euclidean distance between the points P_i^k and P_i^{k+1}, hence

$$\left\|P_i^k P_i^{k+1}\right\| = \left|P_i^{k+1} - P_i^k\right|.$$

The $\widehat{T}_i^{(k-1,k)}$ is the normalized displacement vector as:

$$\widehat{T}_i^{(k-1,k)} = \frac{P_i^{k-1}P_i^k}{\left\|P_i^{k-1}P_i^k\right\|}.$$

In the equation 3.1, if the three points lie on the same line, the first term is zero, while if the distance between the points P_i^{k-1} and P_i^k is equal to the distance between the points P_i^k and P_i^{k+1}, the second term is zero.

For application to latitude-longitude data, 3D Cartesian space is used (Hodges 1995). $P_i^k P_i^{k+1}$ is the directed arc of a great circle from P_i^k and P_i^{k+1}. The distance measure uses the geodesic norm as:

$$\left\|P_i^k P_i^{k+1}\right\| = \arccos(P_i^k \cdot P_i^{k+1}).$$

The directional changes are determined with triple vector cross product $t_i^{(k,k+1)}$ (Hodges 1995):

$$t_i^{(k,k+1)} = (P_i^k \times P_i^{k+1}) \times P_i^k \text{ and } \widehat{t}_i^{(k,k+1)} = \frac{t_i^{(k,k+1)}}{\left|t_i^{(k,k+1)}\right|}.$$

Thus, $\widehat{T}_i^{(k-1,k)} = -\widehat{t}_i^{(k,k-1)}$ and $\widehat{T}_i^{(k,k+1)} = \widehat{t}_i^{(k,k+1)}$ are given in equation 3.1.

To maximize the track smoothness, the cost function (Eq. 3.1) is minimized and subject to the maximum displacement constraint $\left\|P_i^{k-1}P_i^k\right\| \le d_{\max}$ and the maximum smoothness constraint $\psi_{\max}$. If the systems move fast and the similarities of direction and speed is high,

$$\widehat{T}_i^{(k-1,k)} \cdot \widehat{T}_i^{(k,k+1)} \propto 1 \text{ and } 1 - \frac{2[\left\|P_i^{k-1}P_i^k\right\|\left\|P_i^k P_i^{k+1}\right\|]^{1/2}}{[\left\|P_i^{k-1}P_i^k\right\| + \left\|P_i^k P_i^{k+1}\right\|]} \propto 0,$$

then $\psi(P_i^{k-1}, P_i^k, P_i^{k+1})$ could be small. Thus, a more restrict constraint is required for the smoothness. If the systems move slowly, $\psi(P_i^{k-1}, P_i^k, P_i^{k+1})$ is large and a less restrict constraint is required for the smoothness. So adaptive smoothness constraints $\psi_{\max}$ which depend on the regionally varying upper-bound displacement constraints $d_{\max}$ are applied (Hodges 1999) as shown in Table 3.1. This study investigates extratropical cyclones in the Northern Hemisphere. The adaptive smoothness constraints are chosen following a limited sensitive study and could be different to those used by Hodges (1999) due to the analysis of different datasets. The minimization proceeds both forward and backward for one track to ensure that every point is checked.

Table 3.1 Adaptive smoothness constraints used in the study. The last row indicates the maximum speed in each zone.

Zonal upper-bound displacements					
Zones	1	2	3	4	5
Lower (deg lat)	-90.0	-20.0	20.0	30.0	70.0
Upper (deg lat)	-20.0	20.0	30.0	70.0	90.0
$d_{\max}$ (deg)	0.5	4.0	7.0	12.0	7.0
Max. speed (m/s)	1	10	18	30	18
Adaptive track smoothness					
$\bar{d}$ (deg)	0.0	2.0	6.0	13.0	>13.0
$\psi_{\max}(\bar{d})$	0.7	0.5	0.1	0.0	0.0

3.3.2 Cyclone trend

Extratropical cyclones in winter are tracked based on MSLP fields for the time period 1001 – 1990 AD of the quasi-millennial ECHO-G simulation. The natural variability of cyclones on long time scales can be studied here and tracks of cyclones are also available for clustering analysis.

For validation purposes tracks obtained from the ECHO-G simulations are compared to those derived from NCEP/NCAR reanalysis data (Kalnay et al., 1996). To establish a proper basis for comparisons with the ECHO-G simulations, the NCEP/NCAR reanalysis data were coarsened to T30 and 12 hourly outputs and the same tracking setting was applied on both data sets. The numbers of tracks from the ECHO-G simulation data are similar to those derived from the NCEP/NCAR reanalysis data. Spatial densities for regions with cyclone genesis in winter representing the origins of storm tracks are compared in Figure 3.2.

Both data sets show the well-known genesis maxima for Pacific storms located over Mongolia, northeast of China, around southeastern China, east of Japan and in the central Pacific. This result is consistent with the studies by Adachi and Kimura (2007) and Inatsu (2009). Genesis maxima of Atlantic storms are located over continental North America in the lee of the northern Rocky Mountains, along the eastern coast of the United States and around Iceland, in accordance to Hoskins and Hodges (2002). Further genesis regions are found over the Norwegian Sea, over the western Mediterranean and over the Caspian Sea. In general, the distributions of genesis density in the ECHO-G simulation data agree reasonably well with those derived from the NCEP/NCAR reanalysis data.

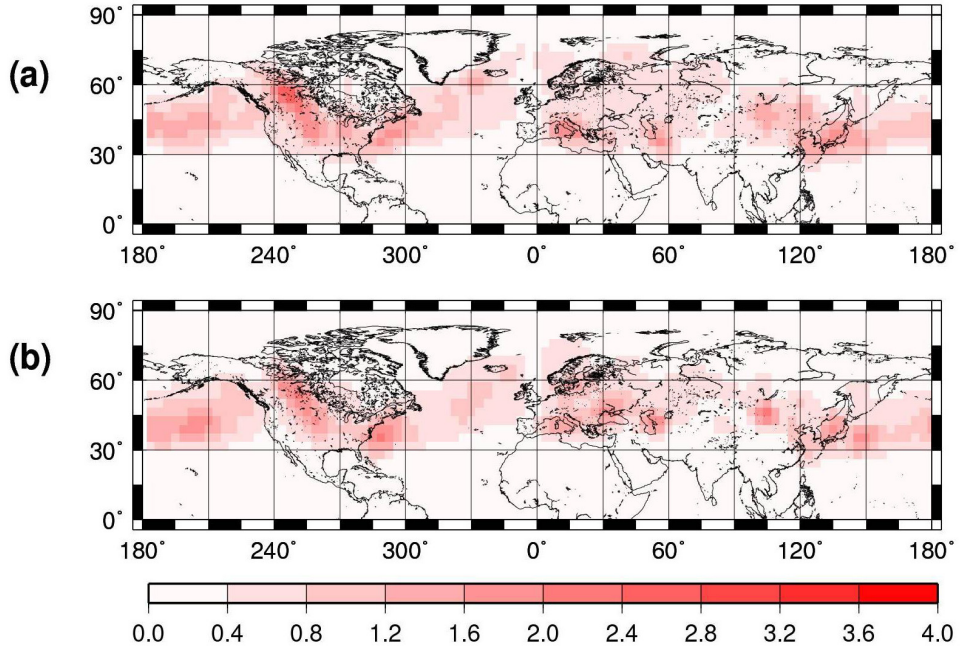

Fig. 3.2 40-years (1951-1990) average density distribution of cyclone genesis in winter (December – February, DJF): (a) coarsened NCEP/NCAR reanalysis data; (b) ECHO-G simulation data.

The cyclone density defined as cyclone occurrences per time step and area (218000km^2) is shown in Figure 3.3. Figure 3.3a shows the mean winter storm density for the period from 1951 – 1990 with the coarsened NCEP/NCAR reanalysis data and Figure 3.3b displays the difference between the ECHO-G simulation data and the coarsened NCEP/NCAR reanalysis data. The primary difference can be found in the western Pacific and in the Gulf of Alaska over the North Pacific, along the coast of North America, in the southeast of Greenland, and the Barents Sea. The ECHO-G simulation overestimates the cyclone density over the Gulf of Alaska, the region south of Greenland, and Western Europe. Underestimations are evident over southeast China, the east of Japan and over the western Mediterranean Sea (Figure 3.3b). However, differences are not large and the general cyclone density pattern is in accordance with results obtained by other studies (Gulev et al. 2001, Hoskins and Hodges 2002). Therefore we conclude that the midlatitude cyclone statistics of the ECHO-G simulation data are realistic to be used for further analyses.

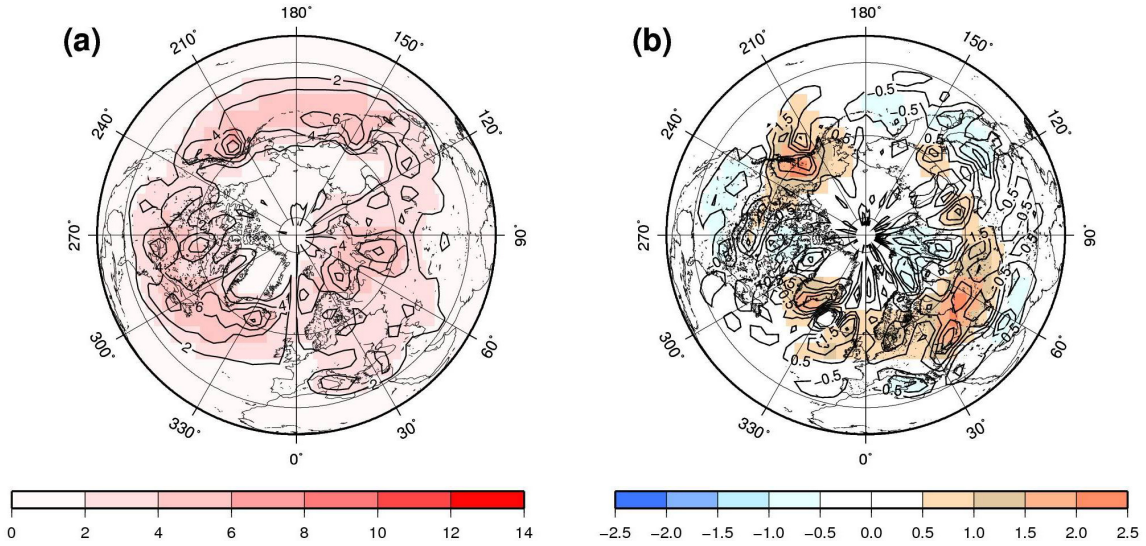

Fig. 3.3 40-years (1951-1990) mean cyclone density (unit: cyclones/winter per 218000km^2) for the Northern Hemisphere: (a) coarsened NCEP/NCAR reanalysis data; (b) difference between ECHO-G simulation data and interpolated NCEP/NCAR reanalysis data.

The quasi-millennium trend for the period 1001-1990 AD of extratropical cyclones in winter is gained by means of Hodges's tracking algorithm (1994, 1995 and 1999) based on MSLP fields. The 990-year time series of winter cyclone numbers for the NH are shown in Figure 3.4. Accordingly, a high amount of inter-annual variability in cyclone numbers is evident. The average cyclone numbers for each century are shown in Figure 3.5. The lowest average cyclone number of 179/yr occurs in the twentieth century (1901–1990 AD). In the thirteenth (1201–1300 AD) and fourteenth (1301–1400 AD) century also relatively few storms are counted, with 180 per year. Largest numbers (182 counts per year) emerge in the fifteenth (1401–1500 AD) century. However, in general the average cyclone frequency for different centuries is quite similar with only little century-to-century variability (Figure 3.5), while the year-to-year variations for storm numbers are quite large (Figure 3.4). Long-term trends in cyclone frequency can not be detected during the quasi-millennial period between 1001 and 1990 AD.

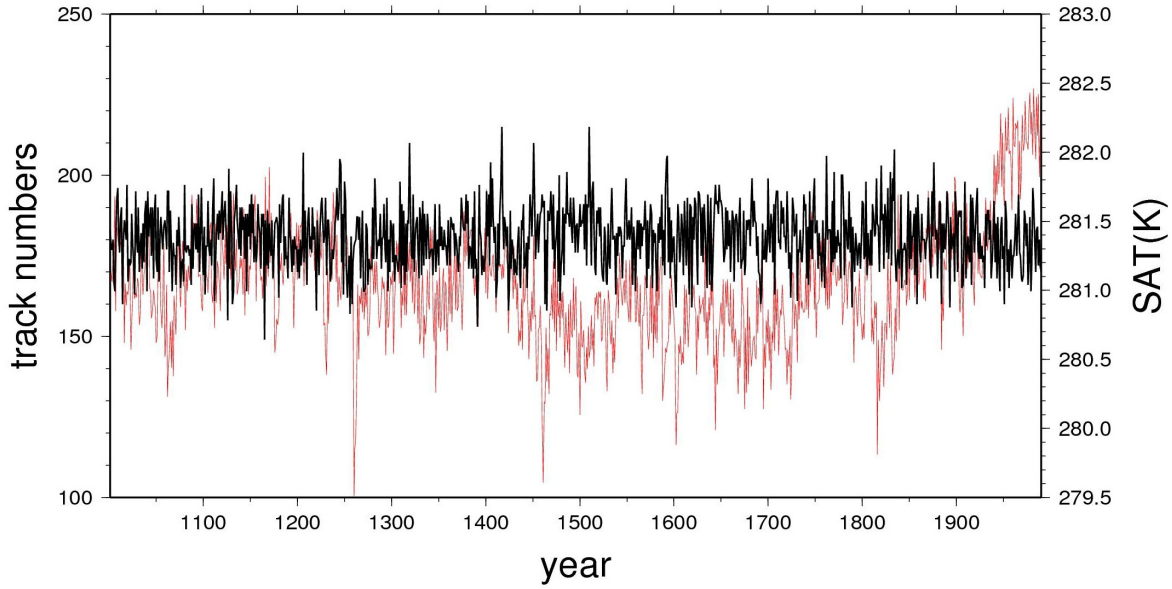

Fig. 3.4 Time series of the numbers of winter (DJF) extratropical cyclones (black line) and winter surface air temperature (SAT: K) (red line) in the Northern Hemisphere (NH) (years 1001–1990 AD).

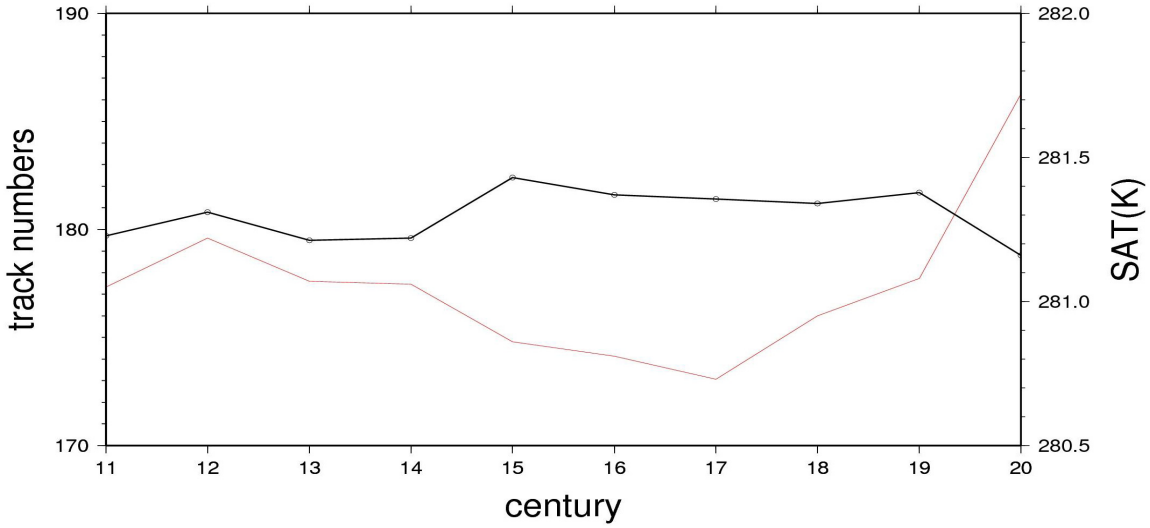

Fig. 3.5 Average annual numbers of winter (DJF) extratropical cyclones (black line) and average winter SAT (K) (red line) in the NH for different centuries (11^{th} -20^{th} century).

This result is very similar to those obtained by Fischer-Bruns et al. (2005) based on a shorter ECHO-G simulation using the maximum wind speed to define storm days. They compared the storm day frequency between pre-industrial times (1551–1850 AD) and industrial times (1851–1990 AD) and found no noticeable differences. They stated that during historical times storm statistics for both hemispheres are remarkably stable with little variability and

storminess mostly decoupled from temperature variations. Only for climate change scenarios (A2 and B2), which describe possible developments in the 21st century, forced with a strong increase of greenhouse gas concentrations, the distributions of high storm frequency exhibited a poleward shift. However, for the area-averaged values for the Northern Hemisphere no increase in the numbers of storms is evident. Also here, we find the large variations in temperature not reflected in parallel variations of cyclone counts (Figure 3.4 and 3.5).

As previously mentioned, compared to datasets carried out with higher spatial and temporal resolution, track numbers derived from coarsely resolved temporal and spatial datasets are underestimated (Blender and Schubert 2000, Jung et al. 2006, Zolina and Gulev 2002). According to the study of Jung et al. (2006), cyclones in the northern Pacific, the Arctic, Baffin Bay, the Labrador Sea and the Mediterranean Sea are specifically sensitive to the horizontal resolution. Numbers of extratropical cyclones within the low resolution model data are 40% smaller compared to the reanalysis data (Jung et al., 2006). This can be explained partly by topography which is described not very well by spatially coarse resolved simulations. Our result differs from those obtained by Gulev et al. (2001) related to the fact that cyclone density of the ECHO-G simulation data is up to 12 cyclones per winter per 218000 km^2 (Figure 3.3). This is considerable less than the number given by Gulev et al. (2001) (up to 20 cyclones per winter per 218000 km^2). This difference may partly be due to the different spatial and temporal resolution of the different simulations under investigation or other deficits of the model ECHO-G. In addition, the differences may also reflect different tracking settings for the detection of storm tracks. However, most important are the similarity of the overall patterns and the relative cyclone frequencies of storm tracks.

3.4 Clustering analysis

3.4.1 Processing

The estimated storm tracks are not equal length and refer to many dimensions. Prior to clustering, further processing is required to describe the tracks by only a few characteristic parameters. Different approaches have been used in this respect. For instance, Blender et al. (1997) used the relative displacement of a cyclone from its initial positions within 3 days. The relative displacements are defined as:

$$d_j(t) = [dx_j(t), dy_j(t)] = [x_j(t) - x_j(0), y_j(t) - y_j(0)]. \qquad \text{(Eq. 3.2)}$$

All cyclones are presented by the displacements within same life span T,

$$D_j = [d_j(t=0), \cdots, d_j(t=T)]. \quad \text{(Eq. 3.3)}$$

The threshold T=3 days is chosen. This requires cyclones to last for more than 3 days. The remaining part over 3 days is not considered in clustering. Considering the time step is 6h, the cyclone displacements are related to:

$$[dx(t=6h), dy(t=6h), \cdots, dx(t=T), dy(t=T)]. \quad \text{(Eq. 3.4)}$$

24 numbers are used for describing every track in the clustering algorithm. Elsner et al. (2000) used latitude and longitude coordinates at the positions of maximum and final hurricane intensities. Nakamura et al. (2009) used the location of maximum wind intensity of the storm track and variance ellipse by measuring the shape of the cyclone track as shown in Figure 3.6. The centroid (see the asterisk in Figure 3.6) uses the location of the x and y coordinates of the maximum and final hurricane intensities. Three variances (x, y and xy directions) illustrate the ellipse in Figure 3.6 providing a summary of the shape of the storm. Afterwards five numbers (two coordinates and three variances) describe the track information forming the basis for track clustering. Chu et al. (2010) fitted a second-order polynomial function to the tracks.

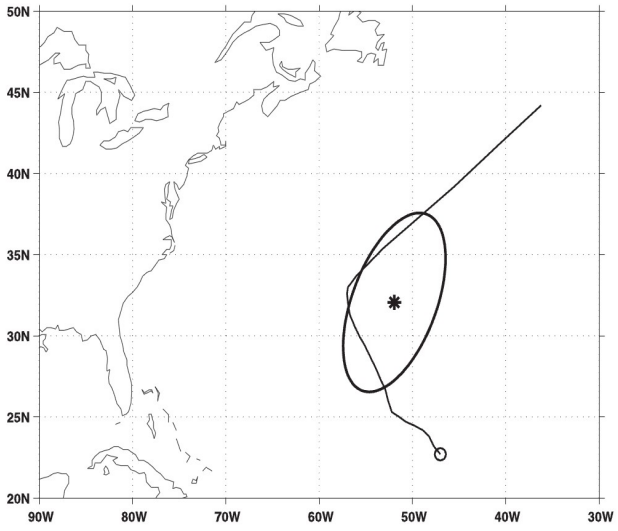

Fig. 3.6 Examples of the centroid (asterisk) and variance ellipse for the storm track (Nakamura et al. 2009).

Here we also adopt Chu et al. (2010)'s procedure and fit to each track a second-order polynomial function with six free parameters. For each cyclone path, this is represented by the latitudes, longitudes and time according to:

$$z = [z_{lat}, z_{long}] = \begin{bmatrix} z_{1,lat} & z_{1,long} \\ \cdots & \cdots \\ z_{n,lat} & z_{n,long} \end{bmatrix} \quad \text{(Eq. 3.5)}$$

with n being the length of cyclone track, $z_{i,lat}$ and $z_{i,long}$ presenting the i –th time step location of the track with $i = 1,\cdots,n.$

Each track can be polyfited as second order polynomial function by the following formula:

$$z = T\beta + \varepsilon, \qquad \text{(Eq. 3.6)}$$

where T is the time vector for the second order polynomial function by

$$T = \begin{bmatrix} 1 & t_1 & t_1^2 \\ \cdots & \cdots & \cdots \\ 1 & t_n & t_n^2 \end{bmatrix} \qquad \text{(Eq. 3.7)}$$

and

$$\beta = \begin{bmatrix} \beta_{0,lat} & \beta_{0,long} \\ \beta_{1,lat} & \beta_{1,long} \\ \beta_{2,lat} & \beta_{2,long} \end{bmatrix}. \qquad \text{(Eq. 3.8)}$$

The resulting formula reads as follows:

$$z = \begin{bmatrix} z_{1,lat} & z_{1,long} \\ \cdots & \cdots \\ z_{n,lat} & z_{n,long} \end{bmatrix} = \begin{bmatrix} 1 & t_1 & t_1^2 \\ \cdots & \cdots & \cdots \\ 1 & t_n & t_n^2 \end{bmatrix} \begin{bmatrix} \beta_{0,lat} & \beta_{0,long} \\ \beta_{1,lat} & \beta_{1,long} \\ \beta_{2,lat} & \beta_{2,long} \end{bmatrix} + \varepsilon \qquad \text{(Eq. 3.9)}$$

i.e.

$$\begin{aligned} z_{1,lat} &= \beta_{0,lat} + t_1\beta_{1,lat} + t_1^2\beta_{2,lat} \\ z_{1,long} &= \beta_{0,long} + t_1\beta_{1,long} + t_1^2\beta_{2,long} \\ &\cdots \\ z_{n,lat} &= \beta_{0,lat} + t_n\beta_{1,lat} + t_n^2\beta_{2,lat} \\ z_{n,long} &= \beta_{0,long} + t_n\beta_{1,long} + t_n^2\beta_{2,long} \end{aligned} \qquad \text{(Eq. 3.10)}$$

where ε is the deviation between cyclone track and the second order polynomial function of the track.

The zero-order coefficients provide the information about the genesis locations of a track, the first-order coefficients describe the direction of track and the second-order terms represent the curvature of the track. Every track can be described by these six parameters and the clustering is done in this 6-dimensional space. Afterward all tracks are clustered into ten groups by the K-means method in each century.

3.4.2 Clustering method

Clustering analysis allows to objectively classify cyclones and storms over different oceans or land areas into categories. It provides a way to separate tracks into groups depending on the

specific characteristics of the cyclones, such as track geographical locations, genesis, track shapes and directions. Table 3.2 shows the different clustering analyses for cyclones in different ocean basins. Blender et al. (1997) classified cyclone tracks in the North Atlantic/European region into three distinct groups of stationary, zonally and north-eastward travelling storms. Elsner (2003) also clustered North Atlantic tropical cyclones into three clusters. Nakamura et al. (2009) used the locations and shapes of tropical cyclone tracks over the North Atlantic and classified the according cyclones into six clusters. Chu et al. (2010) classified tropical storms over the western North Pacific into three straight types, four recurved types and one mixed straight-recurved type. Clustering analysis is potentially helpful to study in greater detail the physical and geometrical characteristics of different groups of cyclones. Different clusters differ in the genesis locations, cyclone counts, intensities, lifetimes, track shapes, travelling directions, deepening rates, landfalls, seasonal patterns, and trends, respectively.

Table 3.2: Clustering analysis applied for different ocean basins with different numbers of clusters and methods related to several studies.

Name	**method**	**clusters**	**type**	**areas**
Blender et al. (1997)	K-means	3	winter extratropical cyclones	North Atlantic
Elsner et al. (2003)	K-means	3	tropical cyclones	North Atlantic
Nakamura et al. (2009)	K-means	6	tropical cyclones	North Atlantic
Chu et al. (2010)	Expectation-maximization(EM) algorithm	8	tropical cyclones	Western North Pacific

The interaction among clusters and their relation with large scale patterns can also be investigated using classification. Schubert et al. (1998) did the same classifications in the North Atlantic as Blender et al. (1997) for different scenarios. The authors find that northeastward travelling cyclones increase in the $2\times CO_2$ scenario, but not in the $3\times CO_2$ scenario. Moreover, cyclone density shifts northward in both scenarios. Sickmöller et al. (2000) also applied Blender et al.'s clustering analysis (1997) but in the Northern Hemisphere

over the North Atlantic and Pacific Ocean, respectively. They found that there are correlations between the north-eastward travelling cyclones in the Pacific and the north-eastward and zonally travelling ones in the Atlantic. More stationary cyclones occur in the Atlantic in conjunction with a positive phase of the North Antlantic Oscillation (deeper Icelandic lows) during winter. In addition, more zonally travelling cyclones develop in the Atlantic when the center of the Aleutian low in the North Pacific is deeper. The study of Raible and Blender (2004) supports the finding that the northward shift of the storm tracks and cyclone intensities in the North Pacific are mainly caused by northeastward and zonally travelling cyclones, controlled by the El Niño Southern Oscillation (ENSO).

Table 3.2 indicates that the K-means method is applied more widely for the cluster analysis (Blender et al. 1997, Elsner et al. 2003, and Nakamura et al. 2009). Chu et al. (2010) used the Expectation-Maximization (EM) algorithm in their clustering algorithm. In section 4.4.1, every track is polyfitted by a second order polynomial function and can be described by six parameters. Thus the clustering is done based on a 6-dimensional space. We also use the K-means method to cluster all cyclone tracks into ten groups for each century.

For k clusters, the K-means method minimizes the sum S of the point-to-cluster-centroid distances as

$$S = \sum_{i=1}^{N} \sum_{j=1}^{L} (\beta_{i,j} - \mu_{k(i),j})^2 \ , \qquad \text{(Eq. 3.11)}$$

where the N represents the cyclone counts, β denotes the second order polynomial parameters for each track. In this study, every track is described by six parameters so the index j counts these parameters with a total number L=6. This (Eq. 3.11) measures the squared Euclidean distance of cyclone tracks to their respective cluster centers. For the k-th cluster, $\mu_{k(i),j}$ are the centroids of this cluster, i.e. the mean of parameters $\beta_{i,j}$ for cyclone i belonging to cluster k:

$$\mu_{k(i),j} = \frac{1}{n_k} \sum_{i \in k} \beta_{i,j} \qquad \text{(Eq. 3.12)}$$

where n_k is the total number of cyclone tracks in cluster k. The K-means algorithm determines the clusters by iteratively swapping points between clusters to minimize S.

The K-means algorithm depends on the initial cluster centroid positions known as seeds. In order to minimize this dependency, the clustering was repeated 20 times by choosing a new

set of track parameters as initial centroid positions each time (Blender et al. 1997). Sensitivity experiments have also been carried out within different cluster numbers k . The cluster numbers k =10 are chosen in order to cover all cyclone genesis areas. This will be discussed in greater details in the following.

3.4.3 Clustering results

All tracks were clustered into ten groups by applying the K-means method in each century (Figure 3.7). The centroid track is the mean track of each cluster. According to Figure 3.7 all 10 clusters form a midlatitude ring around the Northern Hemisphere with a poleward extension at their ends. The pattern is similar to the schematic illustration of principal tracks (Figure 15 of Hoskins and Hodges, 2002) and is also consistent with the location of the genesis areas (Figure 3.2).

Across the Pacific, tracks are separated into three clusters: cluster 4 extending from the southeast of China into the Japan Sea, cluster 5 extending from the east of Japan towards the center of the Pacific, and cluster 6 in the eastern Pacific. In the Atlantic, there are also 3 clusters: cluster 8 along the eastern North American coast, cluster 9 over southern Greenland, and cluster 10 extending from southeastern Iceland into the Norwegian Sea. Cluster 7 corresponds to the tracks generated from continental North America in the lee of the northern Rocky Mountains. The classifications in the Pacific and Atlantic are quite similar to those of Gulev et al. (2001) except that only two clusters appear for the Pacific. Cluster 1 represents the cyclones originated from the Baltic Sea, North Sea and Mediterranean Sea in northern and western Europe. Cluster 2 represents cyclones originated in the Caspian Sea and cluster 3 represents the cyclones from the northeast of China.

Table 3.3 displays the numbers of tracks per cluster for the whole time period 1001 – 1990 AD. Cluster 1 which emanates from the North Sea, Baltic Sea and the western Mediterranean contains most members. In the Pacific, the eastern cluster 6 shows the largest numbers of tracks, while the central cluster 5 contains the lowest number. Over the Atlantic, the western cluster 8 shows most tracks, whereas the lowest number is found in the central cluster 9. The sum of cyclone counts for the three Pacific clusters (4, 5, 6) is larger compared to the three Atlantic clusters (8, 9, 10).

Table 3.3: Cyclone numbers of the ten clusters shown in Fig. 3.7 for the quasi- millennial time period (years 1001 – 1990 AD).

cluster	1	2	3	4	5	6	7	8	9	10
numbers	23955	16625	15519	20219	16720	21510	21435	15899	13079	13918

Table 3.4: Lifespan (days) distribution rates of the ten clusters shown in Fig. 3.7 for the quasi-millennial time period (years 1001 – 1990 AD). Unit: %.

lifetime(days)	2~4	4~6	6~8	8~10	>10
Cluster 1	43.25	30.20	16.70	6.19	3.65
Cluster 2	60.82	25.86	7.99	3.04	2.29
Cluster 3	63.12	15.11	10.02	6.60	5.15
Cluster 4	36.02	28.98	19.96	9.40	5.64
Cluster 5	50.19	29.93	12.40	4.45	3.03
Cluster 6	60.38	24.42	8.51	3.84	2.86
Cluster 7	56.66	18.03	13.28	6.80	5.23
Cluster 8	39.10	29.74	16.48	7.72	6.96
Cluster 9	55.68	23.62	10.54	5.25	4.92
Cluster 10	47.96	24.68	14.59	7.77	5.01

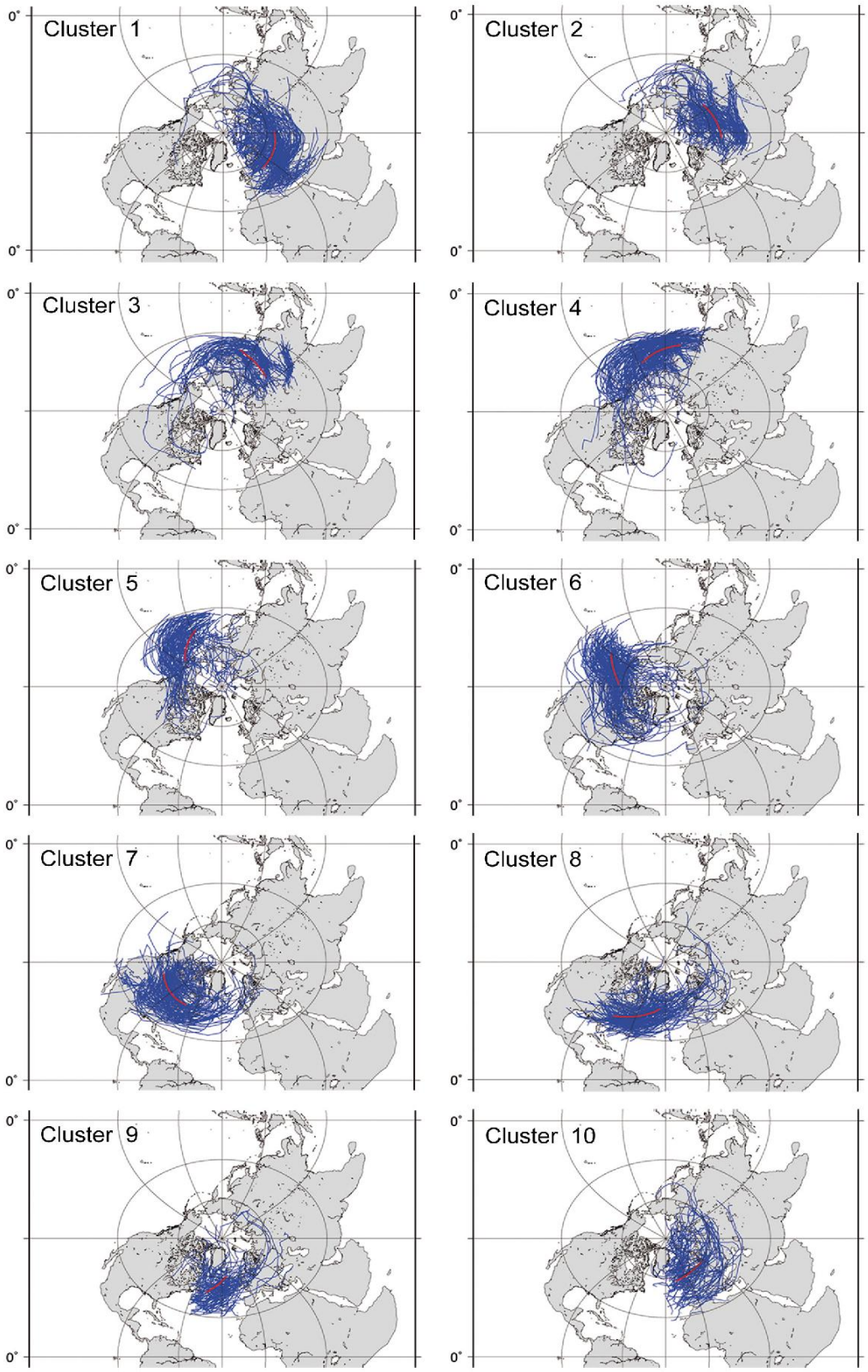

Fig. 3.7 Winter (DJF) extratropical cyclone tracks of the 20th century (years 1901 – 1990 AD) in the NH clustered into ten clusters by applying the K-means method: member tracks (blue) and centroid tracks (red) of the ten clusters.

Many studies found poleward shift of tracks or track density in simulations forced with future greenhouse gas scenarios (Schubert et al. 1998, Ulbrich and Christoph 1999, Fischer-Bruns et al. 2005, and Pinto et al. 2007). Observations based on satellite data also indicate that the storm cloudiness shows a poleward shift (Bender et al. 2012). Figure 3.8 displays the centroid (mean) tracks of the ten clusters for the 11th century (years 1001 – 1100 AD) and the 20th century (years 1901 – 1990 AD). Almost all of them show little variability. Obviously, the geometric positions of the tracks were quite similar in the first and last century of the last millennium. The results obtained by Fischer-Bruns et al. (2005) indicate that it is not the hemispheric temperature, but other factors, such as the zone of maximum baroclinicity that is related to the change in tracks.

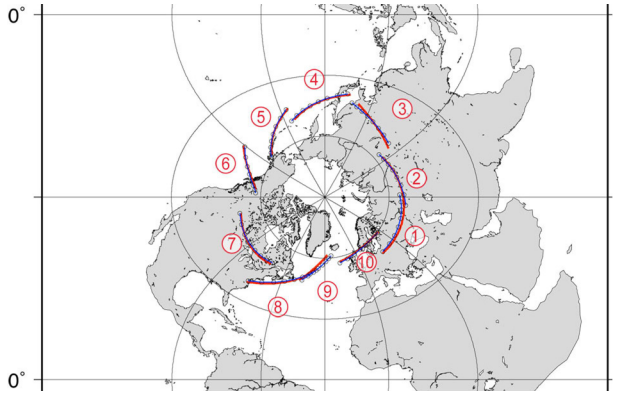

Fig. 3.8 Mean tracks of ten clusters (red numbers) for the NH in the 11th and 20th century: red ones are the mean tracks of the ten clusters in the11th century (years 1001–1100 AD), blue ones with circles are the mean tracks of the ten clusters in the 20th century (years 1901–1990 AD).

Figure 3.9 shows the average cyclone numbers for the 10 clusters in different centuries. There are no large variations between different centuries and the large differences in cyclone counts between the clusters vary very little from century to century. An interesting phenomenon are the variations of cyclone counts over the North Atlantic (Figure 3.9: cluster 8, 9 and 10) in anomalous climatic periods, like the Medieval Climate Anomaly (MCA, 950 – 1250 AD) and the Little Ice Age (LIA, 1500 – 1700 AD) (Keigwin 1996). For example, Raible et al. (2007) found that cyclone density is accompanied by high strong wind speed and precipitation southward shifts in the North Atlantic and Pacific, with concurrent increases in cyclone intensity during winter. However, the differences of cyclone counts over different centuries

can only hardly be recognized (Figure 3.9). Fischer-Bruns et al. (2005) stated that the variations of storm activity are not linearly related to temperature variability within historical times in the ECHO-G simulation between 1500 and 1990 AD. For scenario simulations, however, cyclone trends and density are highly probable to emerge in parallel to temperature changes (Schubert et al. 1998, Ulbrich and Christoph 1999, Fischer-Bruns et al. 2005, and Pinto et al. 2007). This indicates that the possible relationship is more relevant to the rate of temperature change or baroclinic instability (Fischer-Bruns et al. 2005). Nevertheless, there are still uncertainties in storm tracks responding to anthropogenic forcing due to ocean circulation changes (Raible and Blender 2004, Wolling et al. 2012).

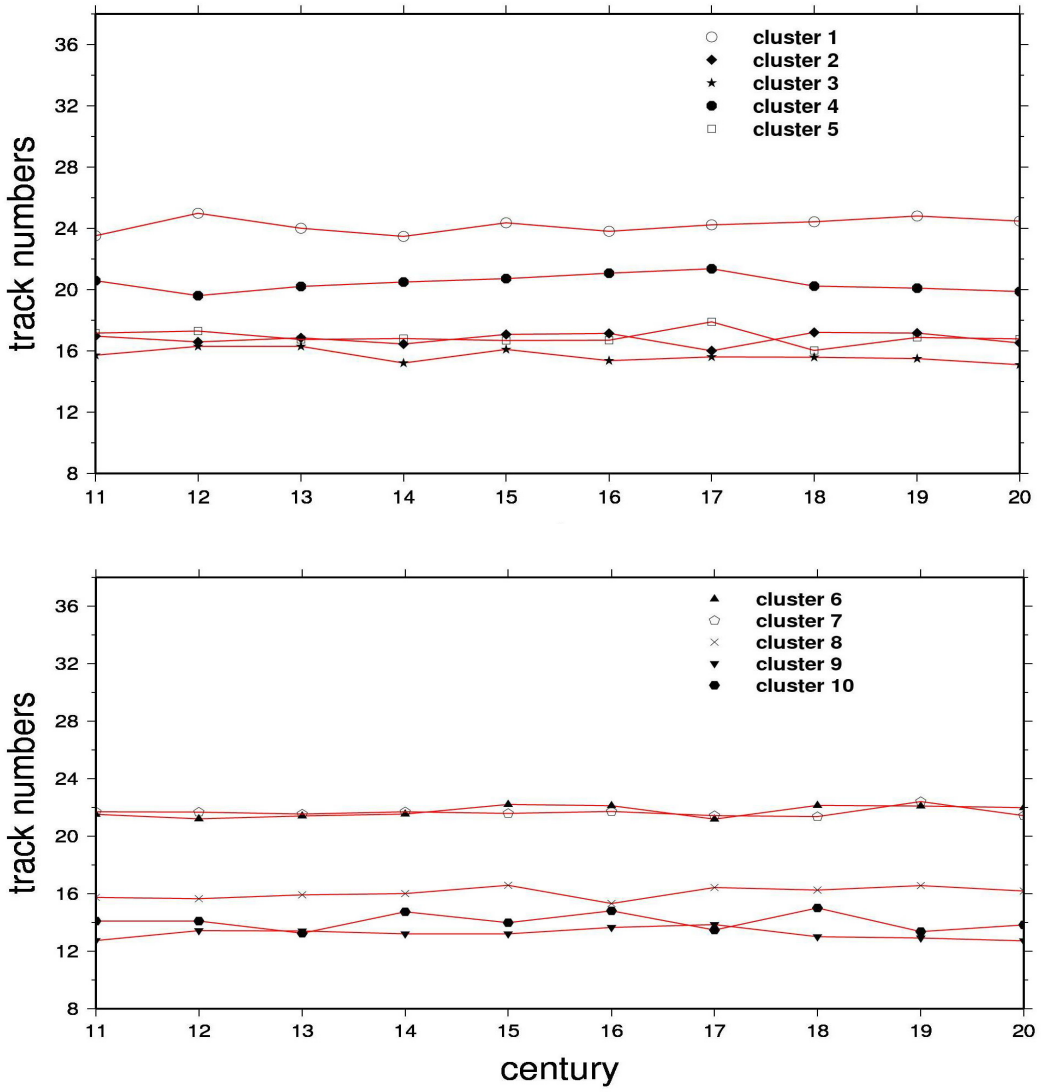

Fig. 3.9 Average annual numbers of winter (DJF) extratropical cyclones over the NH for the ten clusters in different centuries (11^{th} - 20^{th} century).

Table 3.4 shows the distribution of lifetimes for all clusters. Overall, the highest percentage is found for the lifetimes of 2-4 days. For clusters 2, 3 and 6 over 60% of tracks last between 2 and 4 days. Cluster 8, primarily located over the eastern North American coast, contains most long-lived (more than 10 days) cyclones with about 7% of all its cyclones (Table 3.4 and Figure 3.10 b). Over the Atlantic, the eastern cluster 10, extending from southeastern Iceland to the Norwegian Sea, shows an average lifetime of about 5 days. The number of long-lived cyclones (5.0%) is a slightly increased compared to cluster 9. For the Pacific, cluster 4 contains the highest percentage (5.6%) of cyclones lasting more than 10 days with a mean lifetime of about 6 days (Figure 3.10 a). In general, cyclones travelling from land to the ocean tend to exist for a longer time, such as those in clusters 3 and 7. The warm Kuroshio current in the Pacific and the Gulf stream in the Atlantic play important roles in generating baroclinic situations favoring the existence of cyclones. Latent heat release and moisture convergence over the ocean also contribute to the development and persistence of cyclones.

In addition to analyses presented above, also deepening rates for each track were determined, and frequency distributions for these rates for all tracks in a cluster were derived. The "averaged" deepening rate is calculated for the period from genesis location to the maximum pressure value. The "maximum" deepening rate" is the largest pressure decrease along a track.

Table 3.5:Mean deepening rate (hPa/12h) distributions of the ten clusters shown in Fig. 3.7 for the quasi- millennial time period (years 1001 – 1990 AD). Unit: %.

Mean deepening rates (hPa/12h)	<-10	-10~-8	-8~-6	-6~-4	-4~-2	-2~0
Cluster 1	0.08	0.34	1.95	11.44	45.79	40.40
Cluster 2	0.07	0.27	1.52	9.01	38.62	50.51
Cluster 3	0.10	0.57	2.86	14.54	36.98	44.95
Cluster 4	2.15	5.05	13.99	30.70	31.69	16.42
Cluster 5	7.12	9.90	18.13	26.01	25.44	13.40
Cluster 6	6.23	7.83	13.65	22.73	30.92	18.63
Cluster 7	0.23	0.69	3.41	14.84	42.22	38.61
Cluster 8	1.55	4.37	12.40	29.49	38.19	14.00
Cluster 9	2.65	4.19	9.60	21.67	38.37	23.51
Cluster 10	0.59	1.22	4.45	15.17	45.00	33.56

Table 3.5 shows the mean deepening rates per 12 hours for the ten clusters for the whole time period 1001 – 1990 AD. In the Atlantic, the average deepening rates are mainly between 2-4 hPa/12h for clusters 8, 9 and 10 with 38.2%, 38.4% and 45.0%, respectively (Figure 3.10 d and Table 3.5). Cluster 8 for the eastern North American coast also shows an elevated average deepening rate of 4-6 hPa/12h. In the Pacific, there are more cyclones with an average deepening rate between 4 to 6 hPa/12h compared with Atlantic cyclones, most evident in cluster 4 over the western Pacific (30.7%, Figure 3.10 c). For the other clusters average deepening rates are mostly around 0 to 2 hPa/12h, except for clusters 1 and 7 showing their largest deepening rate percentage between 2 to 4 hPa per 12 hours (Table 3.5).

Table 3.6 lists the distributions of maximum deepening rates per 12 hours. Figure 3.10 e and f show maximum deepening rates for the Pacific and the Atlantic. In the Pacific, more than about 25% of all cyclones are related with a rapid maximum deepening of more than 10hPa/12h. Cluster 5 over the central Pacific shows the highest maximum deepening rate (36.6%) with more than 10 hPa per 12h (Figure 3.10 e). Over the Atlantic, the maximum deepening rates of more than 10 hPa per 12h occur less often than over the Pacific. Only cluster 8 over the eastern North American coast shows a maximum deepening over 10 hPa per 12h for 23.4% of all its cyclones (Figure 3.10 f). Cluster 9 (22.2%) over southern Greenland, and cluster 10 (26.9%) extending from southeastern Iceland into the Norwegian Sea show mainly maximum deepening rates of 4-6 hPa/12h. From the studies of Gulev et al. (2001) analyzing NCEP/NCAR re-analysis and from Uccellini (1990) it is known that the largest deepening takes place over the oceans. Thus, the statistics of the ECHO-G cyclone clusters are found to be consistent with the previous studies of "observed" cyclone activity.

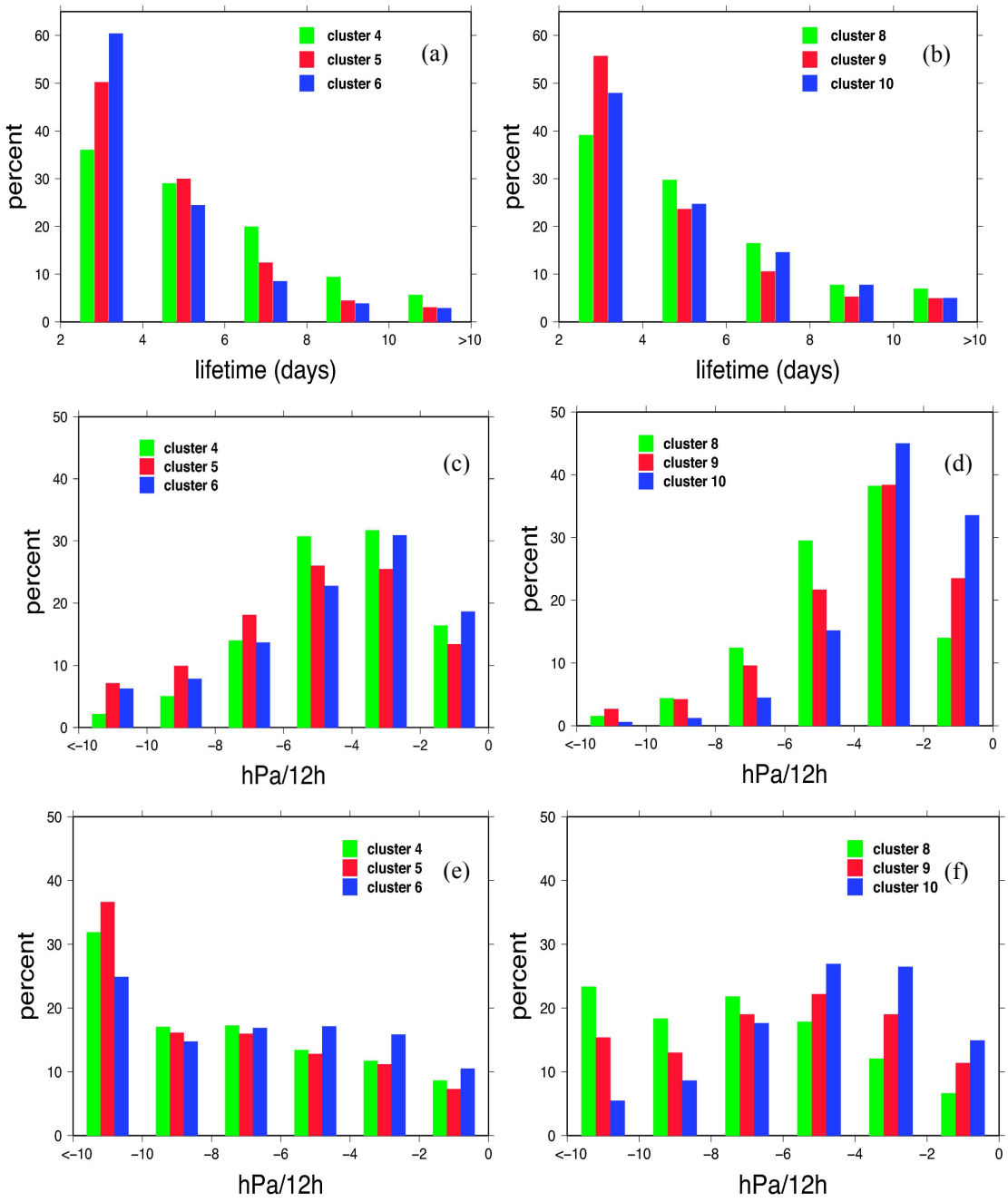

Fig. 3.10 Distributions (%) of cyclone lifetime (days) (a and b), mean deepening rates (hPa/12h) (c and d), and maximum deepening rates (hPa/12h) (e and f) for winter cyclones over the Pacific (a, c and e) and the Atlantic (b, d and f) for the whole time period (years 1001 − 1990 AD).

Figure 3.11 shows changes of the maximum deepening rates for the Atlantic and Pacific clusters during different centuries. In the 20th century maximum deepening rates larger than 10 hPa per 12h become less frequent for cluster 8 but more frequent for cluster 10 in the Atlantic (Figure 3.11 right). Between the 17th and 18th century the maximum deepening rates for cluster 8 of between 6 to 8 hPa per 12h become more frequent, but those larger than 8 hPa per 12h less frequent. There are tendencies of decreases in the frequency of deep cyclones in the 16th-17th and 19th century for cluster 9 and in the 16th and 19th century for cluster 10. In the Pacific, in the 20th century frequencies of rapidly deepening cyclones (over 10 hPa/12h) slightly increase for cluster 4 and 5 (Figure 3.11 left), and relatively slowly deepening cyclones (2-4 hPa/12h) appear more often in cluster 4 but less so in cluster 6. There are decreases in the frequency of deep cyclones in the 11th and 19th century for cluster 4, during the15th to 16th century for cluster 5, and in the 12th century and during the 14th to 16th century for cluster 6.

Table 3.6: Maximum deepening rate (hPa/12h) distributions of the ten clusters shown in Fig. 3.7 for the quasi- millennial time period (years 1001 – 1990 AD). Unit: %.

Maximum deepening rates(hPa/12h)	<-10	-10~-8	-8~-6	-6~-4	-4~-2	-2~0
Cluster 1	2.27	5.58	15.03	28.81	32.05	16.26
Cluster 2	2.08	3.24	9.57	22.48	36.44	26.19
Cluster 3	9.31	7.15	10.76	16.89	28.23	27.66
Cluster 4	31.89	17.06	17.27	13.42	11.72	8.64
Cluster 5	36.64	16.12	15.96	12.78	11.18	7.31
Cluster 6	24.89	14.76	16.89	17.14	15.84	10.48
Cluster 7	9.45	8.78	14.33	19.74	24.68	23.03
Cluster 8	23.35	18.33	21.81	17.83	12.03	6.64
Cluster 9	15.38	13.01	19.01	22.18	19.02	11.39
Cluster 10	5.47	8.63	17.62	26.91	26.44	14.93

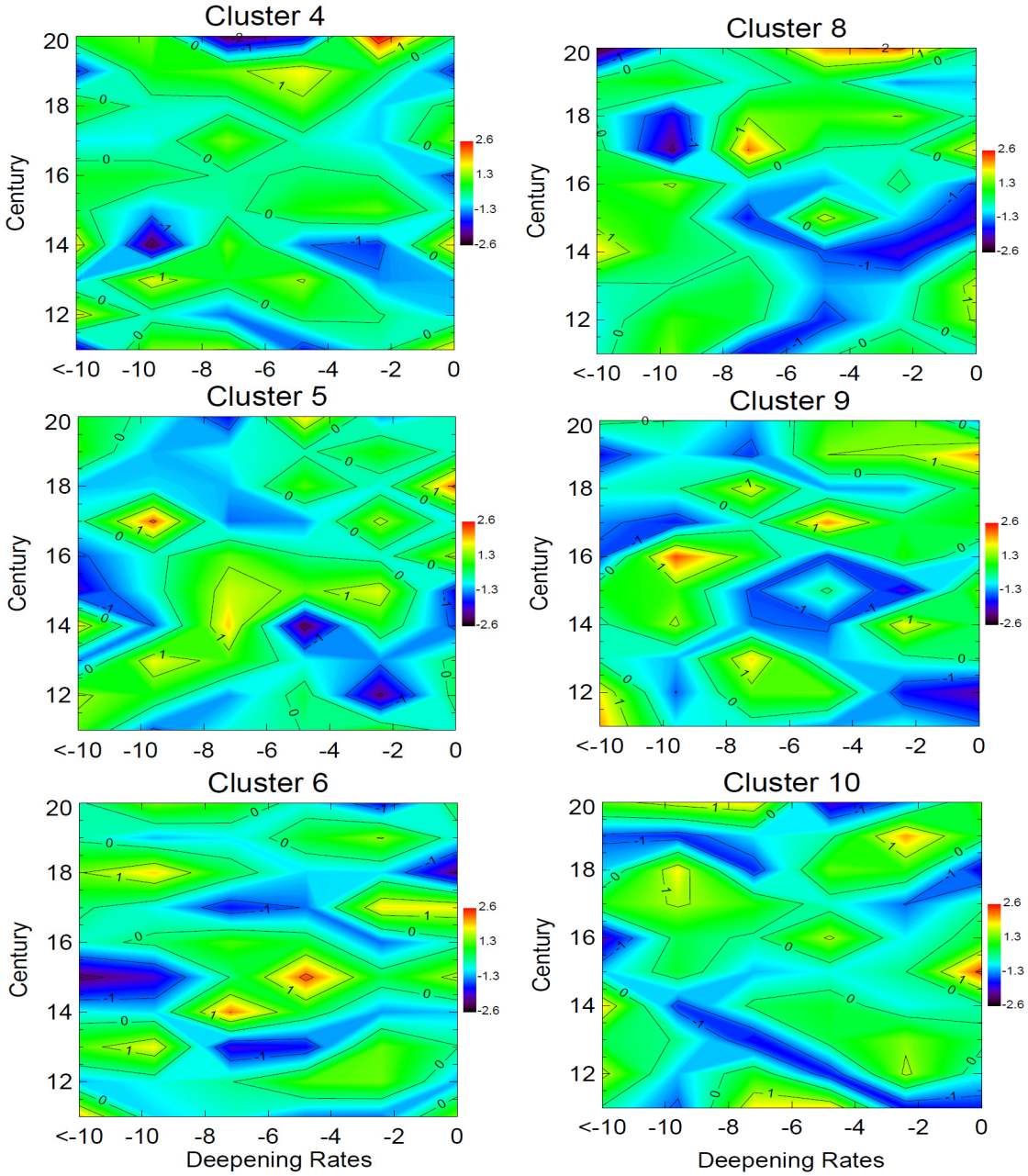

Fig. 3.11 Normalized anomalies of the maximum deepening rate distributions for cluster members over the Pacific (cluster 4, 5 and 6) and the Atlantic (cluster 8, 9 and 10) across different centuries (11^{th} -20^{th} century).

3.4.4 Interactions between clusters

The presence of linkages between cyclonic activities in the Pacific and the Atlantic has been studied before (May and Bengtsson 1998, Sickmöller et al. 2000). Sickmöller et al. (2000) showed that the numbers of north-eastward travelling cyclones in the North Pacific are related to the frequency of the north-eastward and zonal travelling cyclones in the North Atlantic. It was also suggested by Sickmöller et al. (2000) that upper-level Pacific depressions could cross North America and influence the genesis of cyclones over the western Atlantic.

We analyzed the correlations of the numbers between the ten clusters (Table 3.7), as derived from all 990 years of the simulation. The numbers of tracks for each cluster show no obvious serial correlations. The main feature is the negative correlations between neighboring clusters, which is statistically significant at the 5% level. However, negative correlations between neighboring clusters are not very large, e.g., between the Atlantic clusters 8 and 9 (r=-0.23), the Pacific clusters 4/5 (r=-0.22) and 5/6 (r=-0.32), the continental clusters 7/8 (r=-0.22) and 1/10 (r=-0.21). Also small and mostly statistically non-significant correlations emerge between non-neighboring clusters across the North American continent such as clusters 6/8 (r=-0.12), 6/9 (r=+0.13), and 6/10 (r=+0.11). Thus even though the linkage between neighboring clusters is not strong it resembles a robust feature, while the remote linkages are very weak.

Table 3.7: Correlations of time series of winter cyclone numbers between the ten clusters shown in Fig. 3.7 (years 1001-1990): blue ones denote statistically significant correlation coefficients at the 5% level according to a t-test.

clusters	2	3	4	5	6	7	8	9	10
1	-0.17	0.02	0.01	0	0.03	-0.02	-0.03	-0.01	-0.21
2		-0.04	0	0	0.01	-0.02	-0.03	0.06	-0.02
3			-0.11	-0.11	0.02	-0.08	0.02	0.03	-0.02
4				-0.22	-0.10	0.02	-0.03	0.01	0
5					-0.32	-0.09	0.09	-0.02	-0.04
6						-0.06	-0.12	0.13	0.11
7							-0.22	0.01	-0.01
8								-0.23	-0.10
9									0.01

3.4.5 Links to large-scale pressure patterns

In the following we investigate how annual mean MSLP patterns are related to the annual numbers of cyclones in the Pacific and the Atlantic. The Canonical Correlation Analysis (CCA) (von Storch and Zwiers 1999, Zahn and von Storch 2008b) is used to determine systematic mutual dependencies in the annual MSLP fields and yearly cyclone counts for the three clusters in the North Pacific and the North Atlantic sector separately.

Prior to the CCA, a data compression was carried out by truncating the high-dimensional MSLP fields into the leading thirteen Empirical Orthogonal Functions (EOFs) (Gulev et al. 2001, Zahn and von Storch 2008b). The fields, both EOF-truncated MSLP as well as cluster counts, are based on deviations from the long-term (990 years) mean, i.e. annual anomalies.

Figures 3.12 and 3.13 show the two most important patterns linking MSLP and cyclone frequency anomalies in the North Pacific sector. The canonical correlation between the time coefficients of the first (second) CCA pattern are r=0.6 (r=0.4) and the pattern represent 48% (35%) of the variance of winter cyclone counts in the Pacific.

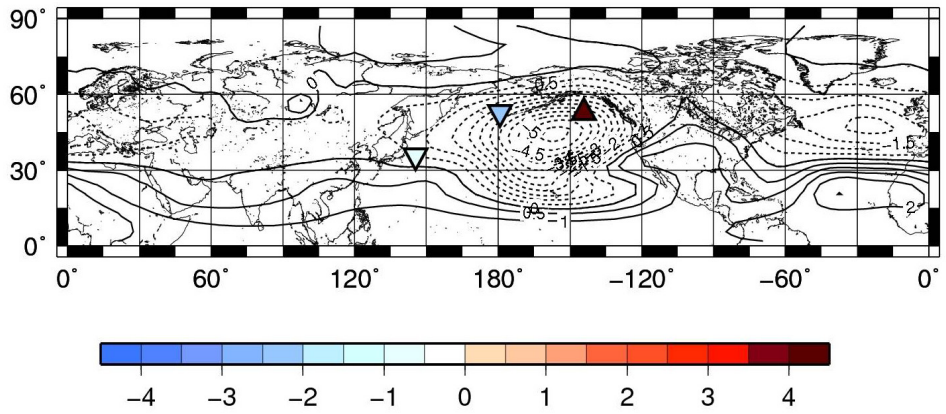

Fig. 3.12 Canonical correlation patterns between time series of winter (DJF) cyclone numbers in the Pacific (clusters 4, 5 and 6) (triangles: for positive values, inverted triangles: for negative values) and mean sea level pressure fields in hPa (isolines: dashed for negative and solid for positive). The first CCA pair shares a correlation coefficient of r=0.59 and represents 48% of the variance of winter cyclone numbers for the period 1001 – 1990 AD. Cyclone frequency anomalies are -0.6 for cluster 4, -2.2 for cluster 5, and +4.6 for cluster 6.

The first Pacific pattern (Figure 3.12) represents a unipolar pressure pattern with a center around the Aleutian Islands with minimum values below -4.5 hPa. For example, given the CCA coefficient at a certain time equals 1, then the maximum annual mean Aleutian pressure anomaly is below -4.5 hPa and the number of cyclones in cluster 4 is decreased by 0.6, in cluster 5 decreased by 2.2 and increased in cluster 6 by 4.6. Thus, when the CCA pattern shows a positive time coefficient, the Aleutian Low tends to be stronger (lower pressure) and cyclone numbers of the eastern cluster 6 increase whereas cyclone counts in the western cluster 4 and central cluster 5 over the North Pacific tend to be lower.

The second pattern (Figure 3.13) describes a bipolar pressure pattern between the Aleutian Islands and North America with a pressure difference of more than 3 hPa. This relates to a decrease/increase of cyclone counts in the western North Pacific (cluster 4) but increase/decrease in the central (cluster 5) and eastern North Pacific (cluster 6). This pattern seems to be related to the Pacific North American Oscillation (PNA) pattern, albeit with a shift. The PNA pattern is associated with the East Asian jet stream and could influence cyclone genesis in the eastern North Pacific to a high degree (Sickmöller et al. 2000, Gulev et al. 2001). Christoph and Ulbrich (2000) also suggested the PNA patterns as important for impacts on cyclone activity in the western North Atlantic.

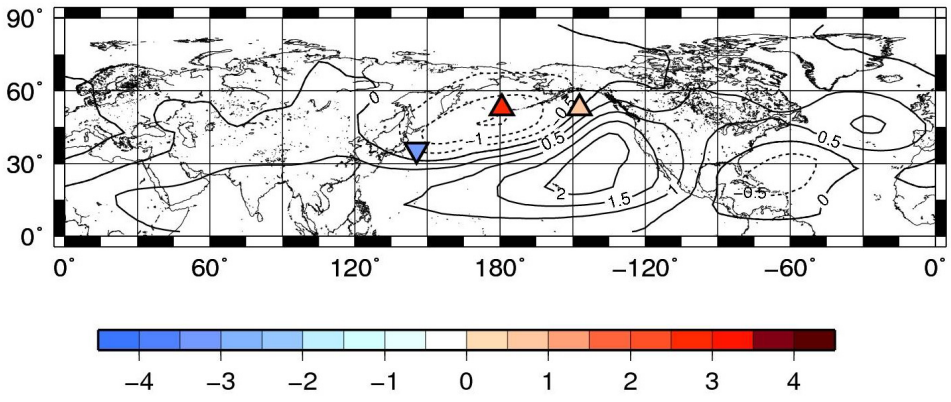

Fig. 3.13 Same as Fig. 3.12 for the second CCA pair: The canonical correlation is r=0.39 and represents 35% of the variance of winter cyclone numbers for the period 1001 – 1990 AD. Cyclone frequency anomalies are -3.2 for cluster 4, +2.9 for cluster 5, and +0.6 for cluster 6.

Figure 3.14 and 3.15 are the CCA patterns for clusters 8, 9 and 10 over the North Atlantic. The first pattern has a canonical correlation of r=0.5 and the second pattern shares a correlation of r=0.3. The patterns represent about 39% and 31% of the year-to-year variance for winter cyclone counts, respectively.

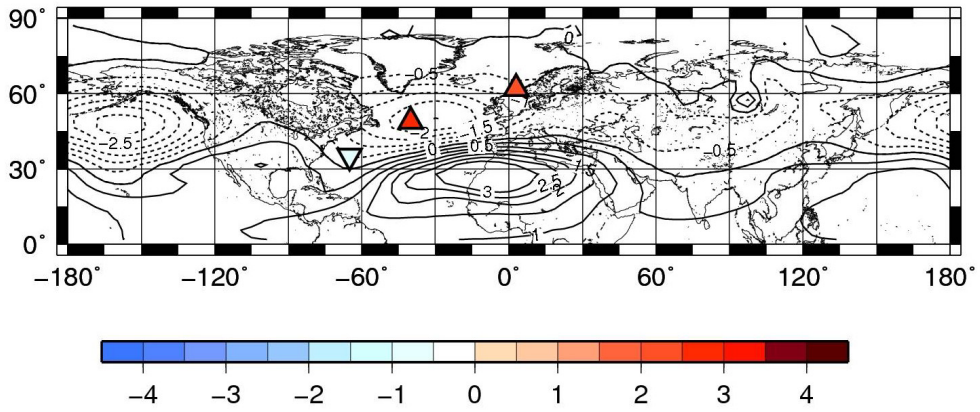

Fig. 3.14 Canonical correlation patterns between time series of winter (DJF) cyclone numbers in the Atlantic (clusters 8, 9 and 10) (triangles: for positive values, inverted triangles: for negative values) and mean sea level pressure fields in hPa (isolines: dashed for negative and solid for positive). The first CCA pair shares a correlation coefficient of r=0.51 and represents 39% of the variance of winter cyclone numbers for the period 1001 – 1990 AD. Cyclone frequency anomalies are -0.9 for cluster 8, +3.0 for cluster 9, and +2.0 for cluster 10.

The first pattern (Figure 3.14) indicates a dipole located over the Iceland region and the subtropical North Atlantic with a pressure difference of more than 4 hPa. This pattern is obviously related to the North Atlantic Oscillation (NAO) pattern with deeper/higher Iceland low and higher/shallower subtropical high. In the positive phase (deeper Icelandic Low) there are more cyclones for cluster 9 and cluster 10 over the southeast of Greenland and northeastern Atlantic, in accordance with the study of Sickmöller et al. (2000). The NAO is known to be associated with variations of storm activity over the North Atlantic (Ulbrich and Christoph 1999, Sickmöller et al. 2000, Gulev et al. 2001, Pinto et al. 2007 and Raible et al. 2007). In its positive phase, cold air from Arctic areas is encountering the warm North Atlantic current, and baroclinicity increases over the North Atlantic. The zonal winds also strengthen to further increase baroclinicity. This leads to more cyclone activity over the northeastern Atlantic. A systematic shift of NAO variability could results in changes of cyclone density or intensity (Ulbich and Christoph 1999, Pinto et al. 2007). In its negative

phase, with a shallower Icelandic Low, cyclones shift southward and more intense cyclones occur over the Mediterranean area (Raible et al. 2007).

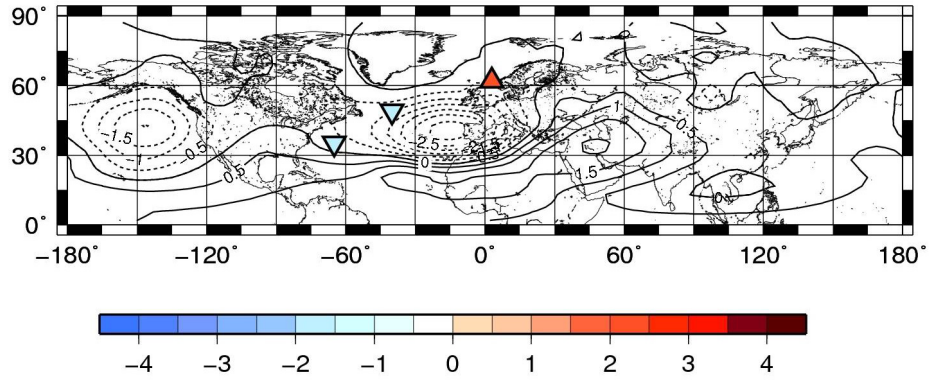

Fig. 3.15 Same as Fig. 3.14 for the second CCA pair: it shares a correlation coefficient of r=0.27 and represents 31% of the variance of winter cyclone numbers for the period 1001 –1990 AD. Cyclone frequency anomalies are -1.7 for cluster 8, -1.7 for cluster 9, and +2.3 for cluster 10.

The second pattern (Figure 3.15) shows a unipolar pattern located over the North Atlantic with negative values of more than -2.5 hPa. According to the sign of the cyclone cluster pattern, more cyclones occur in conjunction with this pressure anomaly pattern along the eastern North Atlantic (cluster 10). At the same time fewer cyclones occur along the coast of North America (cluster 8) and over southern Greenland (cluster 9).

3.5 Conclusions

A coupled global atmosphere-ocean model (ECHO-G) simulation for the last about one thousand years was analyzed for changes in winter storm activity over the Northern Hemisphere. The ECHO-G model was forced with variations of shortwave solar input, volcanic activity changes, and slowly changing greenhouse gas concentrations during the last millennium for the period 1000 – 1990 AD. An automatic tracking algorithm (Hodges 1994, 1995, and 1999) was used to locate extratropical cyclones within the simulated MSLP fields. For validation reasons, the tracks were also compared with coarsened NCEP/NCAR reanalysis data. The main result of the study is that the time series of cyclone counts for the years 1001 to 1990 AD show strong year to year variations, but an obvious trend was not

found. The centennial variability of storm tracks is very small, whereas the centennial variation of hemispheric mean temperature is large.

Tracks were clustered into ten groups by applying the K-means method. The clusters mainly correspond to the cyclone genesis areas. Frequency and distributions of lifetime as well as deepening rates were studied for the ten clusters. The oceanic cyclones show rapid deepening rates and a relatively long lifetime. Storm tracks in the Pacific are clustered into three groups: tracks over the western North Pacific, in the central North Pacific and in the eastern Pacific. In the North Atlantic, tracks are also grouped into three clusters: tracks are located over the eastern North American coast, southern Greenland, and southeastern Iceland and the Norwegian Sea. The frequencies of cyclones in these two oceans are connected to large-scale pressure patterns. The main results for the North Pacific and North Atlantic sectors are as follows:

North Pacific: Most cyclones occur in the eastern North Pacific, and fewest in the central North Pacific. Cyclones in the western North Pacific show longest lifetime (average lifetime of 6 days) and also show the highest percentage of cyclones lasting for more than 10 days. Cyclones over the central North Pacific indicate the highest proportions to deepen rapidly (>10 hPa per 12h). In the 20th century those cyclones that deepen rapidly (> 10hPa per 12h) become slightly more frequent over the western and central North Pacific. Frequencies of cyclones over the western, central and eastern North Pacific are correlated among each other and are also related to the intensity of the Aleutian Low. When the Aleutian Low is stronger, the number of cyclones in the eastern North Pacific increases. Cyclones in the eastern North Pacific show only weak teleconnections across the North American continent to cyclones in the North Atlantic.

North Atlantic: Cyclones located over the eastern North American coast show the largest total numbers, the longest lifetimes with an average lifespan of 6 days, and also most cyclones which deepen rapidly (>10 hPa per 12h) occur in this region. In the 20th century those rapidly deepening cyclones become less frequent over the eastern North American coast, but more frequent over southeastern Iceland and the Norwegian Sea. Cyclone counts over the North Atlantic are correlated with the NAO pattern. During the positive NAO phase, there are more cyclones over the region southeast of Greenland, the northeastern Atlantic and northwest Europe. In general, the cyclone numbers over the North Atlantic are lower compared to the

North Pacific. In addition, more cyclones over the North Pacific than over the North Atlantic show a strong deepening rate of at least 10hPa/12h.

We conclude that the simulation of the last millennium shows only smaller variations on centennial time scale and no long-term trends for the whole period. This is valid for the location and numbers of cyclone tracks which are changing only marginally.

There are a number of caveats: First, the data are generated by a model as a response to prescribed, estimated external forcing (solar, volcanic material, greenhouse gases). These estimated external forcing factors may deviate from the real evolution due to uncertainties involved in their reconstruction. For example, discussions so far point to an overestimation of solar and volcanic factors. Assuming this overestimation in the amplitude and impact of changes in external forcing factors, the conclusions of "little centennial variations of storm track statistics" would not be affected. Also the model may show too small variations of storm activity, in particular related to the coarse spatial resolution of T30. Comparison with other studies indicates that there may be an underestimation, but this would be stationary in time, so that our conclusion about temporal variability would not be affected. Finally, the relatively infrequent storing of MSLP fields, only once in every 12 hours, may have lead to too few detectable storms. We consider this possibility also less relevant, first because of successful previous studies with this "coarse" gridding. Again, such a bias would hardly affect the strength of the variations of cyclone numbers. But all in all, these caveats must be acknowledged, and future studies of similar millennial simulations, with better horizontal and temporal gridding, will help to disentangle the influence of the different external and model specific factors on the results obtained in this study.

Chapter 4 Summary, discussions and outlook

4.1 Summary

In this study, the variability of storm track characteristics is studied in terms of polar lows in the North Atlantic and extratropical cyclones in the Northern Hemisphere. According to the questions raised in Section 1.4, two main investigations were carried out: first, two identification and tracking algorithms are compared for tracking polar lows with relatively high resolution data from the regional climate model CCLM. Second, the centennial scale variability of extratropical winter storm numbers in the Northern Hemisphere is studied in the lens of tracking and clustering analysis using a global climate simulation covering the last millennium. The main conclusions can be summarized as follows:

1. The tracking method from Hodges (1994, 1995, and 1999) (KH method), which was originally designed for tracking cyclones in general, can be adapted to track polar lows. Compared with the method of Zahn and von Storch (2008a) (MZ method) that is especially designed for detecting polar lows, the main difference arises from the different filters applied in both methods. The detection and tracking parts of both methods also influence the numbers of tracks although less critically.

2. Quasi-stationarity is shown for Northern Hemisphere midlatitude winter storm tracks at the centennial time scales. There are only smaller variations on centennial time scale for extratropical cyclone counts, whereas the centennial variation of hemispheric mean temperature is larger. In addition, there are no long-term trends of extratropical cyclones for the whole period from 1001 to 1990 AD. This stationarity is also valid for the track locations indicating only minor changes.

For the first conclusion, it is important to know that the digital filter used by Zahn and von Storch (2008a) is less precise at scale separation according to wave numbers. When filtering variables like MSLP, the wave number parts that stem from the imperfect scale separation contain large values that influence the filter results. Hence we recommend that the DCT filter is better suited, especially for MSLP fields. The filtered vorticity fields obtained by the digital and DCT filters are much more similar, hence it might be expected that smaller differences might occur between polar lows detected by the KH and MZ methods when applied to this field. After a selection process that applies criteria to identify tracks of potential polar lows,

differences between both methods are still visible, although the major systems are identified by both schemes.

For the second part of this study tracks were clustered into ten groups by applying the K-means method. The cluster results mainly correspond to the cyclone genesis areas. Frequency and distributions of lifetime as well as deepening rates were studied for the ten clusters. The oceanic cyclones show rapid deepening rates and a relatively long lifetime.

Storm tracks in the North Pacific are clustered into three groups representing regions over the western, central, and the eastern North Pacific, respectively. Most cyclones occur in the eastern North Pacific, whereas fewest are in the central North Pacific. Cyclones in the western North Pacific show highest persistence with an average lifetime of 6 days and also show the highest percentage of cyclones lasting more than 10 days. Frequencies of cyclones over the North Pacific are related to the Aleutian Low. Periods with intensified Aleutian Low are related to a larger number of cyclones in the eastern Pacific. Cyclones over the eastern Pacific show weak teleconnections across the American continent with cyclones over the North Atlantic.

Over the North Atlantic, tracks are also grouped into three clusters representing regions over the eastern North American coast, southern Greenland, and southeastern Iceland and the Norwegian Sea. Cyclones located over the eastern North American coast show the highest total numbers, the longest lifetimes with an average lifespan of 6 days, and also most cyclones which deepen rapidly occur in this region. The number of cyclones over the North Atlantic is correlated to the phase of the North Atlantic Oscillation (NAO). During the positive NAO phase, more cyclones occur over the southeast of Greenland, the northeastern Atlantic and northwestern Europe. Cyclone numbers over the Atlantic are lower than for the Pacific. In addition, more cyclones occur over the North Pacific than over the North Atlantic in conjunction with pronounced deepening rates of at least 10hPa/12h.

Results of a clustering analysis related to long-term cyclone changes over the last millennium indicate that only smaller cyclone number variations occur on decadal to centennial time scales for ten clusters. The mean location of cyclone tracks within the ten clusters changes only marginally compared between the 11th century and 20th century. The total number of winter cyclones over the Northern Hemisphere for years 1001 to 1990 shows strong year to

year variations, but an obvious trend was not found. The centennial variations of storm tracks over the Northern Hemisphere are quite small and seem to be independent from hemispheric temperature variability during historical times in the ECHO-G simulation.

4.2 Discussions

There are many studies to assess method-related uncertainties on cyclone detection and tracking, such as Raible et al. (2008) who compared three different algorithms with the same input data. Actually the method-related uncertainties are quite important due to contradictory climate trends of cyclones that can result even from analyses based on identical datasets (Ulbrich et al. 2009). Therefore it is essential to study the uncertainties with regard to the different methods used. The project IMILAST (Intercomparison of MId-LAtitude STorm diagnostics) was initiated to intercompare extratropical cyclone detection and tracking algorithms. Fifteen detection and tracking algorithms were compared for extratropical cyclones (Neu et al. 2012). They found that methods are consistent for globally patterns in geographical distribution and interannual variability, but there are largest spreads between different algorithms on the total numbers of cyclones especially the numbers of weak cyclones. Diagnosing the detailed reasons for differences associated with characteristics of different schemes will be in the next phase of IMILAST work. Although these investigations mainly compared methods designed to study extratropical cyclones in general, not for very specific types like polar lows, the consequences of IMILAST are similar with those in our study that various selections and settings in filtering, detection and tracking of different methods could influence the numbers of polar lows.

In order to extract mesoscale systems like polar lows, band-pass filtering is applied before detection and tracking. This differs from tracking general extratropical cyclones. For tracking extratropical cyclones, detection is applied directly on MSLP or vorticity fields to extract extremes (Serreze 1995, Murray and Simmonds 1991, Zolina and Gulev 2002) or using high-pass filtered fields (Hoskins and Hodges 2002). However, based on results from this study, it can be concluded that different filters used in two tracking schemes lead to different numbers and locations of tracks. In this context the filter's influence on the numbers of polar low tracks is far more crucial than the detection and tracking parts of different schemes.

One important result is related to the fact that the digital filter and DCT show much larger similarity for vorticity fields than for MSLP fields. Indeed there are wide discussions about

the choices of MSLP or vortiticy as a basis for tracking in different methods (Hodges et al. 2003, Rudeva and Gulev 2007, Ulbrich et al. 2009). MSLP represents relatively slower moving systems and is more influenced by large scales and background flow as discussed in Chapter 2, while vorticity is more suitable to identify small-scale systems and less influenced by the large-scale background flow (Hodges et al. 2003). Moreover, MSLP is more sensitive to the topography due to extrapolation applied and there might be artificial minima occurring along coastlines or over areas with complex terrain after filtering. In constrast to MSLP, vorticity fields could be very noisy when using high-resolution data. In addition pressure minima are not definitely connected with vorticity maxima and therefore different cyclone centres may be identified. Thus it would be quite interesting for future work to explore this issue to assess if the spatially filtered vorticity fields are a better alternative to the spatially filtered MSLP fields by applying both tracking schemes to the vorticity for tracking polar lows.

For the second parts on the quasi-millennium cyclone activities, the data are derived from a climate model as a response to prescribed estimated external forcing (solar, volcanic eruptions, greenhouse gases). The change in the external forcing applied to the model, such as orbital parameters, also might impact the density and location of storm tracks. For example, greater obliquity and eccentricity combined with changes in the perihelion in northern hemisphere summer resulted in the Eemian interglacial at 125 000 years before present, while the opposite angle of perihelion results in the onset of last glacial at 115 000 years before present. In this context, Kaspar et al. (2007) set the parameters of the Earth's orbit to conditions of 125 000 and 115 000 years before present (yr BP) to force the ECHO-G model. They found that the North Atlantic storm track strengthens and shifts northward and extends further to the east in the simulation of the Eemian at 125 kyr BP. The opposite was found, albeit weaker in amplitude, for the simulation of the last glacial inception at115 kyr BP. Actually the changes in frequency of winter storm days for the Eemian (Kaspar et al. 2007) show similar signals as an ECHO-G climate change simulation for IPCC-SRES scenario A2 and B2 obtained by Fischer-Bruns et al. (2005). Fischer-Bruns et al. (2005) also found poleward storm tracks shift in future scenarios with a strong increase of greenhouse gas concentrations.

The interannual variations in the number of cyclones are likely reduced within the ECHO-G simulation due to the coarse spatial and temporal resolution. Although such a bias would

hardly affect the strength of variations, future studies using similar millennial simulations, with increased horizontal resolution and more frequent temporal output, will help to disentangle the influence of the different external and model-specific factors on the results obtained in this study.

A third aspect addressed in the ECHO-G simulation was the estimation of a linear relationship between the numbers of cyclones over the North Pacific or Atlantic and winter large-scale atmospheric circulation patterns by means of canonical correlation analysis (CCA). According to the time series of winter extratropical cyclone numbers from year 1001 to 1990 AD, it indicates a couple of extreme years with higher or lower cyclone numbers. It would be interesting to see the characteristics of large-scale circulation patterns favoring to these extreme years and investigate their relation to the extremely number of cyclones in greater detail. As preliminary work, we investigated the structure of the mean atmospheric circulation of these extreme years. However, the patterns are not exactly corresponding to the extreme characteristics we previously expected. We suspect that these extreme years are influenced by many moderate or shallow cyclones. Future work might therefore include investigations on the mean atmospheric circulation patterns of extreme years with deepest cyclones. These cyclones are characterized by very low pressure or strengthened deepening rates potentially leading to higher risks of disasters of heavy precipitation and strong winds.

4.3 Outlook

There are different emissions scenarios describing the future release of greenhouse gases and aerosol emissions in the Intergovernmental Panel on Climate Change (IPCC) (Nakicenovic and Swart 2000) which can be used to investigate future global climate changes. It could be also interesting to apply tracking methods on future scenarios to test whether the cyclone locations indicate a shift and to which extent the cyclone numbers changes. Clustering analysis could also be applied to investigate regional cyclone changes. The simulation with the ECHO-G model forced by the IPCC scenario A2 and B2 has been previously analysed to study the storm activity (Fischer-Bruns et al. 2005). Here the simulation of the IPCC scenario A2 by ECHO-G is also used to study the Northern Hemispherical extratropical cyclones responding to climate change. To date, this is the only preliminary analysis and further investigations are currently undertaken.

Figure 4.1 shows the changes of winter extratropical cyclone numbers and temperature in the Northern Hemisphere (NH) for the future climate change scenario A2. The main characteristics of scenario A2 related to increasing emissions with a continuously increasing population but a slow economic and technological development (Nakicenovic and Swart 2000). So there is a strong warming in winter in the Northern Hemisphere (Figure 4.1 red line). The winter extratropical cyclone numbers shows a high year-to-year variability and a slight decrease after 2060. This result is different to Fischer-Bruns et al. (2005) suggesting that Northern Hemispherical storm frequency did not change with scenario A2. However, the result agrees with Pinto et al. (2007) who used ECHAM5/MPI-OM1 simulations for three climate change scenarios (A1B, A2 and B1) and found reductions in cyclone tracks over the northern hemispherical mid-latitudes for all scenario runs. A separate analysis of the cyclone numbers for the North Pacific and North Atlantic, results indicate a decrease in cyclone numbers for the North Pacific (Figure 4.3) in scenario A2, which is consistent with the results of Fischer-Bruns et al. (2005). For the North Atlantic, cyclone numbers do not show distinct changes (Figure 4.4).

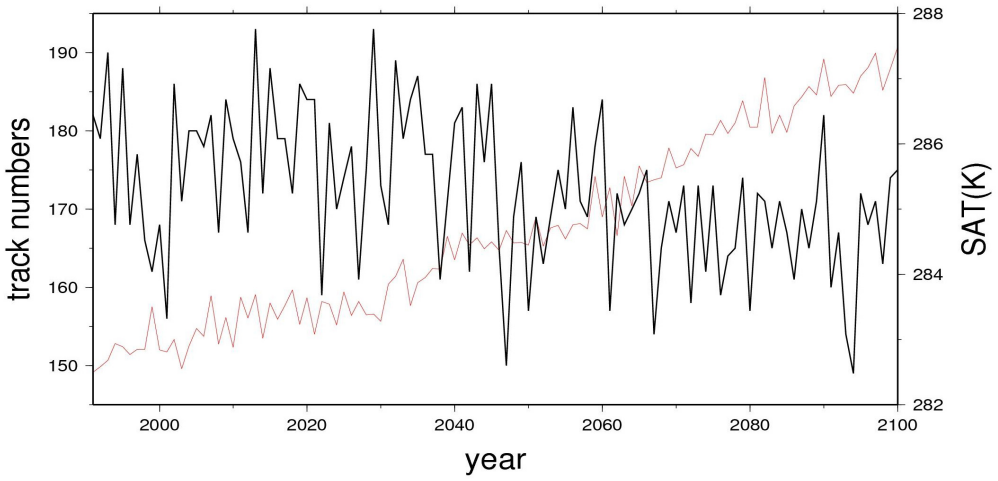

Fig. 4.1 Time series of the numbers of winter (DJF) extratropical cyclones (black line) and winter surface air temperature (SAT: K) (red line) in the Northern Hemisphere (NH) for climate change experiment A2 (years 1991–2100).

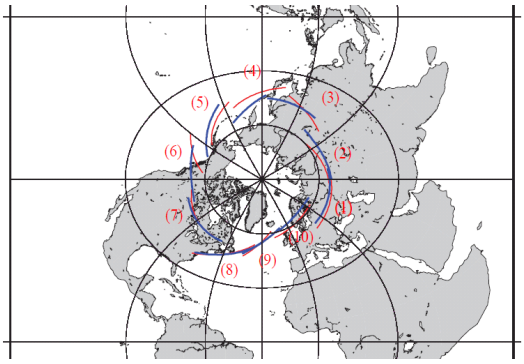

Fig. 4.2 Mean tracks of the ten clusters (red numbers) in the NH for climate change experiment A2: red lines are the mean tracks of the ten clusters in the first decade (years 1991-2000), blue lines are the mean tracks of the ten clusters in the last decade (years 2091-2100).

Cyclone tracks of scenario A2 are also grouped into ten clusters and results indicate that there is a northeastward shift of the mean tracks of the ten clusters with future warming (Figure 4.2). Cluster 4 in the northwestern Pacific and cluster 10 in the northeastern Atlantic show a poleward shift. Other clusters shift eastward, such as cluster 5 and 6 in the North Pacific. Fischer-Bruns et al. (2005) also found that storm day frequency regions shift poleward on both hemispheres in climate change experiment A2. They explained this phenomenon by baroclinicity increases in high latitude areas causing a northward shift of the cyclone genesis and cyclone tracks.

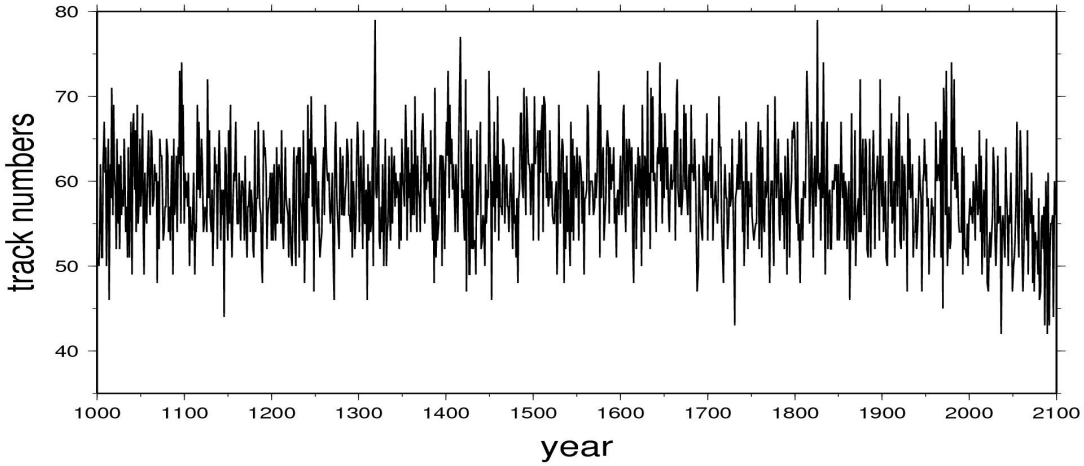

Fig. 4.3 Time series of the numbers of winter (DJF) extratropical cyclones in the North Pacific (sum of track numbers for cluster 4, 5 and 6) for the ECHO-G historical simulation (years 1001-1990) and climate change experiment A2 (years 1991–2100).

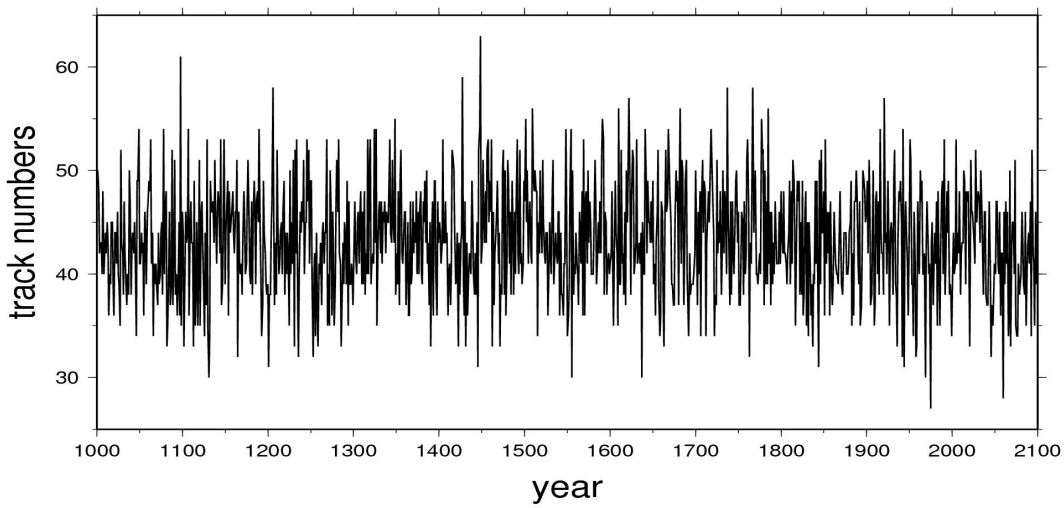

Fig. 4.4 Time series of the numbers of winter (DJF) extratropical cyclones in the North Atlantic (sum of track numbers for cluster 8, 9 and 10) for the ECHO-G historical simulation (years 1001-1990) and climate change experiment A2 (years 1991–2100).

Figure 4.5 compares the maximum deepening rates for winter cyclones over the North Pacific (Figure 4.5 a, c and e) and North Atlantic (Figure 4.5 b, d and f) for different sub-periods. Figure 4.6 is same for the North Pacific (Figure 4.6 a, c and e) and North Atlantic (Figure 4.6 b, d and f) but for the mean deepening rates. It is noteworthy to see the maximum and mean deepening rates change in parallel with increasing temperature between 1991 − 2100. For the North Pacific, the deepening rates exceeding 10hPa/12h decrease considerably for cluster 4, 5 and 6 in scenario A2 (Figure 4.5 a, c and e: blue bar) in comparison with the historical simulations between 1001−1100 and 1901−1990. The maximum deepening rates from 0−6hPa/12h are much higher with climate warming background compared to historical periods. The same is evident for the mean deepening rates that more cyclones with the mean deepening rates from 0−4hPa/12h for the North Pacific region in the scenario time period (Figure 4.6 a, c and e).

Over the North Atlantic, the maximum deepening rates exceeding 10hPa/12h (0−4hPa/12h) of cluster 8 (Figure 4.5 b) located over the eastern North American coast, show clear decreases (increases) between 1991 − 2100. Cluster 9 (Figure 4.5 d) located over southern Greenland reveals a higher percentage of maximum deepening rates from 0−2hPa/12h within climate warming. However, the maximum deepening rates exceeding 10hPa/12h of cluster 10 located around southeastern Iceland and the Norwegian Sea primarily increase within the climate change experiment A2 (Figure 4.5 f). Mean deepening rates of cluster 10 (Figure 4.6 f) also indicate that there are more cyclones deepening fast (increased percentages of the mean

deepening rates over 6hPa/12h) over the northeastern Atlantic in the scenario time period. Other studies analyzing different climate change experiments with other models also indicate increased cyclone intensification rates or intensities in the eastern North Atlantic and Western Europe (Ulbrich an Christoph 1999, Knippertz et al. 2000, and Pinto et al. 2005). Ulbrich and Christoph (1999) and Pinto et al. (2005) link the increased cyclone intensities over the northeastern Atlantic with the enforcing of the North Atlantic Oscillation (NAO) and a north-eastward shift of the NAO centers in the climate change experiments. Knippertz et al. (2000) assumed that the increased upper baroclinity leads to the strong cyclone activity over the North Atlantic. This aspect will be investigated in future research.

Similar analysis for cyclone activities by cyclone tracking and clustering methods will be carried out with other emission scenarios, such as B2 related to moderate emissions and less warming compared to the A2 scenario. Moreover, the influence of climate change on severe hazards, for example strong wind storms, sand storms and floods will be studied as well. These investigations will be accompanied by analyses of potential driving moments, for example related to the changes of the North Atlantic Oscillation under increased greenhouse gas concentrations.

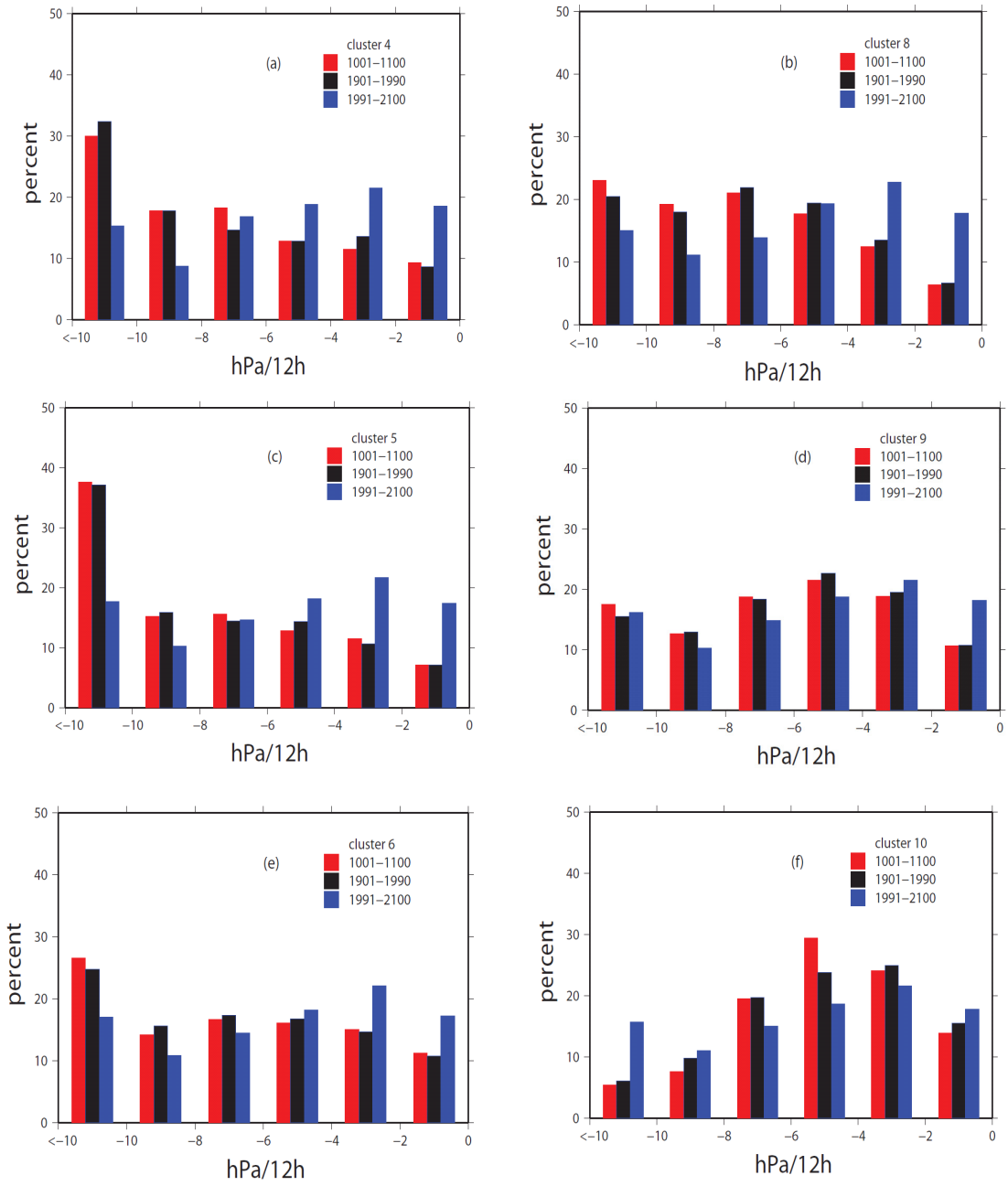

Fig. 4.5 Distributions (%) of cyclone maximum deepening rates (hPa/12h) for the North Pacific (a, c and e) and the North Atlantic (b, d and f) for different sub-period.

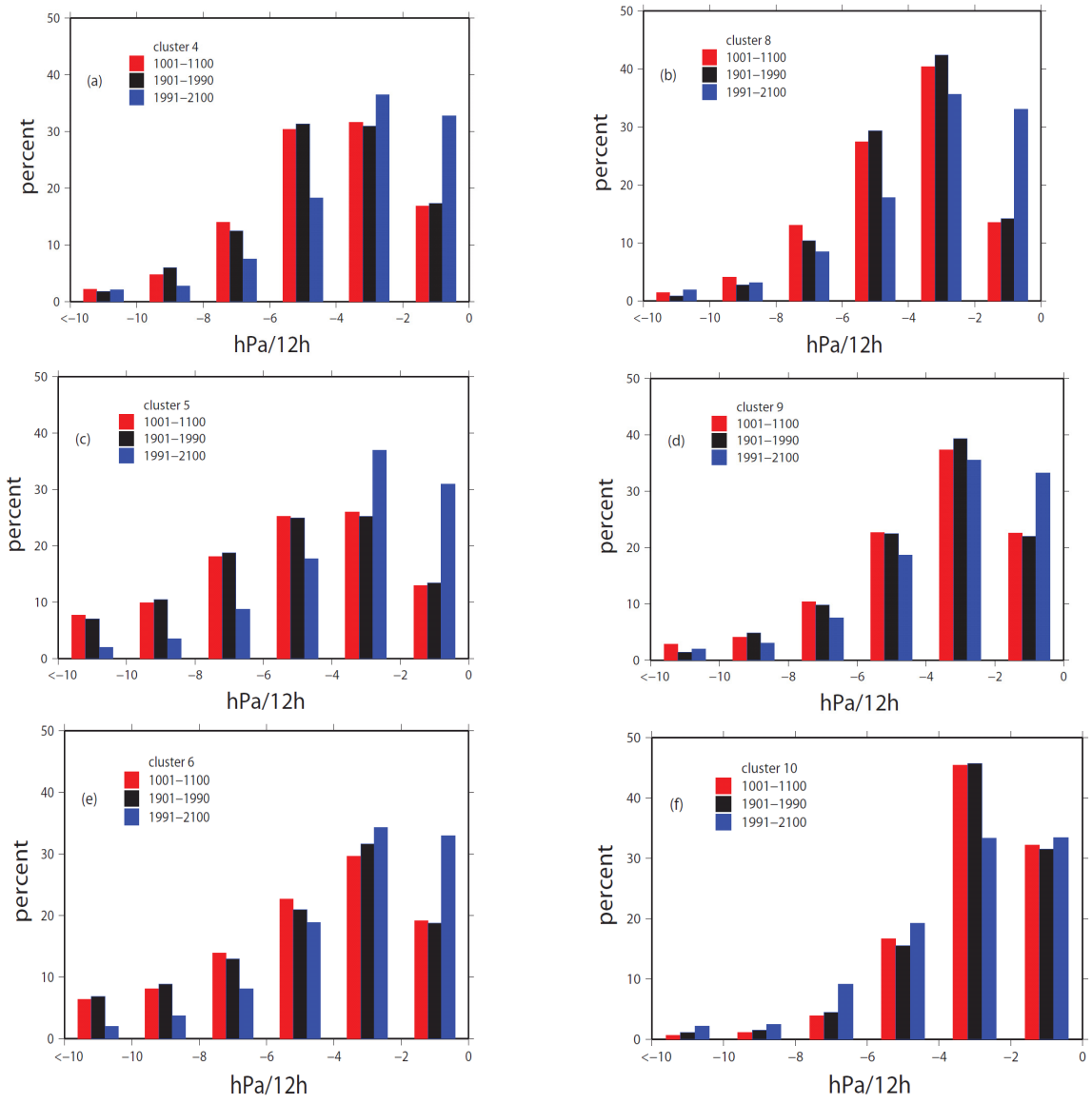

Fig. 4.6 Distributions (%) of cyclone mean deepening rates (hPa/12h) for the North Pacific (a, c and e) and the North Atlantic (b, d and f) for different sub-period.

Reference

Adachi S. and F. Kimura, 2007: A 36-year climatology of surface cyclogenesis in East Asia using high-resolution reanalysis data. *Sola*, **3**, 113-116.

Alexandersson H, T. Schmith, K. Iden, and H. Tuomenvirta, 1998: Longterm variations of the storm climate over NW Europe. *Global Atmosphere Ocean System*, **6**, 97–120.

Alexander L. V., S. F. B. Tett, and T. Jonsson, 2005: Recent observed changes in severe storms over the United Kingdom and Iceland. *Geophysical Research Letters*, **32**, L13704.

Anderson D., K. I. Hodges, and B. J. Hoskins, 2003: Sensitivity of Feature Based Analysis Methods of Storm Tracks to the Form of Background Field Removal, *Monthly Weather Review*, **131**, 565-573.

Bärring L. and H. von Storch, 2004: Scandinavian storminess since about 1800. *Geophysical Research Letters*, **31**, L20202.

Bengtsson L. and K. I. Hodges, 2006: Storm tracks and climate change. *Journal of Climate*, **19**, 3518-3543.

Bender F. A-M., V. Ramanathan, and G. Tselioudis, 2012: Changes in extratropical storm track cloudiness 1983-2008: Observation support for a poleward shift. *Climate Dynamics*, **38**, 2037-2053.

Böhm U., M. Kücken, D. Hauffe, F.-W. Gerstengarbe, P. C. Werner, M. Flechsig and co-authors, 2004: Reliability of regional climate model simulation of extremes and of long-term climate. *Natural Hazards and Earth System Sciences*, **4**, 417-431.

Böhm U, M. Kücken, W. Ahrens, A. Block, D. Hauffe, K. Keuler and co-authors, 2006: CLM − The climate version of LM: brief description and long-term applications. *COSMO Newsletter*, **6**, 225-235.

Blackmon M. L., 1976: A climatological spectral study of the 500 mb geopotential height of the Northern Hemisphere. *Journal of the Atmospheric Science*, **33**, 1607-1623.

Blender R., K. Fraedrich and F. Lunkeit, 1997: Identification of cyclone-track regimes in the North Atlantic. *Quarterly Journal of the Royal Meteorological Society*, **123**, 727-741.

Blender R. and M. Schubert, 2000: Cyclone tracking in different spatial and temporal resolutions. *Monthly Weather Review*, **128**, 377-384.

Brayshaw D. J., B. Hoskin, and M. Blackburn, 2008: The storm-track response to idealized SST perturbations in an aquaplanet GCM. *Journal of the Atmospheric Sciences*, **65**, 2842-2860.

Christoph M. and U. Ulbrich, 2000: Can NAO-PNA relationship be established via the North Atlantic storm track? *Geophysical Research Abstracts*, **2**, 215.

Chu P., X. Zhao and J. Kim, 2010: Regional typhoon activity as revealed by track patterns and climate change. *Hurricanes and Climate Change*, **2**, 137-148.

Chen F., B. Geyer, M. Zahn, and H. von Storch, 2012: Toward a multi-decadal climatology of North Pacific polar lows employing dynamical downscaling. *Terrestrial Atmospheric and Ocean Sciences*, **23(3)**, 291-301.

Claud C., G. Heinemann, E. Raustein, and L. Mcmurdie, 2004: Polar low le Cygne: satellite observations and numerical simulations. *Quarterly Journal of the Royal Meteorological Society*, **130**, 1075-1102.

Davies H. C., 1976: A lateral boundary formulation for multi-level prediction models. *Quarterly Journal of the Royal Meteorological Society*, **102**, 405-418.

Denis B., J. Cote, and R. Laprise, 2002: Spectral decomposition of two-dimensional atmospheric fields on limited-area domains using the discrete cosine transform (DCT). *Monthly Weather Review*, **130**, 1812-1829.

Déqué M., R. Jones, M. Wold, F. Giorgi, J. Christensen and co-authors, 2005: Global high resolution versus limited area model climate change projections over Europe: quantifying confidence level from PRUDENCE results. *Climate Dynamics*, **25**, 653-670.

Dierckx P., 1981: An algorithm for surface-fitting with spline functions. *IMA J. Numer. Anal.* **1(3)**, 267-283.

Dierckx P., 1984: Algorithms for smoothing data on the sphere with tensor product splines. *Computing*, **32**, 319-342.

Duncan C. N., 1977: A numerical investigation of polar lows, *Quarterly Journal of the Royal Meteorological Society*, **103**, 255-267.

Elsner J. B., K.-b. Liu, and B. Kocher, 2000: Spatial variations in major U.S. hurricane activity: Statistics and a physical mechanism. *Journal of Climate,* **13,** 2293–2305.

Elsner J. B., 2003: Tracking hurricanes. *Bulletin of the American Meteorological Society*, **84**, 353-356.

Emanuel K.A., and R. Rotunno, 1989: Polar lows as arctic hurricanes. *Tellus A*, **41**, 1-17.

Feser F. and H. von Storch, 2005: A spatial two-dimensional discrete filter for limited-area-model evaluation purposes. *Monthly Weather Review*, **133**, 1774-1786.

Feser F. and H. von Storch, 2008a: A dynamical downscaling case study for typhoons in SE Asia using a regional climate model. *Monthly Weather Review*, **136 (5)**, 1806-1815.

Feser F. and H. von Storch, 2008b: Regional modelling of the western Pacific typhoon season 2004. *Meteorologische Zeitshrift*, **17(4)**, 519-528.

Fischer-Bruns I., H. von Storch, J. F. González-Rouco and E. Zorita, 2005: Modelling the variablility of midlatitude storm activity on decadal to century time scales. *Climate Dynamics*, **25(5)**, 461-476.

Fu G., H. Niino, R. Kimura, and T. Kato, 2004: Multiple polar mesocyclones over the Japan Sea on 11 February 1997. *Monthly Weather Review*, **132**, 793-814.

Geng Q. and M. Sugi, 2001: Variability of the North Atlantic activity in winter analyzed from NCEP-NCAR reanalysis data. *Journal of Climate*, **14**, 3863-3873.

González-Rouco F., H. von Storch, and E. Zorita, 2003: Deep soil temperature as proxy for surface air-temperature in a coupled model simulation of the last thousand years. *Geophysical Research Letters*, **30(21)**, 2116.

Gouirand I., V. Moron, and E. Zorita, 2007: Teleconnections between ENSO and North Atlantic in an ECHO-G simulation of the 1000-1990 period. *Geophysical Research Letters*, **34**, L06705.

Grønås S. and N. Kvamstø, 1995: Numerical simulations of the synoptic conditions and development of arctic outbreak polar lows. *Tellus A*, **47**, 797–814.

Gulev S. K., O. Zolina and S. Grigoriev, 2001: Extratropical cyclone varibility in the Northern Hemisphere winter from the NCEP/NCAR reanalysis data. *Climate Dynamics*, **17**, 795-809.

Hewson T. D., 2009: Diminutive frontal waves − a link between fronts and cyclones. *Journal of the Atmospheric Sciences*, **66**, 116-132.

Hodges K. I., 1994: A general method for tracking analysis and its application to meteorological data. *Monthly Weather Review*, **122**, 2573-2586.

Hodges K. I., 1995: Feature tracking on the unit sphere. *Monthly Weather Review*, **123**, 3458-3465.

Hodges K. I., 1999: Adaptive constraints for feature tracking. *Monthly Weather Review*, **127**, 1362-1373.

Hodges K. I., B. J. Hoskins, J. Boyle, and C. Thorncroft, 2003: A comparison of recent reanalysis data sets using objective feature tracking: storm tracks and tropical easterly waves. *Monthly Weather Review*, **131**, 2012-2037.

Hoskins B. J. and K. I. Hodges, 2002: New Perspectives on Northern Hemisphere Storm Tracks, *Journal of the Atmospheric Sciences*, **59**, 1041-1061.

Hoskins B. J. and K. I. Hodges, 2005: A new perspective on Southern Hemisphere storm tracks. *Journal of Climate*, **18**, 4108-4129.

Hurrell J. W., 1995: Decadal trends in the North Atlantic Oscillation: regional temperatures and precipitation. *Science*, **269**, 676-679.

International Detection and Attribution Group (IDAG), 2005: Detecting and attributing external influences on the climate system: A review of recent advances. *Journal of Climate*, **18**, 1291-1314.

Inatsu M., 2009: The neighbor enclosed area tracking algorithm for extratropical wintertime cyclones. *Atmospheric Science Letters*, **10**, 267-272.

Jones S. C., P. A. Harr, J. Abraham, L. F. Bosart, P. J. Bowyer, and co-authors, 2003: The extratropical transition of tropical cyclones: forecast challenges, current understanding, and future directions. *Weather and Forecasting*, **18**, 1052-1092.

Jung T., S. K. Gulev, I. Rudeva and V. Soloviov, 2006: Sensitivity of extratropical cyclone characteristic to horizontal resolution in ECMWF model. *Quarterly Journal of the Royal Meteorological Society*, **132**, 1839-1857.

Kalnay, E., Kanamitsu, M., Kistler, R., Collins, W., Deaven, D. and co-authors. 1996. The NCEP/NCAR 40-year reanalysis project. *Bulletin of the American Meteorological Society*, **77**, 437–471.

Kaspar K., T. Spangehl, and U. Cubasch, 2007: Northern hemisphere winter storm tracks of the Eemian interglacial and the last glacial inception. *Climate of the Past*, **3**, 181-192.

Keigwin L. D., 1996: The Little Ice Age and Medieval Warm Period in the Sargasso Sea. *Science*, **274**, 1503-1508.

KIHZ-Consortium: Zinke J., H. von Storch, B. Müller, E. Zorita, B. Rein, H. B. Mieding, H. Miller, A. Lücke, G.H. Schleser, M.J. Schwab, J.F.W. Negendank, U. Kienel, J.F. González-Rouco, C. Dullo and A. Eisenhauser, 2004: Evidence for the climate during the Late Maunder Minimum from proxy data available within KIHZ. In Fischer H., T. Kumke, G. Lohmann, G. Flöser, H. Miller, H von Storch and J. F. W. Negendank (Eds.): The Climate in Historical Times. Towards a synthesis of Holocene proxy data and climate models, Springer, Berlin - Heidelberg - New York, 487 pp., ISBN 3-540-20601-9, 397-414.

Knippertz P., U. Ulbrich, and P. Speth, 2000: Changing cyclones and surface wind speeds over the North Atlantic and Europe in a transient GHG experiment. *Climate Research*, **15**, 109-122.

Legutke S., E. Maier-Reimer, U. Cubasch, and A. Hellbach, 1996: Sensitivity of an OGCM to the resolution of atmospheric forcing data. In: CAS/JSC Working Group Numerical Experimentation, Report No. 20 (ed. G. J.Boer). World Climate Research Program, WMO.

Legutke S. and R. Voss, 1999: The Hamburg atmosphere–ocean coupled circulation model ECHO-G. Technical report No. 18, German Climate Computer Centre (DKRZ), Hamburg, Germany, 62 pp.

Mansfield D. A., 1974: Polar lows: the development of baroclinic disturbances in cold air outbreaks, *Quarterly Journal of the Royal Meteorological Society*, **100**, 541-554.

May W. and L. Bengtsson, 1998: The signature of ENSO in the Northern Hemisphere midlatitude season mean flow and high-frequency intraseasonal variability. *Meteorology and Atmospheric Physics*, **69**, 81-100.

Marchok T. P., 2002: How the NCEP tropical cyclone tracker works. Preprints, 25th Conf. on Hurricanes and Tropical Meteorology, San Diego, CA, Amer. Meteor. Soc. **2**.

Matulla C., W. Schöner, H. Alexandersson, H. von Storch, and X. L. Wang, 2008: European storminess: late nineteenth century to present. *Climate Dynamics*, **31**,125–130.

Min S. K., S. Legutke, A. Hense, and W. T. Kwon, 2005 a: Internal variability in a 1000-yr control simulation with the coupled climate model ECHO-G. I: Near-surface temperature, precipitation and mean sea level pressure, *Tellus A*, **57**, 605-621.

Min S. K., S. Legutke, A. Hense, and W. T. Kwon, 2005 b: Internal variability in a 1000-yr control simulation with the coupled climate model ECHO-G. II: El Niño Southern Oscillation and North Atlantic Oscillation, *Tellus A*, **57**, 622-640.

Moberg A., D. M. Sonechkin, K. Holmgren, N. M. Datsenko and W. Karlén, 2005: Highly variable Northern Hemisphere temperatures reconstructed from low- and high-resolution proxy data, *Nature*, **433**, 613-617.

Mokhov I., M. G. Akperov, V. E. Lagun, and E. I. Lutsenko, 2007: Intense Arctic Mesocyclones. *Atmospheric and Oceanic Physics*, **43(3)**, 259-265.

Murray R. J. and I. Simmonds, 1991: A numerical scheme for tracking cyclone centres from digital data Part I: development and operation of the scheme. *Australian Meteorological Magazine*, **39**, 155-166.

Müller B., 2004: A regional climate simulation for Europe in the time of the Late Maunder Minimum 1675-1705. GKSS-Forschungszentrum Geesthacht GmbH, Geesthacht, Germany.

Muskulus M. and D. Jacob, 2005: Tracking cyclones in regional model data: the future of Mediterranean storms. *Advanced Geosciences*, **2**, 13-19.

Nakamura J., U. Lall, Y. Kushnir and S. J. Camargo, 2009: Classifying North Atlantic tropical cyclone tracks by mass moments. *Journal of Climate*, **15**, 5481-5494.

Neu U., M. G. Akperov, N. Bellenbaum, R. Benestad, R. Blender, and co-authors, 2012: IMILAST − a community effort to intercompare extratropical cyclone detection and tracking algorithms: assessing method-related uncertainties. *Bulletin of the American Meteorological Society*, DOI: 10.1175/BAMS-D-11-00154.1.

Nielsen N. W., 1997: An early autumn polar low formation over the Norwegian Sea. *Journal of Geophysical Research*, **102**, 13955-13973.

Noer G. and M. Ovhed, 2003: Forecasting of polar lows in the Norwegian and the Barents Sea. Proc. Of the 9th meeting of the EGS Polar Lows Working Group, Cambridge, UK.

Pinto J. G., U. Ulbrich, G. C. Leckebusch, T. Spangehl, M. Reyers, and S. Zacharias, 2007: Changes in storm track and cyclone activity in three SRES ensemble experiments with the ECHAM5/MPI-OM1 GCM. *Climate Dynamics*, 29, 195-210.

Rasmussen E., 1979: The polar low as an extratropical CISK disturbance. *Quarterly Journal of the Royal Meteorological Society*, **105**, 531-549.

Rasmussen E. and J. Turner, 2003: Polar lows: mesoscale weather systems in the Polar Regions. Cambridge University Press, Cambridge.

Raible C. C. and R. Blender, 2004: Northern Hemisphere Mid-latitude cyclone variability in different ocean representations. *Climate Dynamics*, **22**, 239-248.

Raible C. C., M. Yoshimori, T. F. Stocker and C. Casty, 2007: Extreme midlatitude cyclones and their implications for precipitation and wind speed extremes in simulations of the Maunder Minimum versus present day conditions. *Climate Dynamics*, **28**, 409-423.

Raible C. C., P. M. Della-Marta, C. Schwierz, and R. Blender, 2008: Northern Hemisphere extratropical cyclones: a comparison of detection and tracking methods and different reanalyses. *Monthly Weather Review*, **136**, 880-897.

Roeckner E., K. Arpe, L. Bengtsson, M. Christoph, M. Claussen, L. Dümenil, M. Esch, M. Giorgetta, U. Schlese, and U. Schulzweida, 1996: The atmopheric general circulation model ECHAM4: model description and simulation of present-day climate. Report No. 218, 90 pp, Max-Planck-Institut für Meteorologie, Bundesstr 55, Hamburg.

Rockel B., A. Will, and A. Hense, 2008: The Regional Climate Model COSMO-CLM (CCLM). *Meteorologische Zeitshrift*, **17(4)**, 347-348.

Rudeva I. and S. K. Gulev, 2007: Climatology of cyclone size characteristic and their changes during the cyclone life cycle. *Monthly Weather Review*, **135**, 2568-2587.

Schubert M., J. Perlwitz, R. Blender, K. Fraedrich and F. Lunkeit, 1998: North Atlantic cyclones in CO_2-induced warm climate simulations: frequency, intensity and tracks. *Climate Dynamics*, **14**, 827-837.

Scharenbroich L., G. Magnusdottir, P. Smyth, H. Stern, and C. Wang, 2010: A Bayesian Framework for Storm Tracking Using a Hidden-State Representation. *Monthly Weather Review*, **138**, 2132–2148.

Serreze M. C., 1995: Climatological aspects of cyclone development and decay in the arctic. *Atmosphere- Ocean*, **33(1)**, 1-23.

Shapiro R., 1975: Linear filtering. *Mathematics of Computation.*, **29(132)**, 1094-1097.

Shuman F. G., 1975: Numerical methods in wether prediction: II. Smoothing and filtering. *Monthly Weather Review*, **85**, 357-361.

Shapiro M. A., L. S. Fedor, and T. Hampel, 1987: Research aircraft measurements of a polar low over the Norwegian Sea. *Tellus A*, **39**, 272-306.

Sinclair M. R., 1997: Objective identification of cyclones and their circulation intensity, and climatology. *Weather and Forecasting*, 12, 591-608.

Sickmöller M., R. Blender and K. Fraedrich, 2000: Observed winter cyclone tracks in the northern hemisphere in re-analysed ECMWF data. *Quarterly Journal of the Royal Meteorological Society*, **126**, 591-620.

Simmonds I. and K. Keay, 2002: Surface fluxes of momentum and mechanical energy over the North Pacific and North Atlantic Oceans. *Meteorology and Atmospheric Physics*, **80**, 1-18.

Stendel M. and E. Roeckner, 1998: Impacts of horizontal resolution on simulated climate statistics in ECHAM4. Report No. 253, Max-Planck-Institut für Meteorologie, Bundesstr 55, Hamburg.

Steppeler, J., Doms, G., Schättler, U., Bitzer, H., Gassmann, A. and co-authors. 2003. Meso-gamma scale forecasts using the nonhydrostatic model LM. *Meteorol. Atmos. Phys.* **82**, 75-96.

Tan M., X. Shao, J. Liu and B. Cai, 2009: Comparative analysis between a proxy-based climate reconstruction and GCM-based simulation of temperature over the last millennium in China. *Journal of Quaternary Science*, **24(5)**, 547-551.

Uccellini L. W., 1990: Process contributing to the rapid development of extratropical cyclones. In: Newton CW, Holopainen EO (eds) Extratropical cyclones. The Eric Palmen memorial volume. AMS, Boston, 81-106.

Ulbrich U. and M. Christoph, 1999: A shift of the NAO and increasing storm track activity over Europe due to anthropogenic greenhouse gas forcing. *Climate Dynamics*, **15**, 551-559.

Ulbrich U., G. C. Leckebusch and J. G. Pinto, 2009: Extra-tropical cyclones in the present and future climate: a review. *Theoretical and Applied Climatology*, **96**, 117-131.

von Storch, J.-S., V. Kharin, U. Cubasch, G. Hegerl, D. Schriever, H. von Storch, and E. Zorita, 1997: A 1260 year control integration with the coupled ECHAM1/LSG general circulation model. *Journal of Climate*, **10**, 1526-154.

von Storch and F. W. Zwiers, 1999: Statistical analysis in climate research. Cambridge University Press, Cambridge, UK, 503pp.

von Storch H., H. Langenberg, and F. Feser, 2000: A spectral nudging technique for dynamical downscaling purposes. *Monthly Weather Review*, **128**, 3664-3673.

von Storch H., E. Zorita, Y. Dimitriev, F. González-Rouco, and S. Tett, 2004: Reconstructing past climate from noisy data. *Science*, **306**, 679-682.

Wang X. L., V. R. Swail, and F. W. Zwiers, 2006: Climatology and changes of extratropical cyclone activity: Comparison of ERA-40 with NCEP/NCAR Reanalysis for 1958-2001. *Journal of Climate*, **19**, 3145-3166.

Weisse R., H. von Storch, and F. Feser, 2005: Northeast Atlantic and North Sea Storminess as Simulated by a Regional Climate Model during 1958-2001 and Comparison with Observations. *Journal of Climate*, **18(3)**, 465-479.

Weisse R. and H. von Storch, 2009: Marine climate and climate change: storm, wind waves and storm surges. Springer Praxis Books, ISBN: 978-3-540-25316-7, 166-173.

Wernli H. and C. Schwierz, 2006: Surface cyclones in the ERA-40 dataset (1958-2001). Part I: novel identification method and global climatology. *Journal of the Atmospheric Sciences*, **63**, 2486-2507.

Wolff J. O., E. Maier-Reimer, and S. Legutke, 1997: The Hamburg Ocean primitive equation model. Technical Report, No. 13, 98 pp, German Climate Computer Center (DKRZ), Hamburg.

Woth K., R. Weisse, and H. von Storch, 2006: Climate change and North Sea storm surge extremes: an ensemble study of storm surge extremes expected in a changed climate projected by four different regional climate models. *Ocean Dynamics*, **56**, 3-15.

Wollings T., J. M. Gregory, J. G. Pinto, M. Reyers, and D. J. Brayshaw, 2012: Response of the North Atlantic storm track to climate change shapes by ocean-atmosphere coupling. *Nature Geoscience*, **5**, 313-317.

Xia L., M. Zahn, K. I. Hodges, F. Feser, and H. von Storch, 2012a: A comparison of two identification and tracking Methods for polar lows. *Tellus A*, **64**, 17196.

Xia L., H. von Storch and F. Feser, 2012b: Quasi-stationarity of centennial Northern Hemisphere midlatitude winter storm tracks. *Climate Dynamics*, DOI: 10.1007/s00382-012-1543-5.

Zahn M. and H. von Storch, 2008a: Tracking polar lows in CLM. *Meteorologische Zeitshrift*, **17(4)**, 445-453.

Zahn M. and H. von Storch, 2008b: A long-term climatology of North Atlantic polar lows. *Geophysical Research Letters*, **35**, L22702.

Zahn M., H. von Storch, and S. Bakan, 2008: Climate mode simulation of North Atlantic polar lows in a limited area model. *Tellus A*, 60, 620-631.

Zahn M. and H. von Storch, 2010: Decreased frequency of North Atlantic polar lows associated with future climate warming. *Nature*, **467**, 309-312.

Zolina O. and S. K. Gulev, 2002: Improving the accuracy of mapping cyclone numbers and frequencies. *Monthly Weather Review*, **130**, 748-759.

Zorita E., J. F. González-Rouco, H. von Storch, J. P. Montávez, and F. Valero, 2005: Natural and anthoropogenic model of surface temperature variations in the last thousand years. *Geophysical Research Letters*, **32**, L08707.

List of Abbreviations

AD	Anno Domini
AGCM	Atmospheric General Circulation Model
AMIP	Atmospheric Model Intercomparison Project
BP	Before Present
CCA	Canonical Correlation Analysis
CISK	Conditional Instability of the Second Kind
CLM or **CCLM**	Regional Climate Model COSMO-CLM of the German Weather Service
DCT	Discrete Cosine Transforms
DJF	December, January, and February
DWD	German Weather Forecast Service
ECHAM4	the 4^{th} generation of the atmospheric general circulation model developed by the Max Planck Institute for Meteorology
ECHO-G	a coupled climate model consisting of the atmospheric model ECHAM4 and the ocean model HOPE-G
ECMWF	European Center for Medium-Range Weather Forecasts
ENSO	El Nino Southern Oscillation
EOF	Empirical Orthogonal Function
ERA-40	the ECMWF reanalysis
GCM	Global Climate Model
HOPE-G	a global version of the Hamburg Ocean Primitive Equation general circulation model HOPE
IMILAST	Intercomparison of MId-LAtitude STorm diagnostics project
IPCC	Intergovernmental Panel of Climate Change
KH	Hodges' detection and tracking method (1994, 1995 and 1999)
LIA	Little Ice Age
LLM	Late Maunder Minimum
MCA	Medieval Climate Anomaly
MOC	Meridional Overturning Circulation
MSLP	Mean Sea Level Pressure
MZ	Zahn and von Storch's detection and tracking method (2008a)
NAO	North Atlantic Oscillation

NCAR	National Center for Atmospheric Research
NCEP	National Centers of Environmental Prediction
NH	Northern Hemisphere
PNA	Pacific/North American Oscillation
RCM	Regional Climate Model
REMO	the Regional Model of Max Planck Institute for Meteorology
SH	Southern Hemisphere
SO	Southern Oscillation
SOI	Southern Oscillation Index
SST	Sea Surface Temperature
Z1000	the 1000hPa geopotential height surface
ξ_{850}	850 hPa vorticity
θ_{pv2}	potential temperature on a potential vorticity=2 surface

List of Figures

List of Tables

Erklärung

Hiermit erkläre ich an Eides statt, dass ich die vorliegende Dissertationsschrift selbst verfasst und keine anderen als die angegebenen Quellen und Hilfsmittel benutzt habe.

_____ _____

Ort, Datum Unterschrift